

**Structural characterization of the two copper proteins  
nitrous oxide reductase from *Pseudomonas stutzeri* and  
laccase Lcc5 from *Coprinopsis cinerea***

Dissertation zur Erlangung des Doktorgrades der Mathematisch-  
Naturwissenschaftlichen Fakultäten der Georg-August-Universität zu  
Göttingen

vorgelegt von Anja Pomowski  
aus Jena

Göttingen, 2010

D7

Referent: Prof. Dr. Oliver Einsle

Korreferentin: Dr. Susana Andrade

Tag der mündlichen Prüfung: 27.10.2010



"The most exciting phrase to hear in science, the one that heralds new discoveries, is not 'Eureka!' (I found it!) but 'That's funny...'"

- Isaac Asimov

# Contents

<b>I</b>	<b>ZUSAMMENFASSUNG</b> .....	<b>IV</b>
<b>II</b>	<b>SUMMARY</b> .....	<b>VI</b>
<b>III</b>	<b>INTRODUCTION</b> .....	<b>1</b>
1	COPPER SITES IN PROTEINS .....	2
1.1	<i>Type-1 copper</i> .....	2
1.2	<i>Type-2 copper</i> .....	4
1.3	<i>Type-3 copper</i> .....	5
1.4	<i>Trinuclear copper center</i> .....	6
1.5	<i>Cu<sub>A</sub> center</i> .....	7
1.6	<i>Cu<sub>B</sub> center</i> .....	9
2	NITROUS OXIDE REDUCTASE .....	10
2.1	<i>The biological nitrogen cycle</i> .....	10
2.1.1	Nitrous oxide .....	12
2.1.2	N <sub>2</sub> O metabolism .....	13
2.1.3	Nitrous oxide reductase .....	14
2.1.3.1	Spectroscopic properties .....	16
2.1.3.2	Structure .....	17
2.1.3.3	Expression, Regulation and Maturation of N <sub>2</sub> OR .....	19
2.1.3.4	Catalysis and theoretical calculations on the reaction mechanism .....	21
2.2	<i>Scope of the study</i> .....	22
3	LACCASES .....	23
3.1	<i>Catalysis</i> .....	24
3.2	<i>Biotechnological applications</i> .....	25
3.3	<i>Laccase Lcc5 from Coprinopsis cinerea</i> .....	26
3.4	<i>Scope of the study</i> .....	27
<b>IV</b>	<b>MATERIAL AND METHODS</b> .....	<b>28</b>
1	PROTEIN CRYSTALLOGRAPHY .....	28
1.1	<i>Theoretical background</i> .....	28
1.1.1	Crystallization .....	28
1.1.2	X-ray diffraction by crystals .....	30
1.1.2.1	Braggs' law .....	30
1.1.3	The electron density function $\rho(x)$ .....	32
1.1.3.1	Molecular replacement .....	33
2	PROTEIN BIOCHEMISTRY .....	34

2.1	<i>Nitrous oxide reductase from Pseudomonas stutzeri</i> .....	35
2.1.1	Crystallization .....	35
2.1.2	Substrate complexes of nitrous oxide reductase .....	35
2.1.3	Data collection and processing.....	36
2.1.4	Molecular replacement .....	36
2.1.5	Model building and Refinement .....	37
2.1.6	Spectroscopy .....	37
2.1.6.1	UV/ vis spectra .....	37
2.1.6.2	Electron Paramagnetic Resonance.....	37
2.2	<i>Laccase Lcc5 from Coprinopsis cinerea</i> .....	38
2.2.1	Crystallization .....	38
2.2.2	Data collection and processing.....	38
2.2.3	Molecular replacement .....	39
2.2.4	Model building and refinement.....	39
<b>V</b>	<b>RESULTS AND DISCUSSION</b> .....	<b>40</b>
1	NITROUS OXIDE REDUCTASE OF <i>PSEUDOMONAS STUTZERI</i> .....	40
1.1	<i>Crystallization</i> .....	40
1.2	<i>Crystal structure</i> .....	41
1.2.1	The Cu <sub>A</sub> site .....	44
1.2.2	The Cu <sub>Z</sub> site.....	46
1.2.2.1	Second sulfur .....	47
1.2.2.2	Spectroscopic characterization of Cu <sub>Z</sub> , Cu <sub>Z</sub> * and Cu <sub>Z</sub> <sup>0</sup> .....	48
1.2.3	The putative gas channel.....	51
1.3	<i>Implications for the reaction mechanism</i> .....	55
1.3.1	Electron transfer from a putative electron donor .....	55
1.3.2	Explanation for the pH dependence of N <sub>2</sub> OR by an engineered Cu <sub>A</sub> azurin .....	57
1.3.3	A structural role for S <sub>Z2</sub> .....	59
1.3.4	Two distinct ways of N <sub>2</sub> O reduction in Cu <sub>Z</sub> and Cu <sub>Z</sub> * .....	59
1.3.5	Iodide as an inhibitor for N <sub>2</sub> OR.....	60
1.3.6	Biosynthetic models of Cu-S cluster .....	61
1.4	<i>Conclusions and Outlook</i> .....	62
2	LACCASE LCC5 OF <i>COPRINOPSIS CINEREA</i> .....	64
2.1	<i>Crystallization</i> .....	64
2.2	<i>Sequence analysis</i> .....	64
2.3	<i>Crystal structure</i> .....	65
2.3.1	The two copper sites .....	67
2.3.2	Glycosylation of Lcc5 .....	70
3	CONCLUSIONS AND OUTLOOK.....	70
<b>VI</b>	<b>APPENDIX</b> .....	<b>72</b>

ABBREVIATIONS.....	72
<b>VII REFERENCES.....</b>	<b>76</b>
<b>VIII ACKNOWLEDGEMENTS.....</b>	<b>89</b>
<b>IX CURRICULUM VITAE.....</b>	<b>91</b>

## I Zusammenfassung

Obwohl die Reduktion von Distickstoffoxid ( $\text{N}_2\text{O}$ ) stark exergonisch ist, verhindert eine hohe Aktivierungsenergie eine spontane Reaktion. Wie Distickstoff benötigt  $\text{N}_2\text{O}$  ein komplexes Metallzentrum, um aktiviert zu werden.

Das einzige bekannte Enzym, welches die Reduktion von  $\text{N}_2\text{O}$  zu  $\text{N}_2$  katalysieren kann, ist das sauerstoffempfindliche Protein Distickstoffmonoxidreduktase ( $\text{N}_2\text{OR}$ ).

Kristallographische Untersuchungen an diesem Protein aus *Paracoccus denitrificans*, *Marinobacter hydrocarbonoclasticus* und *Achromobacter cycloclastes* ermöglichten Einblicke in dessen Struktur: Das Protein formt ein "Head-to-Tail"-Dimer, dessen Bildung notwendig für die enzymatische Reaktion ist. Jedes Monomer besteht aus zwei separaten Domänen, einem N-terminalen  $\beta$ -Propeller mit dem tetranuclear  $\text{Cu}_Z$ -Zentrum und einer C-terminalen Cupredoxin-ähnlichen Domäne, welche ein gemischt-valentes  $\text{Cu}_A$ -Zentrum trägt, ähnlich dem der Cytochrom *c* Oxidase.

Diese  $\text{N}_2\text{O}$ -Reduktasestrukturen repräsentieren jedoch aerob isoliertes Protein, welches nur aktiv ist, nach einer verlängerten Inkubation mit Reduktionsmitteln. Im Gegensatz hierzu zeigt die violette Form der Distickstoffoxidreduktase aus *Pseudomonas stutzeri* physiologische Aktivität, ohne dass eine vorherige reduktive Aktivierung notwendig ist.

In dieser Arbeit wird sowohl die erste Kristallstruktur der physiologisch aktiven Form der  $\text{N}_2\text{O}$ -Reduktase als auch die erste Struktur eines Metall- $\text{N}_2\text{O}$ -Komplexes beschrieben. Dies ermöglicht neue Erkenntnisse hinsichtlich des Bindungsmodus von  $\text{N}_2\text{O}$  an das katalytische Zentrum.

In mit  $\text{N}_2\text{O}$ -begasteten Kristallen bindet Distickstoffoxid zwischen dem  $\text{Cu}_A$  und dem  $\text{Cu}_Z$ -Zentrum. Das  $\text{Cu}_A$ -Zentrum ist wie bereits früher beschrieben ein gemischt-valentes Zentrum, welches zwischen dem oxidiertem  $[\text{Cu}^{+1.5}:\text{Cu}^{+1.5}]$  und dem reduzierten  $[\text{Cu}^+:\text{Cu}^+]$  Zustand alterniert und dadurch ein Elektron pro Zyklus zur Verfügung stellt. Im Gegensatz zu früheren Strukturen ist der Histidinligand von  $\text{Cu}_{A1}$  flexibel und rotiert abhängig von



der Anwesenheit des Substrats, um Wasserstoffbrücken zu einem nahegelegenen Serin- und Aspartatrest zu bilden.

Desweiteren zeigt das  $\text{Cu}_z$  einen entscheidenden strukturellen Unterschied zu früheren Beschreibungen. An der Kante von  $\text{Cu}_{z1}$  und  $\text{Cu}_{z4}$  befindet sich anstelle des beschriebenen Wassermoleküls ein zweiter Schwefel. Dieser ermöglicht die Erklärung verschiedener spektroskopischer Beobachtungen bei den einzelnen Enzymformen.

$\text{Cu}_z$  der violetten Distickstoffoxidreduktase aus *Pseudomonas stutzeri* ist daher ein  $[\text{4Cu:2S}]$  Zentrum, wohingegen das  $[\text{4Cu:1S}]$  Cluster, welches zuvor bei anderen Formen beobachtet wurde, das  $\text{Cu}_z^*$  Zentrum repräsentiert. Der zweite Schwefel stabilisiert vermutlich die Geometrie von  $\text{Cu}_z$  und könnte daher Voraussetzung für eine erfolgreiche Substratbindung darstellen.

Der Bindungsmodus von  $\text{N}_2\text{O}$  deutet an, dass  $\text{Cu}_z$  und  $\text{Cu}_A$  als ein aktives Zentrum fungieren, um das Substrat zu reduzieren.

## II Summary

Although, the reduction of nitrous oxide ( $\text{N}_2\text{O}$ ) is highly exergonic, a high activation barrier hinders a spontaneous reaction. With regard to inertness,  $\text{N}_2\text{O}$  is second only to molecular nitrogen and in both cases a complex metal center is required for activation. The only known enzyme, which catalyzes the reduction of  $\text{N}_2\text{O}$  to  $\text{N}_2$  is the oxygen sensitive copper-protein nitrous oxide reductase ( $\text{N}_2\text{OR}$ ). Crystallographic studies on this enzyme from *Paracoccus denitrificans*, *Marinobacter hydrocarbonoclasticus* and *Achromobacter cycloclastes* provided insight into its structure: The protein forms a head-to-tail homodimer, which was shown to be obligatory for enzyme reaction. Each monomer comprises of two distinct domains, an N-terminal  $\beta$ -propeller with the tetranuclear  $\text{Cu}_Z$  site and a C-terminal cupredoxin-like domain carrying the mixed valent  $\text{Cu}_A$  center, similar to the one found in cytochrome *c* oxidase.

However, these structures represent the aerobically isolated protein, which is only active upon extended incubation with reducing agents. In contrast, the purple form of nitrous oxide reductase from *Pseudomonas stutzeri* shows physiological activity without the necessity of reductive activation.

This work presents the first structure of the purple form of nitrous oxide reductase and as well the first structure of a metal- $\text{N}_2\text{O}$  complex, providing new insights into the binding mode of  $\text{N}_2\text{O}$  to the catalytic site.

In pressurized crystals  $\text{N}_2\text{O}$  binds between  $\text{Cu}_Z$  and  $\text{Cu}_A$  site, which is as previously described a mixed-valent center alternating between the oxidized mixed-valent  $[\text{Cu}^{+1.5}:\text{Cu}^{+1.5}]$  and the reduced  $[\text{Cu}^+:\text{Cu}^+]$  state thereby providing one electron per cycle. In contrast to previous structures, the histidine ligand of  $\text{Cu}_{A1}$  is flexible and rotates to form hydrogen bonds with a near-by serine and aspartate residue in dependence of substrate binding. Additionally, a major structural difference could be observed for the  $\text{Cu}_Z$  site. A second sulfur ion is found at the edge of  $\text{Cu}_{Z1}$  and  $\text{Cu}_{Z4}$  replacing the earlier described water molecule. This observation offers an explanation for several spectroscopic features of the different enzyme forms.

The Cu<sub>2</sub> of purple nitrous oxide reductase from *Pseudomonas stutzeri* is therefore a [4Cu:2S] site, whereas the [4Cu:1S] center observed in previously structures represents the Cu<sub>2</sub>\* state. The second sulfur might stabilize the Cu<sub>2</sub> geometry by binding to Cu<sub>Z1</sub> and Cu<sub>Z4</sub>, which might be a prerequisite for successful substrate binding. The observed binding mode of N<sub>2</sub>O indicates that both copper center act in concert to reduce the substrate.

### III Introduction

Metals and transition metals occur as components of proteins where they can function as active sites for catalysis or as structural elements. Among the redox-active transition metals, copper is the second most abundant after iron, and it is involved in various biological functions (1).

Copper became biologically relevant with the evolution of photosynthesis that resulted in accumulation of oxygen in the atmosphere (2). In contrast to iron, which is water soluble in its  $\text{Fe}^{2+}$  form and insoluble if oxidized to  $\text{Fe}^{3+}$ , copper is insoluble as  $\text{Cu}^+$  but soluble and therefore accessible as  $\text{Cu}^{+2}$ . The low bioavailability of copper during the early colonization of earth by microorganisms led to the consideration that copper proteins have evolved later than their iron counterparts (3).

Before the first photosynthetic bacteria evolved, dioxygen was almost absent in the earth atmosphere (4) and the higher concentrations of  $\text{CH}_4$ ,  $\text{SO}_2$ ,  $\text{H}_2$ ,  $\text{H}_2\text{S}$  (5,6) compared to today's atmosphere resulted in a reducing environment with iron existing therefore mostly in its ferrous form. But with the evolution of photosynthetic microorganisms, the dioxygen levels were rising (4). This led to the precipitation of iron in form of ferric iron hydroxides ( $\text{Fe}(\text{OH})_3$ ) and to an increase in the atmospheric dioxygen concentration (7). A new redox-active metal was therefore required which could be found in copper (3). Nowadays, copper is an essential trace element in all domains of life.

Iron and copper inherit similar functions in proteins ranging from electron transfer in such fundamental processes as photosynthesis and respiration (8) to dioxygen uptake, transport and storage (9) and catalysis. Most of these biological functions of copper depend on the fact that it can adopt two redox states:  $\text{Cu}^+$  ( $d^{10}$ ) and  $\text{Cu}^{2+}$  ( $d^9$ ). Iron on the other hand, occurs as  $\text{Fe}^{2+}$  ( $d^6$ ) and  $\text{Fe}^{3+}$  ( $d^5$ ), but also frequently as  $\text{Fe}^{4+}$  ( $d^4$ ).

Copper sites in proteins were commonly divided into three different groups according to their spectroscopic features: The type-1 or blue copper proteins, type-2 and type-3 copper proteins (10). However, over the last years, more copper sites were found, making

the definition of new classes necessary (11,12). The current classification lists 7 different types of copper centers that will be briefly summarized in the following paragraphs (11).

## 1 Copper sites in proteins

### 1.1 Type-1 copper

Type-1 (T1) copper proteins, also called blue copper proteins or cupredoxins, contain a mononuclear copper site (11,12).

A typical feature for T1 copper proteins is the so called cupredoxin fold: a 6-8 stranded  $\beta$ -barrel with a greek key motif (Fig. 1) that forms a strong scaffold to coordinate the copper (13). It can also be found in different copper proteins such as Cu-nitrite reductase (14,15), nitrous oxide reductase (16,17,18) and cytochrome *c* oxidase (13).

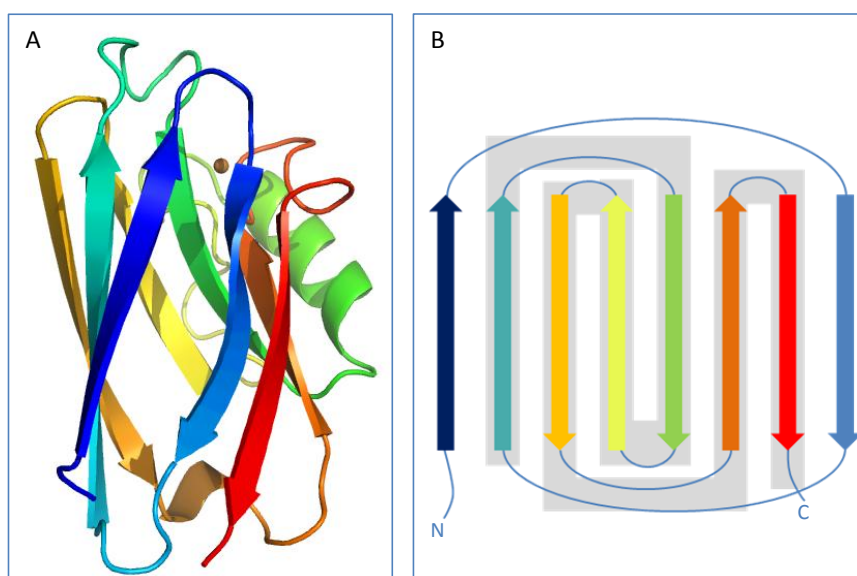


**Fig. 1 A:** Cupredoxin fold of azurin (pdb: 1azu). The  $\beta$ -sheets form a  $\beta$ -barrel with a greek key motif. Coloring from N-terminus (blue) to C-terminus (red).  
**B:** Scheme of greek key motif (grey boxes).

The copper is usually ligated by two histidine residues, one cysteine residue and one or two variable axial ligands, one of them mostly a methionine, in a distorted tetrahedron or as a distorted trigonal bipyramide (Fig. 2, (12)).

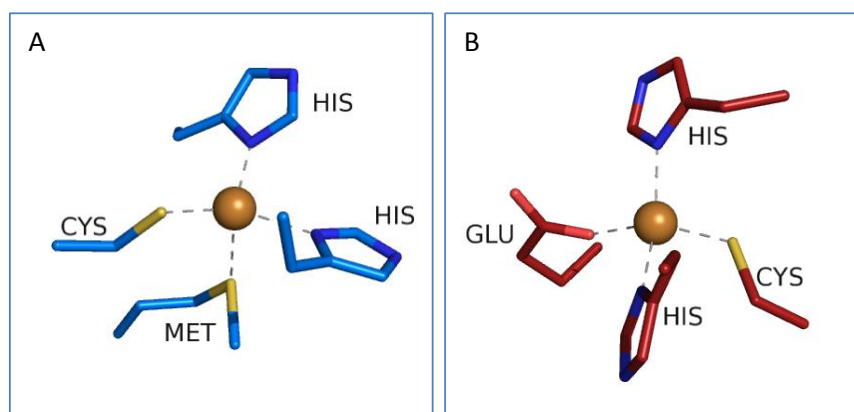


**Fig. 2 A:** Type-1 (T1) copper site of azurin (pdb: 1azu). The copper atom (brown) is bridged by two histidine residues, one cysteine residue and a methionine residue in axial position. **B:** Type-1 copper site of nitrosocyanin (pdb: 1iby). The methionine residue is exchanged against a glutamate residue.

The role of the axial ligands of the copper has been studied extensively (19) and the observation of different redox potentials depending on this ligand suggests a putative role in fine tuning of the redox properties (20,21): Stellacyanin of *Rhus vernicifera* contains a glutamine residue as axial ligand and exhibits one of the lowest redox potentials (184 mV vs. NHE) among the blue copper proteins whereas in fungal laccases and ceruloplasmin (22,23), which can have redox potentials up to almost 1000 mV vs. NHE, a leucine is coordinating the T1 copper (24).

The characteristic feature of T1 proteins which is eponymous for this protein group is the intense ( $\epsilon > 3000 \text{ M}^{-1} \text{ cm}^{-1}$ ) blue color in their oxidized  $\text{Cu}^{2+}$  form that is due to a  $\text{S}(\text{Cys}) \rightarrow \text{Cu}$  ligand-to-metal-charge transfer (LMCT) transition near 600 nm (25). The EPR spectrum exhibits an uncommonly small hyperfine splitting in the  $g_{\parallel}$  region ( $g_{\parallel}=2.3$ ,  $A_{\parallel} = (40-95) \cdot 10^{-4} \text{ cm}^{-1}$ ) (25,26) due to the covalent thiolate S-Cu bond and a delocalized electron spin that decreases its interaction with the nuclear spin of the copper (12). The highly covalent character of the thiolate Cu-S bond and the low reorganization energy favor long-range electron transfer (27) which is represented in the functions of typical examples of this protein group such as azurin, pseudoazurin, rusticyanin, plantacyanin and proteins of the plastocyanin family that are involved in electron-transfer (12,28,29). However, the type-1 site can also be found in multicopper oxidases such as ascorbate oxidase or laccase, which contain more than one copper site. In these proteins, the T1

center is the active site or involved in electron shuttling from and to the catalytically active site (12,30).

Nevertheless, the term "blue copper proteins" can be misleading because some T1 copper centers containing proteins can be green like green Cu-nitrite reductases (14) or even red: Nitrosocyanin of *Nitrosomonas europaea* is a red T1 copper containing protein with unknown function (31,32). The axial methionine residue is exchanged against a glutamate residue (Fig. 2) which leads to a shift of the absorption band to 390 nm ( $\epsilon = 7000 \text{ M}^{-1} \text{ cm}^{-1}$ ) and therefore to the red color (33). The protein exhibits a redox potential of 85 mV vs. NHE that is even lower than that of other blue copper proteins (31). The second axial ligand is a water molecule that is lost upon reduction thereby providing an open coordination site. This observation suggests a role involved in electron transfer or catalysis (32,31).

## 1.2 Type-2 copper

Type-2 (T2) copper centers can be found in enzymes assisting in amine degradation such as phenylalanine hydroxylase (34), cross-linking of collagen and elastin by lysyl oxidase (35,36), in oxidations or oxygenations like galactose oxidase or Cu-Zn superoxide

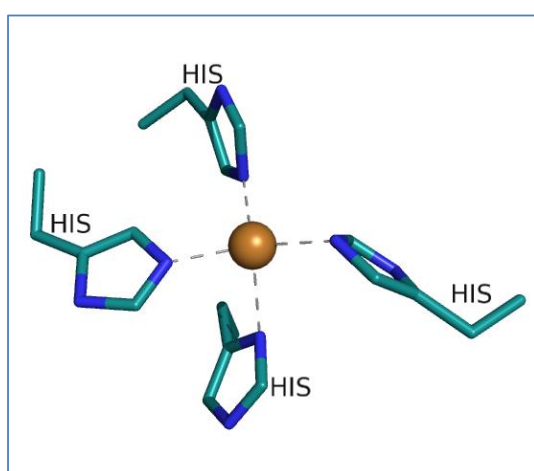


**Fig. 3** Type-2 copper site of Cu,Zn-superoxide dismutase from spinach (pdb: 1srd). The copper atom (brown) is ligated by 4 histidine residues coordinated as a distorted tetrahedron.

dismutase (37,38) or as part of the biological nitrogen cycle, the Cu-nitrite reductase (39,14).

The single copper ion shows a square planar or distorted tetrahedral geometry (Fig. 3) coordinated by four N or N/O ligands but no S ligand (11).

In T1 copper proteins, the blue color is a result of a LMCT transition from S(Cys) to Cu; the absence of a S-providing ligand in type-2 copper proteins explains therefore why

these proteins are nearly colorless. Their axial EPR spectrum shows a hyperfine splitting characteristic for square-planar Cu(II) complexes, which distinguish them from type-1 copper centers.

### 1.3 Type-3 copper

Type-3 (T3) copper sites are binuclear, laying within a conserved four-helix bundle motif with the two copper ions ligated by three N(His) each (Fig. 4).

They are EPR silent due to strong antiferromagnetic coupling of the  $d^9$  nuclei. Proteins

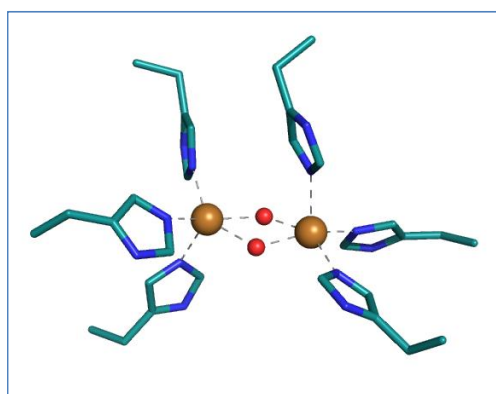


**Fig. 4** Type-3 copper site of hemocyanin (pdb: 1nol). Both copper atoms (brown) are ligated by three histidine each. A peroxide molecule (red) is bridging both Cu atoms.

belonging to this group are involved in dioxygen transport and activation like tyrosinase, hemocyanins and catechol oxidases (40,30). Upon dioxygen uptake, an intensive absorption at 350 nm and 600 nm can be observed as a result of two peroxide-copper charge transfer transitions (41,42).

This feature can be seen very well in molluscs like cephalopods: their hemolymph contains hemocyanin instead of hemoglobin for transport of dioxygen. As a result, their

"blood" is colorless when deoxygenated and blue if dioxygen is bound.

Even though their function is similar to that of hemoglobin, several significant differences regarding structure and mechanism can be observed: In contrast to their heme-containing counterparts, hemocyanins are located in any kind of blood cell. A reason for this behavior is the size of these proteins. Depending on the species, they form dimers or hexamers containing subunits of 50-400 kDa arranged in clusters or chains that can exceed 1,500 kDa (43). Another difference is the accommodation of the metal ion: In hemoglobin, the iron is coordinated via porphyrin, in hemocyanin however, the copper is directly ligated by histidine residues.



## 1.4 Trinuclear copper center

Trinuclear copper center also referred as type-4 copper sites (11) are composed of a type-2 and type-3 active site with 8 histidine residues that coordinate the three coppers and two bridging water or hydroxyl ligands (Fig. 5).

This center can be found in enzymes such as laccases and ascorbate oxidase (44,23) that have an additional type-1 center that is connected to the trinuclear site by a cysteine-histidine electron pathway (30). These proteins are referred as multicopper oxidases or blue oxidases (30).

A prominent example for this protein group is ceruloplasmin, a pseudohexameric protein (45) with one trinuclear site and three type-1 copper centers (45,44,22). It is the only multicopper oxidase in humans: The most remarkable feature of the different copper sites is the redoxpotential of  $\sim 1.0$  V for one of the T1 copper (22) whose physiological role is still under discussion. The function of ceruloplasmin has been studied extensively (46,47,48,49): It could be shown that the protein catalyzes the oxidation of  $\text{Fe}^{2+}$  to  $\text{Fe}^{3+}$  under physiological conditions which supports the putative function as a plasma ferroxidase in humans (50,51,52). Nevertheless, additional activity towards homeostasis and transport of copper, NO homeostasis by oxidation of NO to  $\text{NO}_2^-$  and amine oxidase activity have been postulated as well (53,54).

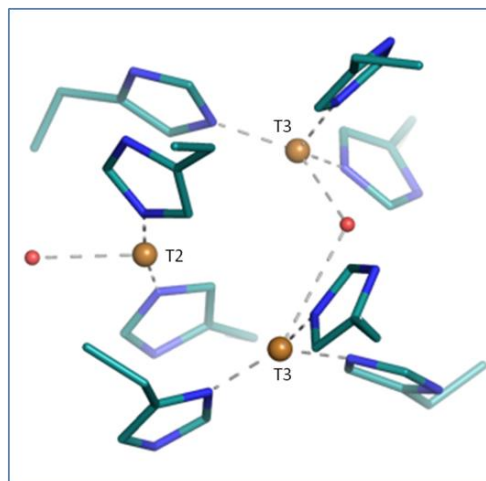


**Fig. 5** Type-4 (T4) copper center of laccase Lcc1 of *C. cinerea* (pdb: 1hfu) (216). The trinuclear center consists of one T2 copper atom (brown) that is ligated by two histidine residues and one hydroxyl or water molecule. The two T3 copper atoms (brown), are coordinated by three histidine residues each and one hydroxyl or water molecule.

## 1.5 Cu<sub>A</sub> center

The Cu<sub>A</sub> site is a mixed-valent [Cu<sup>+1.5</sup>:Cu<sup>+1.5</sup>] binuclear copper site (55) in physiologically oxidized form that can be reduced to a [Cu<sup>+</sup>:Cu<sup>+</sup>] state. It can be found in cytochrome *c* oxidase (COX), menaquinol-oxidizing NO-reductase of *Bacillus azotoformans* (17,56,57,58,59) and nitrous oxide reductase (N<sub>2</sub>OR) (60) and has been engineered into the type I copper center of azurin (61,62).

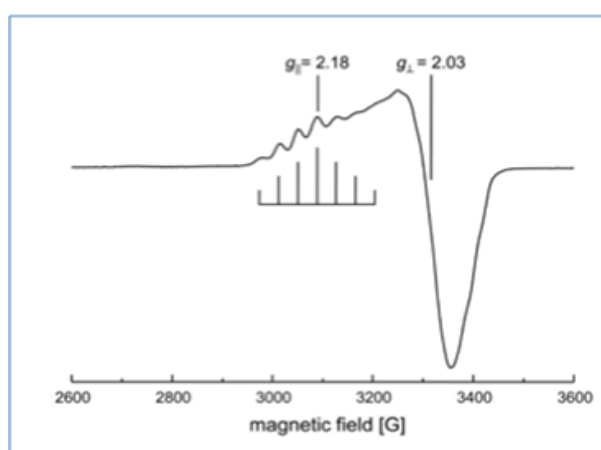


**Fig. 6** X-band EPR spectrum of purple N<sub>2</sub>O reductase of *P. stutzeri* showing the characteristic 7-line hyperfine pattern with a 1:2:3:4:3:2:1 intensity ratio.

The Cu<sub>A</sub> site has a characteristic purple color as a result of S(cys) → Cu charge transfer bands at 485 nm and 525 nm, a class III mixed-valence charge transfer band at around 790 nm and a very unique EPR spectrum (63,12,64,65): The one of N<sub>2</sub>OR exhibits a 7-line hyperfine pattern in a 1:2:3:4:3:2:1 intensity ratio (Fig. 6) in the g<sub>||</sub> region at around 2.18 (X-band) (63,66). Multifrequency EPR

spectroscopy at 2.5-35 GHz indicated a binuclear composition with a mixed-valent S=1/2 state of the two copper atoms (60,66,67). Upon reduction, the center becomes EPR silent. Even though the EPR spectra of COX are not as well resolved as the spectra obtained from N<sub>2</sub>OR (68,55,63,64,66,69), the same binuclear mixed-valent [Cu<sup>1.5</sup>:Cu<sup>1.5</sup>] character of Cu<sub>A</sub> was expected, which could then be confirmed by the crystal structures of COX from *Paracoccus denitrificans* (57) and bovine heart (58) and N<sub>2</sub>OR (16,70,17).

The structures of cytochrome C oxidase and N<sub>2</sub>OR show a binuclear site where each copper is ligated by a histidine residue and additionally bridged by two cysteine derived S atoms (57,58). Additional weak ligands are a methionine and one main chain carbonyl of a tryptophan (N<sub>2</sub>OR) or glutamate (COX) in an axial position (Fig. 7, (57,58,59,16)). And even though the overall center is quite stable, mutations on the copper ligands lead to

decrease or complete loss in catalytic activity in both cytochrome *c* oxidase and nitrous oxide reductase (71,72,73,74,75).

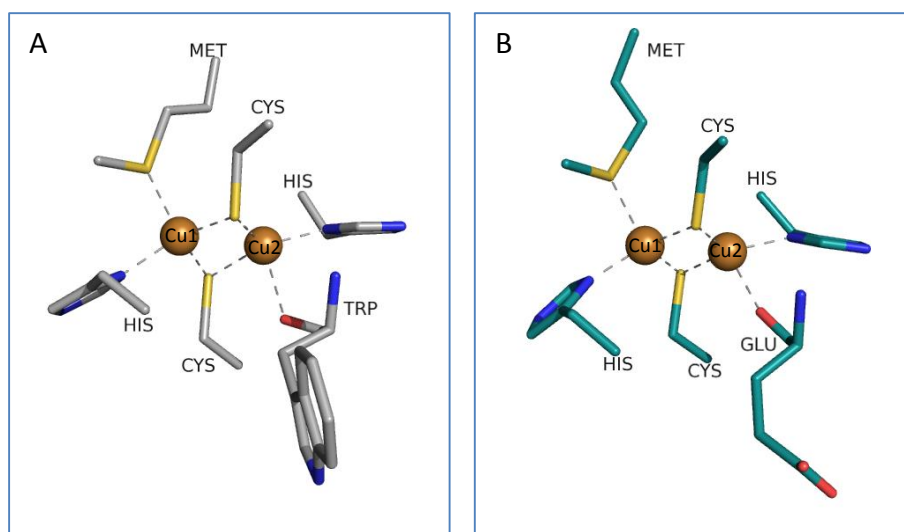


**Fig. 7** Cu<sub>A</sub> site of N<sub>2</sub>OR from **A:** *P. denitrificans* (pdb: 1fwx) and of **B:** bovine COX (pdb: 1occ). Both copper ions are ligated by one histidine and two cysteine residues. Copper 1 is additionally ligated by one methionine and copper 2 by the main chain carbonyl group of a tryptophan (N<sub>2</sub>OR) or glutamate residue (COX).

The unpaired electron is delocalized over the Cu<sub>2</sub>S<sub>2</sub> core and leads to a low reorganization energy that allows fast electron transfer rates in this copper site (27). The covalent character of the Cu-S bond might increase the electron transfer rates additionally (76). This center is considered to transfer one electron from an external electron donor to the active site (77).

## 1.6 Cu<sub>B</sub> center

The Cu<sub>B</sub> site can be found in cytochrome *c* oxidase where it is close to the heme group in the catalytic center (57,58). It contains just one copper ion that is coordinated by three histidine residues (Fig. 8) in a trigonal pyramidal geometry with the open coordination position of the copper oriented towards the open coordination position on the heme iron (57,58).

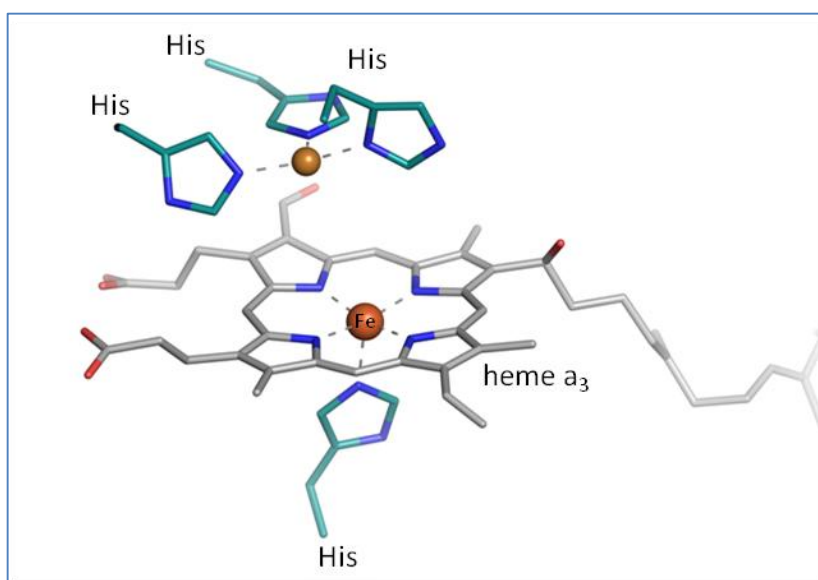


**Fig. 8** Cu<sub>B</sub> site of bovine cytochrome *c* oxidase (pdb: 1occ). The single copper atom (brown) is ligated by three histidine residues. Cu<sub>Z</sub> center

The Cu<sub>Z</sub> center is unique for nitrous oxide reductase where it is the putative catalytically site involved in reduction of N<sub>2</sub>O to N<sub>2</sub>. It has been described as a tetranuclear,  $\mu$ 4-sulfide-bridged center (78,17) and presents therefore the first biological example of a Cu-S cluster (79). The copper ions are arranged as a distorted tetrahedron with seven ligating histidine residues. Cu<sub>Z1</sub>, Cu<sub>Z2</sub> and Cu<sub>Z3</sub> have two histidine ligands each whereas Cu<sub>Z4</sub> has only one (Fig. 9).

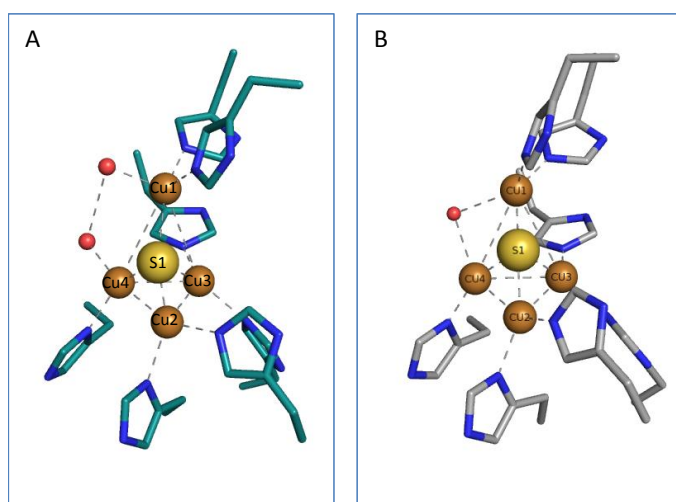


**Fig. 9** Cu<sub>2</sub> site of N<sub>2</sub>OR of **A:** *Achromobacter cycloclastes* (pdb: 2iwf) and of **B:** *Paracoccus denitrificans* (pdb: 1fwx). The four copper are arranged as a distorted tetrahedron with seven ligating histidine residues. Cu<sub>Z1</sub> to Cu<sub>Z3</sub> have two ligands each, whereas Cu<sub>Z4</sub> has just one ligand. The four copper are bridged by an inorganic sulfur. At the edge of Cu<sub>Z1</sub> and Cu<sub>Z4</sub>, one (*P. denitrificans*) or two (*A. cycloclastes*) hydroxyl or water molecules can be found.

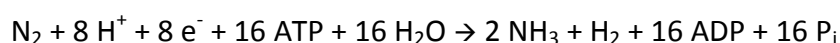
The Cu-Cu distances between the four copper ions are not equal: Cu<sub>Z2</sub>, Cu<sub>Z3</sub> and Cu<sub>Z4</sub> have similar bond length of around 2.3 Å in contrast to Cu<sub>Z1</sub> which is 3.4 Å separated from Cu<sub>Z2</sub> and Cu<sub>Z4</sub>. The so far published structural models of nitrous oxide reductases show one or two additional oxygen moieties bridging Cu<sub>Z1</sub> and Cu<sub>Z4</sub> (Fig. 9) that is thought to be either water molecules or hydroxyl ions (17,18).

## 2 Nitrous oxide reductase

### 2.1 The biological nitrogen cycle

Nitrogen is an essential component of nucleic acids, amino acids and amino sugars. But in contrast to hydrogen, oxygen or carbon, its bioavailability is limited even though it is the most frequent element in the atmosphere with approximately 80 vol. %. The inertness of dinitrogen (bond enthalpy: 944 kJ/ mol (80)) makes a conversion difficult.

Ammonia (NH<sub>3</sub>) is the only form that can be assimilated into biomass. The reduction of dinitrogen to ammonia, termed nitrogen fixation, is catalyzed by the enzyme nitrogenase in a highly energy consuming reaction.



Ammonia can be oxidized to nitrate via hydroxylamine ( $\text{H}_2\text{NOH}$ ) and nitrite ( $\text{NO}_2^-$ ) in the nitrification pathway, catalyzed by the three enzymes ammonia oxygenase, hydroxylamine oxidoreductase and nitrite oxidase (Fig. 10).

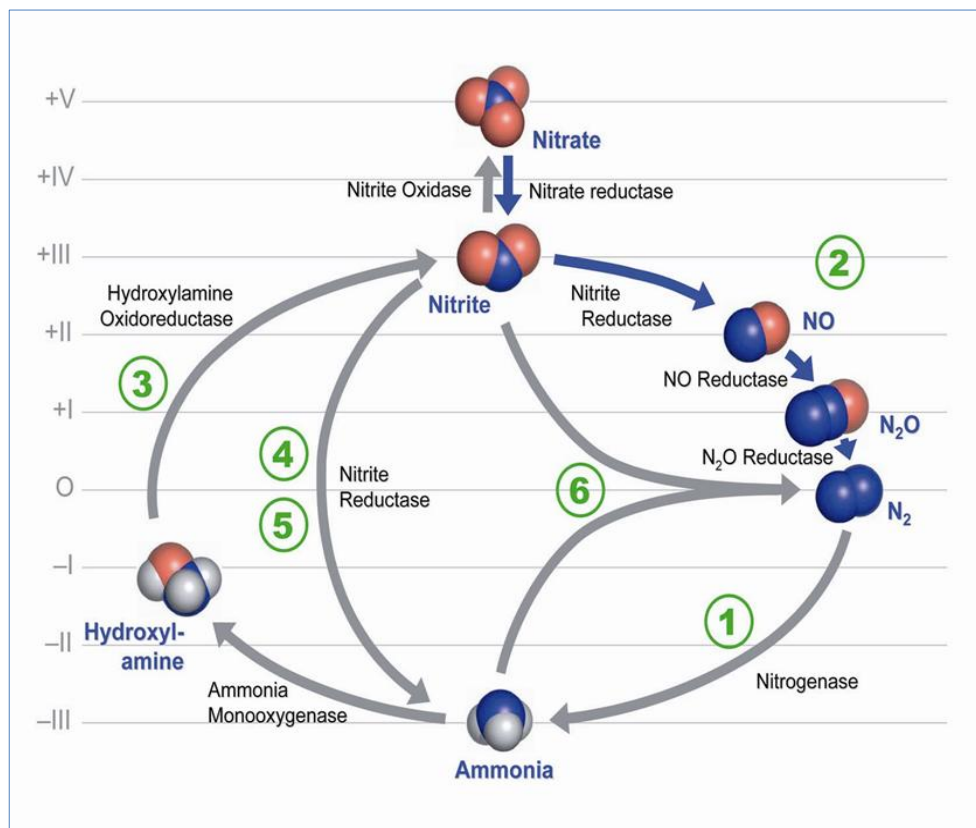


**Fig. 10** Scheme of the biological nitrogen cycle as published by Einsle (81).

Nitrogen compounds are arranged according to their oxidation states as shown by the left margin. The metabolic pathways are: (1) nitrogen fixation, (2) denitrification, (3) nitrification, (4) and (5) assimilatory and dissimilatory nitrate ammonification, respectively and (6) Anammox (anaerobic ammonia oxidation). Every enzyme contributing to one of the reactions is represented by an arrow.

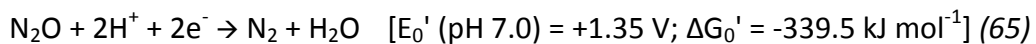
On the other hand, nitrate ( $\text{NO}_3^-$ ) can be used by bacteria, higher plants, algae and fungi as they reduce nitrate directly to ammonia (assimilatory nitrate ammonification) (82,83) or under anaerobic conditions by microorganisms where nitrate serves as the terminal electron acceptor instead of oxygen thereby producing ammonia (dissimilatory nitrate ammonification) (84,85,86). A third pathway to reduce nitrate is denitrification. This metabolic pathway comprises four single steps and requires anoxic conditions (87,81): Nitrate is first reduced to nitrite ( $\text{NO}_2^-$ ) catalyzed by nitrate reductase. Nitrite is then

further reduced to nitric oxide (NO) by the enzyme nitrite reductase, nitrous oxide (N<sub>2</sub>O) catalyzed by nitric oxide reductase and eventually to dinitrogen (81,87,88) by nitrous oxide reductase.

Recently, a second pathway was discovered that results in significant N<sub>2</sub> production: Under anaerobic conditions, ammonia can be oxidized by several microorganisms like *Kuenenia stuttgartiensis* to nitrogen. It is a comproportionation in which ammonia (NH<sub>4</sub><sup>+</sup>) reacts with nitrite (NO<sub>2</sub><sup>-</sup>) to nitrogen (N<sub>2</sub>) and two water molecules. The process is called Anammox as an abbreviation of anaerobic ammonia oxidation (89,90).

### 2.1.1 Nitrous oxide

N<sub>2</sub>O is a colorless gas characterized by kinetical inertness due to a high activation barrier of approx. 250 kJ mol<sup>-1</sup> (91), even though the reduction to N<sub>2</sub> is thermodynamically favorable:

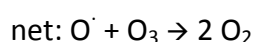
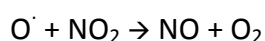
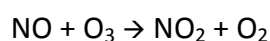


In the last years, the impact of nitrous oxide on the earth's climate has drawn more and more attention. Besides water vapor, CO<sub>2</sub>, CH<sub>4</sub>, tropospheric O<sub>3</sub> (92) and chlorofluorocarbons, N<sub>2</sub>O has become one of the most important greenhouse gases (93,94,95). It is one of the natural regulators of the stratospheric ozone-layer and emitted by biotic (denitrification) and abiotic processes such as hypersaline ponds in the Antarctic (96). But its emission into the atmosphere is exponentially increasing. Alone 70 % of the atmospheric budget of N<sub>2</sub>O has its origin in microbial processes as a by-product in nitrification and as an intermediate during denitrification (97). However, the main sources for the increase in atmospheric N<sub>2</sub>O concentration are of anthropogenic origin, such as burning of fossil fuels, wastewater treatment (98,99,91,87,17) and most of all agriculture (100,95,93). Especially the increasing N input to agricultural soils by fertilization (101) leads to an exponentially rising concentration of N<sub>2</sub>O in the atmosphere. Since 1750 the

atmospheric level has risen by 15 % and is increasing every four years by one percent (94,100).

Nitrous oxide influences the climate in two ways: The global warming potential (GWP) of N<sub>2</sub>O considered over a range of 100 years is 12 times stronger than that of CH<sub>4</sub> and exceeds the one of CO<sub>2</sub> by a factor of almost 300, partially because of its long lifetime of approx. 114 years (93,94).

Besides its effect on global warming, it is additionally highly potent in stratospheric ozone depletion (95,93,100). Upon emission into the troposphere, nitrous oxide is transported into the stratosphere, where it is converted into nitrogen oxides (NO<sub>x</sub>) that catalyze ozone depletion via (102,103):



The ozone-depletion potential of nitrous oxide is similar to the one of hydrochlorofluorocarbons (HCFCs) (93). Even though, in contrast to chlorines that deplete ozone below and above the maximum concentration in stratosphere, NO<sub>x</sub> act in areas where ozone concentration is highest. Parts of the chlorine react with NO<sub>x</sub> into benign forms like ClONO<sub>2</sub> (93). But since the HCFCs are now regulated by the Montreal Protocol (104) their concentration in the stratosphere is decreasing. Ravishankara and co-workers calculations revealed that the ODP of N<sub>2</sub>O might increase by roughly 50 % when the chlorine levels go back to the value of the year 1960 (93).

From all ozone-depleting substances (ODSs), the current anthropogenic ODP-weighted nitrogen oxide emissions are the largest and they are predicted to remain the largest of all ODS for this century being now a bigger threat than HCFCs (93,94,95,100).

### 2.1.2 N<sub>2</sub>O metabolism

Nitrous oxide is produced by many microorganisms and fungi mostly from nitrate and nitrite in various processes, such as denitrification (65) or associated with hydroxylamine



oxidation (105). Among these only one dissimilatory reaction is known, where nitrous oxide is reduced to molecular nitrogen. The two main microbial processes involved in nitrous oxide reduction are denitrification and N<sub>2</sub>O respiration (65). In denitrification, the nitrous oxide occurs as an intermediate that is further reduced to N<sub>2</sub>. However, due to truncated denitrification nitrous oxide can be emitted into the atmosphere (65). This phenomenon has been described for several bacteria such as *Thauera aromatica* (106), *Pseudomonas fluorescens* (107), *Roseobacter denitrificans* (108,109) and is caused by the absence of a gene encoding for nitrous oxide reductase (65) that results in early termination at the level of N<sub>2</sub>O (110,107,111,106,112).

On the other hand, some microorganisms that do not have the full set of enzymes required for denitrification encode a nitrous oxide reductase and are therefore able to grow by N<sub>2</sub>O respiration such as *Wolinella succinogenes* (113,114).

Both processes, denitrification and N<sub>2</sub>O respiration, can be found in Gram-positive and Gram-negative bacteria as well as in archaea even in extreme habitats with temperatures ranging from -1 °C (*Colwellia psychrerythraea*, (115,116)) to 104 °C (*Pyrobaculum aerophilum* (117)), high salinity to 30 % NaCl (*Salinibacter ruber*, (118)) or pressures up to 20 MPa (*Photobacterium profundum*, (119)). In many of these cases, a dimeric copper protein was found to be responsible for the N<sub>2</sub>O reduction (65). However, there are several denitrifying archaea and bacteria like *Nitrosomonas europaea* (120), *Halobacterium sp. NRC-1* (121), *Haloferax volcanii* (122,123) or *Pyrobaculum aerophilum* (117,124,125) known that do not contain this enzyme. Therefore, the existence of another type of nitrous oxide reductase is assumed. Just recently, a multicopper oxidase of the archeon *Pyrobaculum aerophilum* was found to be active in N<sub>2</sub>O reduction (125) and is now under close investigation.

### 2.1.3 Nitrous oxide reductase

Nitrous oxide reductase is a copper containing protein that was first identified and isolated from the periplasm of the Gram-negative  $\gamma$ -proteobacterium *Pseudomonas*

*stutzeri* ZoBell (previously *Pseudomonas perfectomarina*) (119) by Zumft and coworkers showing catalytic activity towards the reduction of N<sub>2</sub>O (126,127,128).

The necessity of copper for this protein was studied even before the actual enzyme could be identified (129,130,126). This observations and the knowledge, that N<sub>2</sub>O can react with transition metals helped to direct the search for a N<sub>2</sub>O reductase towards Cu-containing enzymes and eventually identify and isolate the protein (65). The purified enzyme of *P. stutzeri* is composed of two identical subunits of 638 residues (74 kDa) with a copper content determined to approx. 8 coppers per dimer (130 kDa) (63,64). Several spectroscopically distinguishable forms were described depending on the purification strategy: under oxic conditions, a pink form was isolated whereas anoxic purifications yielded a purple form (63,64). X-band EPR spectra showed an unusual 7-line hyperfine splitting in the g<sub>II</sub> region for both forms, although the spectra of pink N<sub>2</sub>OR was less defined (63,64). Activity assays based on the oxidation of photochemically reduced benzyl-viologen showed that the enzyme has an optimum activity at pH 8-9.5 depending on the organism (63,131,132) and that the purple form is up to 5 times more active than the pink protein indicating sensitivity to dioxygen (63). Nevertheless, this activity could not be reestablished with Cu(en)<sub>2</sub>SO<sub>4</sub> if the copper had been removed with KCN (63).

Redox titrations gave a redox potential of 260 mV vs. NHE (63), a value comparable to that of azurin (19) and cytochrome *c* oxidase (63).

To date, nitrous oxide reductase has been found in various bacteria and archaea such as *Pseudomonas aeruginosa*, *Thiobacillus denitrificans*, *Wolinella succinogenes* *Bacillus azotoformans*, and *Rhodobacter capsulatus*. Characterizations of those N<sub>2</sub>OR orthologs showed common properties: The enzyme is usually a 2x65 kDa homodimer with a high sensitivity towards oxygen, and in all cases copper is essential for the catalytic activity (133,134,135,136).

The N<sub>2</sub>OR of Gram-negative bacteria are localized in the periplasm, while in Gram-positive bacteria a membrane-bound or membrane associated N<sub>2</sub>OR is suggested (65,137).

### 2.1.3.1 Spectroscopic properties

There are 5 forms of the *P. stutzeri* enzyme described (Tab. 1), characterized by their spectroscopic (Fig. 11) and catalytic features yielded under different source and purification procedures (65,138,63,64).

**Tab. 1** Forms of nitrous oxide reductase characterized by spectroscopic and kinetic properties (Adapted from (65)).

N <sub>2</sub> OR forms	Enzyme state	Cu/ M <sub>r</sub> <sup>2</sup>	Properties
<b>I (purple)</b>	Anoxic; low Cu <sub>Z</sub> * content	Approx. 8	High catalytic activity; 20-50 % EPR-active Cu; g <sub>II</sub> =2.18, A <sub>II</sub> =3.83 mT (7 equidistant lines), =2.03, =2.8 mT
<b>II (pink)</b>	Oxic; high Cu <sub>Z</sub> * content	Approx. 7	Low catalytic activity; 20-50 % EPR-active Cu; g <sub>II</sub> =2.18, A <sub>II</sub> =3.55 mT, =2.03, not well defined at 9.32 GHz
<b>III (blue)</b>	reduced	Approx. 8	catalytically inactive; 10-30 % EPR-active Cu, broad unstructured EPR signal at 9.32 and 34 GHz, Cu determined as type 1 by resonance Raman
<b>IV</b>	Reconstituted with Cu(en) <sub>2</sub> SO <sub>4</sub>	Approx. 4	catalytically inactive; EPR characteristics similar to N <sub>2</sub> OR V
<b>V</b>	MK402 mutant (defective in chromophore biosynthesis)	Approx. 4	catalytically inactive, 50 % EPR inactive Cu, g <sub>II</sub> =2.18, A <sub>II</sub> =3.55 mT (4-5 equidistant lines), =2.03, not well defined at 9.32 GHz

The availability of a pink Cu<sub>A</sub>-only variant form ( $\Delta nosD$ , form V, Fig. 11) that was purified from a transposon Tn5-induced mutant with a defect in chromophore biosynthesis allowed the differentiation of spectroscopic features belonging either to Cu<sub>A</sub> or Cu<sub>Z</sub> (65,64).

The highly active, purple form (form I, Fig. 11) can only be obtained under dioxygen-free conditions. Here, Cu<sub>A</sub> in its oxidized state is a mixed-valent [Cu<sup>1.5+</sup>:Cu<sup>1.5+</sup>] site that exhibits two peaks at 485 and 525 nm and a broad band at 790 nm while Cu<sub>Z</sub> is characterized by two bands at 552 nm and 660 nm. Aerobic purifications lead to the pink form of N<sub>2</sub>OR (form II, Fig. 11) which is characterized by low activity and an additional band at around 650 nm (65,64).

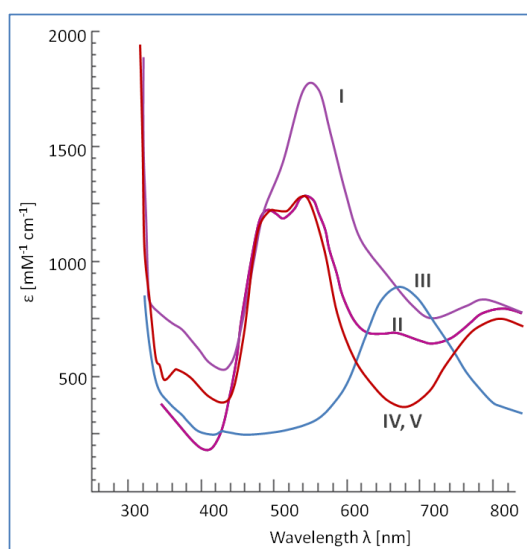


**Fig. 11** UV/ vis spectra of  $N_2OR$ . Five forms have been described that are obtained under different source and purification procedures. Form I (purple), form II (pink), form III (blue), form IV and V (red).

$N_2OR$  is characterized by a peak at around 650 nm; the exact position depended on the mode of reduction (141). It is inactive but had been shown to regain activity if further reduced to a  $[4Cu^+]$  state (142,143,144). However, this observation could not be verified for the enzyme of *P. stutzeri* (64).

### 2.1.3.2 Structure

Sequence comparisons of  $N_2OR$  revealed that the C-terminal cupredoxin-like domain is homologous to cytochrome *c* oxidase subunit II; it even shares a highly conserved sequence motif,  $(H(X)_{34}C(X)_3C(X)_3H(X)_2M)$  (145) that contains the mixed-valent  $Cu_A$  site (146).

Additional evidence for a  $Cu_A$  center came from the highly similar MCD (magnetic circular dichroism) spectra of the oxidized  $N_2OR$  and COX and from the typical 7 hyperfine line pattern of the EPR spectra (87,146,147). The N-terminal domain on the other hand did not have any homology to known proteins at that time, but quantitative elemental analysis that yielded 8 copper per dimer and spectroscopic data suggested another

This corresponded with the appearance of a second paramagnetic species and was assigned to the catalytically inactive form  $Cu_z^*$  (68,65,69,139,79). The  $Cu_z/Cu_z^*$  ratio depended on the purification technique. In *P. stutzeri*  $N_2OR$  its ratio is low if the enzyme is purified under anoxic conditions (69,139,140), but in the presence of dioxygen, more of the  $Cu_z^*$  species is generated.

Both forms, I and II, can be reduced to a blue form (III) with reducing agents like dithionite (63,64). If dioxygen is absent, the reduction of form I is reversible. Form III of

copper center (69). This could be confirmed by mutant studies and spectroscopy (64,71) even though the exact nature of this site stayed elusive until the first X-ray crystal structure of a nitrous oxide reductase, isolated from *Marinobacter hydrocarbonoclasticus* (formerly *Pseudomonas nautica*), became available (70). The crystal structure revealed a dimeric assembly with the monomers lying head-to-tail to each other. Each monomer comprised two distinct domains, a C-terminal cupredoxin domain with the mixed-valent  $\text{Cu}_A$  site (60) and an N-terminal, 7-bladed  $\beta$ -propeller carrying the four copper center  $\text{Cu}_Z$  (Fig. 12). According to its unique  $\text{Cu}_Z$  site, this type of nitrous oxide reductase is referred to as Z-type  $\text{N}_2\text{OR}$  [EC 1.7.99.6] (65).

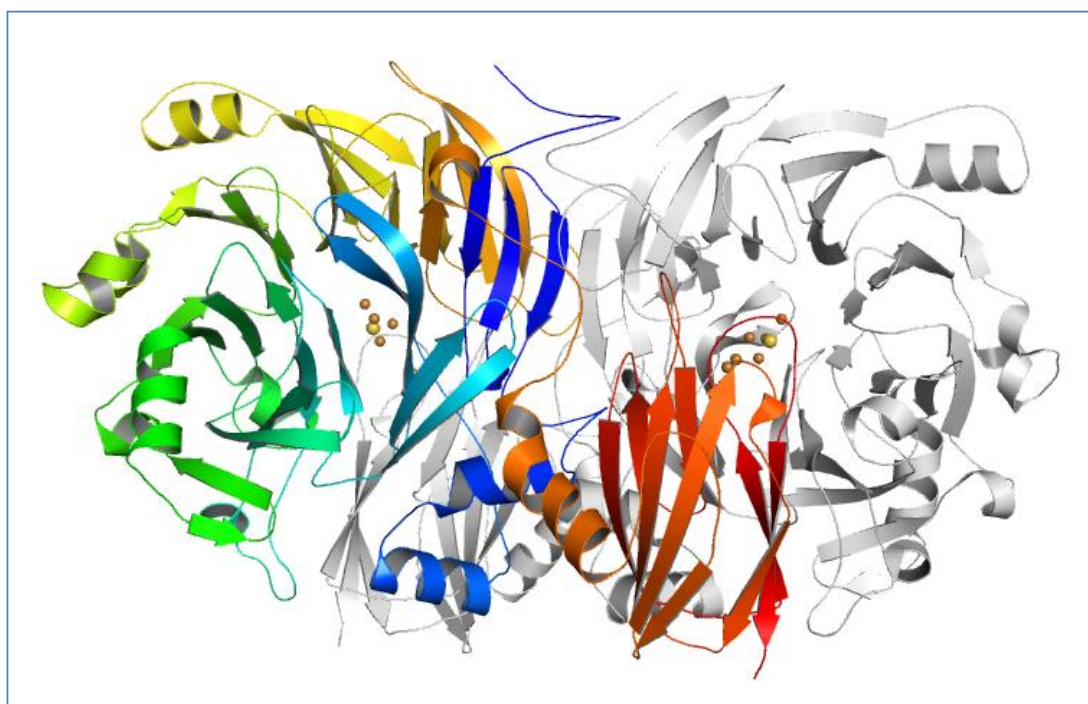


**Fig. 12** Nitrous oxide reductase of *Marinobacter hydrocarbonoclasticus*. The first monomer is colored in grey, the second in rainbow colors with blue at the N-terminus and red at the C-terminus. Copper atoms are in brown, sulfur in yellow. The N-terminal 7-bladed  $\beta$ -propeller (blue to yellow) carries the tetranuclear  $\text{Cu}_Z$  site, while the C-terminal cupredoxin-like domain (orange-red) contains the binuclear  $\text{Cu}_A$  site.

This second tetranuclear copper center was surprising because a binuclear site was assumed due to the results of the copper content analysis (69,146,63). In the structure of the *M. hydrocarbonoclasticus*  $\text{N}_2\text{OR}$ , the  $\text{Cu}_Z$  cluster was modeled with an oxygen bridging

the four copper, but EPR and resonance Raman (RR) spectra demonstrated an acid-labile sulfide (79,139,70). The higher resolution X-ray structure of *Paracoccus denitrificans* N<sub>2</sub>OR that became available shortly afterwards showed indeed an inorganic sulfur bridging the copper ions (71,17,79). This Cu<sub>2</sub> site represents therefore the first Cu-S cluster known for biological systems (79).

The X-ray structure also explained why dimerization is obligatory for N<sub>2</sub>OR to be catalytically active: the Cu<sub>A</sub> and the Cu<sub>Z</sub> site within one monomer are almost 40 Å apart but both centers lie in close proximity when the dimer is formed, separating the Cu<sub>A</sub> of one monomer to the Cu<sub>Z</sub> of the second monomer by just around 10 Å which is in range for effective electron transfer (70,65,17,148).

The putative electron donor is thought to be a *c*-type cytochrome (65,143,149,150) or a cupredoxin like azurin or pseudoazurin (151). The formation of a N<sub>2</sub>OR complex with cytochrome *c* is obligatory for *Paracoccus pantotrophus* enzyme activity (77).

Several bacteria are known to have a modified nitrous oxide reductase like *Campylobacter fetus*, *Wolinella succinogenes* and *Thiomicrospira denitrificans* (134,136,152,114), where the enzyme has a C-terminal extension carrying a heme *c* binding side. This is most likely due to the fusion of the N<sub>2</sub>OR gene and the gene encoding for the electron donor.

### 2.1.3.3 Expression, Regulation and Maturation of N<sub>2</sub>OR

The processing and maturation of the N<sub>2</sub>OR apoprotein involves several genes. So far, 10 *nos* genes have been identified that are expressed growth on N<sub>2</sub>O. Among these, the core *nosRZDFYL* cluster can be found in many bacteria (65). To determine the minimal set of genes required for the maturation of NosZ, Zumft and co-workers transferred the *nosRZDFY* cluster into the non-denitrifying bacterium *Pseudomonas putida* where they obtain an N<sub>2</sub>OR that exhibited *in vitro* activity (153).

The following chapter will give a rough overview over the *nos* gene cluster. However, the exact genetic composition depends highly on the microorganism.

There are three transcriptional units suggested for the *nosRZDFY* cluster comprised of *nosR*, *nosZ* and *nosDFY* (65). The gene products of *nosDFY* might be involved in providing an appropriate sulfur source and maturation of the Cu<sub>z</sub> site (65). A mutant with deleted *nosDFY* produced an inactive enzyme that showed the characteristics of the Cu<sub>A</sub> only form with just ~4 Cu atoms per dimer (154). It is a putative ABC-type transporter (155) consisting of the periplasmic protein NosD, a cytoplasmic ATPase NosF and NosY, a six-helix integral membrane protein (65). NosR is a membrane-bound iron-sulfur flavoprotein regulating *nosZ* and *nosDFY* gene expression (155,156). Upon inactivation of *nosR* either no N<sub>2</sub>OR is formed (156,154) or the transcriptional rate is decreased (157). Besides its role as transcription regulator, another putative role for this protein is maturation of the N<sub>2</sub>OR possibly in the step of insertion of copper into the protein (154,158). Although site-directed mutations in the metal binding sites resulted in expression of N<sub>2</sub>OR, the obtained enzyme form showed the features of the Cu<sub>z</sub>\* state (154).

Even though NosZ is mostly transported to the periplasm by the Tat-system (159,160), the Cu cofactors are not obtained in the cytoplasm but in its designated location (158,153). However, there are some exceptions such as *Wolinella succinogenes*, where NosZ is transported by the Sec system (114). The copper assembly involves the proteins NosL and NosD, whose exact function is unknown. NosL is considered to be a lipoprotein that could be anchored to the membrane (65,161). A possible function would be as a chaperone supported by the fact, that NosL shows a significantly higher affinity towards Cu<sup>+</sup> than for Cu<sup>+2</sup> (162).

In *Paracoccus denitrificans* and several other bacteria an additional *nosX* gene has been found (163,164). Its gene product, a flavoprotein, is transported into the periplasm by the Tat-system as is NosZ (65). Absence of NosX leads to N<sub>2</sub>OR in the Cu<sub>z</sub>\* state as observed after oxic preparation or defective NosR (154) and like the latter, NosX seems to be required for the maintenance of activity of N<sub>2</sub>OR (154,65).

Nitrous oxide as the substrate of N<sub>2</sub>OR is a weak inducer of *nosZ* gene expression, however, the presence of NO leads to a strong upregulation of the *nos* genes and an increase of the cellular N<sub>2</sub>OR content (65). This provides an explanation for the frequent

observation that some bacteria like *Pseudomonas aeruginosa* are not able to grow on N<sub>2</sub>O even though the full set of genes is available (157).

On the other hand, the cells express N<sub>2</sub>OR only at low levels if dioxygen is present (165,166,167).

#### 2.1.3.4 Catalysis and theoretical calculations on the reaction mechanism

The availability of high-resolution crystal structures of N<sub>2</sub>OR provided more insight into the geometry of the copper clusters. The Cu<sub>A</sub> site had already been characterized as an electron transfer site according to its homolog in cytochrome *c* oxidase subunit II. Cu<sub>Z</sub> is assumed to be the catalytical center of this enzyme. In all three crystal structures that have been described so far, one or two water or hydroxyl ligands have been modeled to the edge of Cu<sub>Z1</sub> and Cu<sub>Z4</sub> that is suggested as putative substrate binding site, however the exact nature of this ligand needs to be confirmed.

Spectroscopic analysis of the aerobically purified enzyme had shown that N<sub>2</sub>OR is in an oxidized form with a [1Cu<sup>2+</sup>/3Cu<sup>+</sup>S] redox state (168,169,170). In contrast to the anaerobically purified enzyme of *P. stutzeri* that is already catalytically active in its oxidized form, the N<sub>2</sub>OR of *A. cycloclastes* and *M. hydrocarbonoclasticus* need to be completely reduced to an [4Cu<sup>+</sup>S] state to show catalytic activity (142,143,138,171). The reductive activation of the enzyme is achieved by long-time incubation with dithionite and an excess of methylviologen (143,171) and the [4Cu<sup>+</sup>S] state is regarded as the catalytically active form (142,171) whereas the [1Cu<sup>2+</sup>/3Cu<sup>+</sup>S] state represents the resting form (78,140,170).

Theoretical studies of binding mode and catalysis on the basis of the structures of *A. cycloclastes* and *P. denitrificans* gave more insight into the mechanism of N<sub>2</sub>O reduction at the Cu<sub>Z</sub> site.

To study the reaction, density functional theory (DFT) calculations were carried out based on the structures of the aerobically prepared enzyme (172). The formation of an N<sub>2</sub>O-Cu<sub>Z</sub> complex in the fully reduced state is achieved by enhanced Cu<sub>Z</sub> → N<sub>2</sub>O back donation and the competitive binding mode is better than in the [3Cu<sup>+</sup>/1Cu<sup>2+</sup>S] state (173). N<sub>2</sub>O binds



directly to the  $\text{Cu}_{\text{Z1}}\text{-Cu}_{\text{Z4}}$  edge in a bent  $\mu\text{-1,3-O,N}$ -mode that resembles the transition state. It is stabilized by a strong  $\text{Cu}_{\text{Z4}}^{2+}\text{-O}^-$  bond and non-covalent interactions of the surrounding protein environment (172). The other two copper and the sulfur in the cluster obtain a role in extensive back-bonding. The activation energy that is needed depends on the strength of a proton donor, which might be a close-by lysine residue. Bond cleavage of the bent  $\text{N}_2\text{O}$  is induced by electron transfer from the  $\text{Cu}_2$  cluster into the  $\pi^*$  LUMO of  $\text{N}_2\text{O}$  and is probably facilitated by protonation. Earlier experiments had already shown that  $\text{N}_2\text{OR}$  has a pH optimum around pH 8-9.5 (63,131,132) and further DFT calculations on the effect of pH on enzyme activity confirmed its relevance for catalysis (138).

The complete reaction cycle comprises therefore alternating one electron reduction and protonation steps which at the end turn  $\text{Cu}_2$  back into its fully reduced state.

## 2.2 Scope of the study

Aim of this work was to achieve the crystal structure of the physiologically active nitrous oxide reductase. The so far available  $\text{N}_2\text{OR}$  structures represent form II or form III obtained under oxic conditions. They need to be reduced to an  $[\text{4Cu}^+]$  state to show catalytic activity as described previously. However, this is not a prerequisite for the anaerobically isolated purple nitrous oxide reductase from *Pseudomonas stutzeri*. The question is therefore, if this observation is a result of structural changes upon contact to air.

Because there is no structure of a metal- $\text{N}_2\text{O}$  complex available, all suggested reaction mechanisms are based on the aerobically purified enzymes. Thus, the second objective for this work was to obtain the structure of the enzyme in complex with its substrate  $\text{N}_2\text{O}$  to provide insight in its binding mechanism.

### 3 Laccases

Laccase (p-diphenol:oxygen oxidoreductase (EC 1.10.3.2)) are multi-copper enzymes that catalyze the oxidation of a wide variety of organic (especially aromatic) and inorganic compounds with concomitantly reduction of dioxygen to water. They are expressed by quite diverse organisms ranging from certain bacteria and fungi (174), as well as insects and crustacea (175) or plants (176).

The first laccase was discovered in the Japanese lacquer tree *Rhus vernicifera* (177,178) and to date this enzyme has been identified in a variety of plants such as *Acer pseudoplatanus* (179), *Pinus taeda* (180), *Lolium perenne* (181) or *Zea mays* (182). It is involved in lignin synthesis by catalyzing the free radical polymerization of lignin structural units (183,184,185,186,26,176). Among bacteria, laccases have been found in *Bacillus licheniformis* (187), *Escherichia coli* (188) and *Pseudomonadaceae* (189,190) where they are thought to be involved in functions such as Cu<sup>2+</sup>-resistance, pigmentation processes or sporulation (189,191). In crustacea and insects (192,193,194), laccases take part in processes like melanization and immune response (195,196,197,198,175). However, the main producers of laccases are ligninolytic fungi belonging to the phyla basidiomycota and ascomycota (199). These enzymes are involved in diverse physiological functions such as lignin degradation, pathogenesis, detoxification, development and morphogenesis (200,185,201,202,203).

Laccases are glycoproteins with a molecular weight between 50-130 kDa (26). Most of these enzymes are extracellular but they can be found as well in cell walls, if they take part in, for example, production of melanin (26). The majority of fungi produces intra- as well as extracellular laccases, with the main part (~95 %) being excreted from the cells (204). A common feature for fungi is the multiplicity of laccase genes that encode for different isozymes (205). They differ considerably in substrate specificity, redox potential (420 to 790 mV vs. NHE), and pH and temperature optimum. Their expression is probably controlled depending on the processes they are involved in or on the growth stage of the fungi (206,207,208,23,209). A few fungi, such as *Pleurotus ostreatus*, can express different

isoforms of laccases, which are encoded by the same gene. The expression is controlled as well by different environmental conditions like presence or absence of metals.

In most cases, laccases are monomeric with three consecutively connected cupredoxin-like domains that form a tight globule (26). Nevertheless, examples such as *Trametes villosa* (210) or *Podospora anserine* (211) have been described that express a dimeric protein or a tetramer, respectively.

The active site of laccases contains two copper sites: A mononuclear type-1 site (T1) and one trinuclear type-4 copper site (composed of a type-2 (T2) and type-3 site (T3)). The distance between T1 and the trinuclear center is around 12 Å (212,213,214), whereas the distance between T2 and T3 is ~4 Å. The oxidation of the substrate comprises four single one-electron oxidations and takes place at the T1 center (30,44,215). The electrons are then transferred via a histidine-cysteine pathway from the T1 site to the T2/T3 center where oxygen is reduced to water (30,216,217,218). Sequence comparisons revealed four highly conserved regions (L1-L4) where, among other amino acids, all copper ligands can be found (219). Furthermore, four loops (loop 1-4) could be identified - located between L2 and L3 - that are involved in substrate binding even though these regions are less conserved (220,219).

However, not all laccases are exclusively copper-containing proteins. *Pleurotus ostreatus*, for example, expresses two isoforms of a laccase. One of them contains 4 copper atoms, whereas the second form has one copper, one iron and two zinc atoms (221,206).

### 3.1 Catalysis

Typical substrates of laccases are phenols that are due to their high redox potentials (ranging from 500 to 1000 mV vs. NHE) able to transfer electrons onto the type-1 copper of the enzyme (222).

Recent studies could show, that the redox potential of the T1 copper site is not dependent on a single amino acid residue but rather a combination of different factors like T1 copper coordination geometry, solvent accessibility, hydrogen bonding and dielectric anisotropy of this copper site (222,223,224,225).

Four electrons that are derived from single substrate oxidation reactions at the type-1 copper site are used to reduce molecular oxygen to two water molecules. The electrons are transferred via a conserved His-Cys-His tripeptide to the trinuclear copper site (226). In its resting state  $[4\text{Cu}^{2+}]$ , all copper atoms have open coordination positions that result from nearby charged carboxylate residues within 8 Å of the cluster thereby destabilizing  $\text{H}_2\text{O}/\text{OH}^-/\text{O}^{2-}$  binding to the trinuclear site, which tunes its redox potentials (227,225).

The mechanism of dioxygen reduction at the trinuclear site is still under discussion. It has been extensively studied by Solomon *et al.* who proposed a mechanism based on spectroscopic and kinetic studies mainly on *R. vernicifera* (228,229,212): The fully reduced enzyme will reduce dioxygen generating two intermediates, the peroxy intermediate (PI) and the native intermediate (NI). The first step involves two electron reduction of  $\text{O}_2$  leaving two of the copper atoms in the trinuclear site oxidized. This is the rate limiting step. The native intermediate is generated upon two-electron reductive cleavage of the O-O bond. The NI has a fully oxidized trinuclear site with dioxygen completely reduced but still bound to copper site. It is different from the resting form because it has an internal  $\mu_3$ -oxo-bridge that needs to be reorganized to the external position on the T2 copper to close the catalytic cycle (230,229,231,232).

### 3.2 Biotechnological applications

Their wide range in oxidizing various substrates makes laccases valuable for biotechnological applications.

It has been shown that several laccases are able to reduce phenols, methoxy-substituted phenols, aminophenols, diamines,  $[\text{Mo}(\text{CN})_8]^{4-}$ ,  $[\text{Fe}(\text{CN})_6]^{4-}$ ,  $[\text{Os}(\text{CN})_6]^{4-}$  and  $[\text{W}(\text{CN})_8]^{4-}$  (30,233,234,235,225), which offers other possible applications like bioremediation of soils and waters or detoxification of industrial sewage. They can be used to decontaminate environments that had been polluted with harmful xenobiotic compounds such as organochlorines, pesticides or polycyclic aromatic hydrocarbons (236,237). The direct use of enzymes allows utilization even in environments that are no longer suitable for organisms due to extreme conditions or toxicity (238).

Nowadays, they are already used commercially in dye decolorization and bleaching (239,240,241), for example, in textile and paper industry (242,243,244,245,225) or for production of building material such as medium-density fiberboards (MDF) by enzymatic modification of fibers (246,247,248,249).

### 3.3 Laccase Lcc5 from *Coprinopsis cinerea*

*Coprinopsis cinerea* (inky cap mushroom) belongs to the basidiomycetes. It has the largest fungal laccase family known so far (220). The laccase genes probably diverged from each other by frequent synonymous and non-synonymous codon change which resulted in 17 non-allelic genes encoding for laccases (220). The distribution of introns and analysis of the amino acid sequences allows dividing them into two groups: the first one consists of

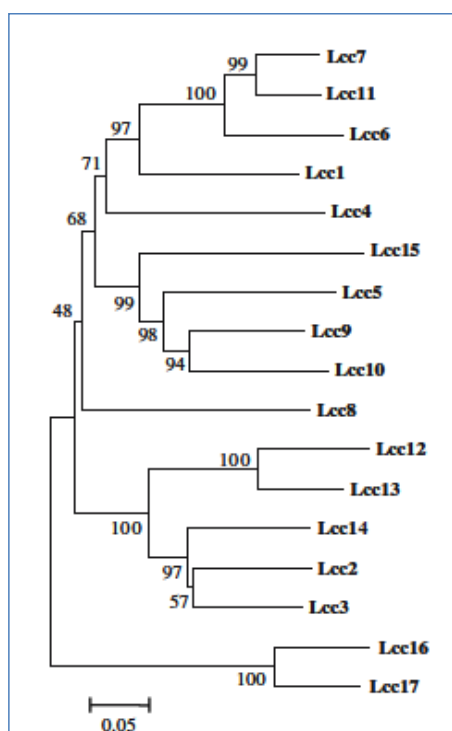


**Fig. 13** Neighbor joining tree of the deduced amino acid sequences of the *C. cinerea* laccases. (Reprinted from (220) with kind permission from Springer).

*lcc1-lcc15* that can be divided into smaller subgroups, and group 2 consists of *lcc16* and *lcc17* (220). Comparisons of the amino acid sequence show Lcc1 to be mostly related to Lcc6, Lcc7 and Lcc11, whereas Lcc5 is related to Lcc9, Lcc10 and Lcc15. A separate subgroup is formed by Lcc2, Lcc3 and Lcc12-14 (Fig. 13).

It is not known so far whether the similarities between different enzymes reflect similar physiological roles (225). However, recent studies showed that at least Lcc1 and Lcc5, Lcc6 and Lcc7 cannot completely substitute each other (225). These studies suggested as well that, based on secretion profiles of *C. cinerea* laccases in liquid medium, Lcc1 and Lcc5 are universal, whereas other laccases are only expressed under specific environmental conditions (225).

Furthermore, Lcc1 seemed to be the most effective enzyme on various substrates, even though Lcc5 was more stable towards organic solvents, such as acetonitrile and ethanol (199,225). This suggests a different adaptation of these proteins to different environmental conditions and substrates (225).

### 3.4 Scope of the study

Objective for this project was the determination of the crystal structure of laccase Lcc5 from *Coprinopsis cinerea*.

## IV Material and Methods

### 1 Protein crystallography

#### 1.1 Theoretical background

Proteins are too small to be studied with conventional microscopes because they work with visible light ranging from around 350 nm to 700 nm. The resolution depends on the numerical aperture  $N_A$  of the used lens, which is determined by  $N_A = n \cdot \sin\theta$  with  $n$  for the refraction index of the surrounding medium and  $\theta$  for half the angle of the marginal ray. The minimal distance that can therefore be resolved is approximately proportional to  $\lambda / N_A$ .

But to examine proteins on an atomic level (~0.1 nm), an appropriate spectral range is needed, which can be provided by X-rays. Nevertheless, X-ray diffraction by a single protein is too weak to be detected. But in crystals the molecules are ordered in a highly regular crystal lattice, so diffraction of an incident beam will thereby be enhanced and detectable. Because there are no lenses available that can focus X-rays, computers have to be used to evaluate the data.

##### 1.1.1 Crystallization

Crystal formation is an energetically favored process because the loss of the hydration shell of the protein causes a decrease of free energy in the system.

One widely used technique to obtain protein crystals is the vapor diffusion method in which a protein solution is brought into a state of supersaturation. This can be achieved in the presence of commonly used precipitants such as ionic compounds, organic solvents like ethanol and isopropanol or polymers like polyethylene glycol that reduce the solubility of the protein and favor growth of crystals.

The different stages of crystallization in dependence of protein and precipitate concentration are shown in the phase diagram (Fig. 14).

In general, crystals will grow if the surrounding solution is supersaturated. The protein solution is mixed with the reservoir solution and equilibrated against the reservoir. The precipitant concentration in the drop is much lower than in the reservoir leading to evaporation of water from the protein solution. This leads to a slow dry-out of the protein drop and thereby to an increase of the protein concentration. So the condition moves towards the state of nucleation where initial clusters of protein can form. By formation of these clusters, the protein concentration in the drop

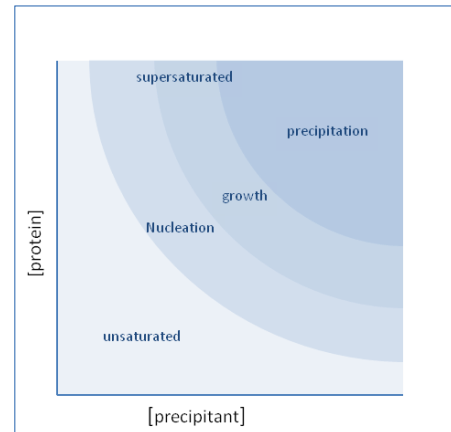


**Fig. 14** Phase diagram for crystallization. If protein and/ or precipitant concentration are too low, neither nucleation nor crystal growth will occur. The protein will precipitate, if protein and/ or precipitant concentration are too high.

decreases leading to a condition that lies in the growth region for crystals. Therefore, by carefully changing the precipitant concentration, the pH of the buffer and the protein concentration, one might be able to produce single crystals.

Nevertheless, the most challenging step is to find the right condition where a protein in solution will crystallize.

In crystals the protein molecules are ordered in a regular lattice that may contain additional elements of internal symmetry. The smallest repeating block that builds up the whole lattice by translation is called the unit cell. So the complete crystal structure can be built by stacking these unit cells in three dimensions with all of them in the same orientation. The smallest unit that does not contain any further elements of crystal symmetry is called the asymmetric unit. From it, the entire unit cell can be constructed by applying crystallographic symmetry operators. The complete description of symmetry operations and the geometry of the unit cell define its space group. Due to the chirality of proteins, only translations, rotations and screw axes are allowed as symmetry operations; there will not be any mirror symmetry in biological molecules. This reduces the possible number of space groups available for protein crystals from 230 to 65.



It is important to identify the exact space group of the crystal to be able to interpret the data obtained from diffraction experiments.

### 1.1.2 X-ray diffraction by crystals

X-rays can be scattered by protein molecules due to interaction of the X-ray photons with electrons. If the photon is absorbed it will set the electron oscillating with the same frequency as the X-ray. Upon return of the electron in its ground state, an X-ray photon of the same wavelength will be emitted in a random direction. This process is called coherent scattering.

On the opposite, incoherent scattering happens if the electron interacts with the atom causing transitions that result in emission of photons of lower energy. This energy release can leave the atom in an excited state and as a consequence, radiation damage can appear. So in order to determine protein structures by X-ray crystallography, coherent scattering is required.

#### 1.1.2.1 Braggs' law

X-rays will be diffracted by the crystal lattice, thereby creating a new virtual lattice of diffraction maxima. This lattice is called reciprocal lattice because its geometric properties are inverse to those of the real crystal.

Braggs' law helps to understand the position of given reflections: A virtual set of lattice planes (hkl) can be seen as virtual mirrors where an incident beam is only reflected if the path difference  $2d_{hkl} \cdot \sin\theta$  between the resulting waves is an integer multiple of the wavelength  $\lambda$  of the incident X-rays (constructive interference, (Fig. 15)).

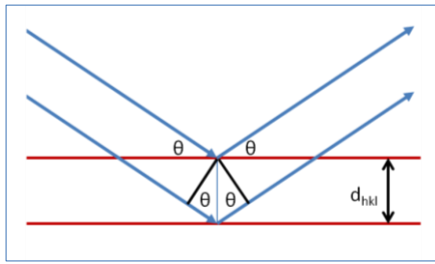


**Fig. 15** Bragg's law. Two waves, which are reflected by adjacent lattice planes with a distance  $d_{hkl}$  have a difference in path length equal to  $2d \cdot \sin\theta$ .

If the path difference is a multiple integer of the used wavelength  $\lambda$ , constructive interference will occur.

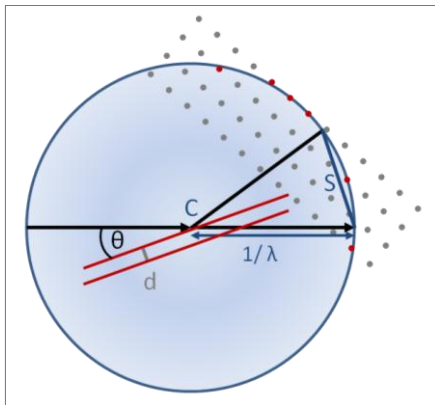


**Fig. 16** Ewald sphere. The crystal (C) is placed in the center with a radius of  $1/\lambda$ . If the crystal rotates, the reciprocal lattice (grey dots) will rotate as well. Diffraction conditions will be fulfilled for those spots, which intersect with the Ewald sphere (red dots).

real-space planes (hkl).

The primary information that can be gained from diffraction experiments on a protein crystal are the space group, the dimensions of the unit cell and based on that the intensity  $I(hkl)$  of every single reflection hkl.

Otherwise, the waves will cancel each other out resulting in destructive interference.

The intensity and the phase depend on the distribution of scattering matter, in this case electrons, in the unit cell. On a given set of planes (hkl) the electron density will produce the reflection hkl on the reflection pattern. The intensity of this reflection corresponds to the electron density in this set of planes, so a high electron density will give a high intensity for the reflection.

A tool to show how the reciprocal-lattice points have to be arranged to fulfill Bragg's law is the creation of a sphere with a radius of  $1/\lambda$  with the crystal as the center, known as Ewald sphere (Fig. 16).

Every reciprocal lattice point that intersects with this sphere gives a detectable reflection. So if the crystal rotates in the X-ray beam, various reciprocal-lattice points will intersect with the sphere and produce a detectable reflection hkl that is caused by reflection from the set of parallel

### 1.1.3 The electron density function $\rho(x)$

Each scattered X-ray photon is described by a complex wave function, with every diffracting atom in the unit cell, represented by its *atomic scattering factor*, contributing to it. A way to describe this summation for every single reflection  $hkl$  is the structure factor  $F_{hkl}$ .

The structure factor is a Fourier sum itself, representing the amplitude ( $|F(hkl)|$ ) and the phase ( ) of a reflection by one lattice plane.

It is therefore possible to calculate the electron density  $\rho$  for every point  $(x,y,z)$  in real space from the inverse Fourier transform of structure factors.

—

An additional factor that has to be taken care of is the thermal vibrations of the atoms and crystal disorder. Therefore, an exponential function is added to the equation. This factor is referred to as B-factor or Debye-Waller-factor and will smear the atomic electron density.

—

So, if both pieces of information, the amplitude and the phase of the scattered wave are known, the electron distribution in the unit cell can be calculated by an inverse Fourier transform. The main problem here is that only the intensity of each diffracted wave can

be detected, but information about the phase is lost. The amplitude can be obtained experimentally from the intensity of the diffracted X-ray beam because it is proportional to the square of the measured intensity.

In contrast, the phase cannot be determined directly. This is referred to as the phase problem of crystallography. To overcome this problem, different methods like the molecular replacement method, multiple-wavelength anomalous dispersion (MAD), single-wavelength anomalous dispersion (SAD), multiple isomorphous replacement (MIR, MIRAS) and single isomorphous replacement (SIR, SIRAS) can be used to overcome this problem.

### 1.1.3.1 Molecular replacement

The previous paragraph emphasized already that different techniques are available to obtain the phases necessary for calculation of the electron density function. One of these techniques is the molecular replacement method (250,251,252). Basis for this method is the already known structure of a protein with sufficiently high similarity to the target protein that can be used as a phasing model.

For both structures, a Patterson function  $P(u,v,w)$  is calculated (253). The amplitude of each term is obtained by squaring the structure factor that is proportional to the measured intensity of a reflection:

—

A map can be derived from the Patterson function. The resulting Patterson map is a vector map that contains a peak for every interatomic distance including vectors of

opposite direction between the same pair of atoms with a large peak at the origin (0,0,0) as a result of vectors that relate atoms to themselves.

If both structures are homologous enough, the Patterson maps should be similar. Thus, the two maps will correlate, if the correct orientation and position within the unit cell has been found. There will be a maximum in this function because the Patterson maps of two homologous proteins will look similar, if both proteins have the same position and orientation in a unit cell with identical dimension and symmetry. So this maximum provides the best orientation of the phasing model in the unit cell of the target protein.

Once the position and orientation of the template match the one of the target protein, the phases can be calculated and used as an estimate.

Since this method is depending on sufficiently homologous models, it cannot be used for every protein.

## 2 Protein biochemistry

For all experiments, standard techniques and materials were used. Unless specified elsewhere, all chemicals were of p.a. quality.

Protein solutions were handled on ice and frozen in liquid nitrogen for storage. *Coprinopsis cinerea* Lcc5 was stored at -80 °C and *P. stutzeri* N<sub>2</sub>OR in liquid nitrogen to assure anoxic conditions for long-term storage. Protein concentrations were determined using bicinchoninic acid (254) with bovine serum albumin as standard.

For *Pseudomonas stutzeri* nitrous oxide reductase, all experiments had to be carried out under oxygen-free conditions in an anaerobic chamber (Coy Laboratory Products, Grass Lake, USA) with a 95 % N<sub>2</sub>/ 5 % H<sub>2</sub> atmosphere. All glass and plastic ware was stored in this chamber for at least 72 hours prior to use. The solutions and buffers used for crystallization trials were evacuated and flushed with N<sub>2</sub> eight times to remove dioxygen.

## 2.1 Nitrous oxide reductase from *Pseudomonas stutzeri*

Nitrous oxide reductase of *Pseudomonas stutzeri* was provided by Prof. Dr. W. G. Zumft, University of Karlsruhe, Germany.

### 2.1.1 Crystallization

All crystallization experiments were set up in an anaerobic chamber with a 95 % N<sub>2</sub>/ 5 % H<sub>2</sub> atmosphere and <1 ppm O<sub>2</sub> using the sitting drop vapor diffusion method.

Initial three-dimensional crystals growing as clusters were obtained from the Footprint Screen I-III in a condition that contained 16 % PEG 4,000 and 0.2 M imidazole/ malate buffer pH 7.5. This condition could be further refined by optimization of the PEG chain length, PEG concentration and the pH of the buffer. Additional fine screening with the detergent screen (Hampton Research) was done to avoid the formation of crystal clusters. The final crystallization condition consisted of 16 % PEG 6,000 and 0.2 M imidazole/ malate pH 7.0 in the reservoir, while the drop contained 2.8-4.5 % (v/v) n-octyl-β-D-glucoside, 1 μl protein solution (15 mg ml<sup>-1</sup>) and 1 μl reservoir solution.

Crystals with purple color appeared after around 2 to 4 days. The temperature seemed to be the major determinant for crystal morphology. Depending on the temperature, the crystal form varied from cuboid (at 293 K) to hexagonal shaped crystals (at 298 K). Both crystal forms diffracted better than 2 Å but belonged to different space groups. The crystals were transferred into cryoprotective buffer that contained the reservoir solution and 10 % (v/v) 2*R*,3*R* butane diol as cryoprotectant.

### 2.1.2 Substrate complexes of nitrous oxide reductase

To obtain the structure of nitrous oxide reductase with the bound substrate N<sub>2</sub>O, freshly grown crystals were pressurized with N<sub>2</sub>O in a pressurization chamber (XeCell, Oxford CryoSystems). The filter of the chamber was soaked in H<sub>2</sub>O to avoid dehydration of the crystals and then subsequently closed and flushed with N<sub>2</sub>O (UHP). The crystals were

incubated for 2, 5, 10, 15 or 20 min with pressure adjusted to 10, 15 or 20 bar and then transferred into the cryoprotective solution and subsequently frozen in liquid nitrogen.

### 2.1.3 Data collection and processing

Diffraction data were collected on beam lines X06SA and X06DA at the Swiss Light Source, Paul Scherrer Institute, Villigen, Switzerland.

Collected data were indexed and processed with MOSFLM and SCALA (255) of the CCP4 suite (256).

The cube-shaped crystals belonged to space group P1 with unit cell parameters  $a = 96.9 \text{ \AA}$ ,  $b = 106.7 \text{ \AA}$ ,  $c = 131.1 \text{ \AA}$ ,  $\alpha = 111.3^\circ$ ,  $\beta = 107.3^\circ$  and  $\gamma = 90.7^\circ$ . Calculation of the Matthews coefficient (257,258) with a molecular mass of 130 kDa per dimer suggested 4 dimers per asymmetric unit and a solvent content of 46 %.

The hexagonal crystals that appeared at higher temperatures belonged to space group P6<sub>5</sub> with  $a = b = 70.3 \text{ \AA}$ ,  $c = 399.7 \text{ \AA}$  and  $\alpha = \beta = 90^\circ$ ,  $\gamma = 120^\circ$  with one dimer per a.s.u. and a solvent content of 45 %. These crystals were merohedrally twinned with two twin domains: the twinning operation -H-K, K, -L.

### 2.1.4 Molecular replacement

The nitrous oxide reductase of *Paracoccus denitrificans* (pdb: 1fwx) shows a sequence identity of 56 % to the N<sub>2</sub>OR of *P. stutzeri*. Upon removal of water, the monomer of this protein was therefore used as search model for molecular replacement with the triclinic dataset using the program PHASER (259) of the CCP4 suite (256). The rotation and translation functions were done for the P1 data set within the resolution range of 35.8 Å to 2.5 Å.

### 2.1.5 Model building and Refinement

The structural model was rebuilt according to the electron density map and the sequence of *P. stutzeri* N<sub>2</sub>OR using the program COOT (260). The model was refined to a resolution of 2.1 Å with REFMAC5 (261) to final  $R_{\text{cryst}}$  and  $R_{\text{free}}$  of 17.8 % and 24.9 %, respectively.

The current model consists of 12 copper, 2 calcium, 2 monovalent ions (sodium or potassium), 2 chlorine atoms per dimer, and 36,801 non-hydrogen atoms and 2,474 solvent molecules in the asymmetric unit. The final r.m.s.d. values are 0.02 Å for bond length and 1.92° for bond angles. A summary of the data collection statistics and refinement statistics can be found in Tab. 2 in the appendix.

From here on, this model of *P. stutzeri* N<sub>2</sub>OR was used for all further data sets as a search model for molecular replacement.

### 2.1.6 Spectroscopy

#### 2.1.6.1 UV/ vis spectra

UV/ vis spectra of the protein (7 mg ml<sup>-1</sup>) in 25 mM TrisHCl pH 7.5 were recorded with a Perkin Elmer Lambda 40 spectrophotometer in a spectral range from 250 to 800 nm at 20 °C. The spectrometer was equipped with a 1 ml sample cell (light path of 1 cm) that could be closed with a septum to assure anoxic conditions during measurement.

Deconvolution of the spectra (provided by Prof. Oliver Einsle) into individual bands was done using Microcal Origin.

#### 2.1.6.2 Electron Paramagnetic Resonance

EPR spectra were recorded at a temperature of 10 K using a Bruker EMX continuous wave spectrometer fitted with an Oxford helium cryostat in X-band ( $\nu = 9.204$  GHz) with 200  $\mu$ W power and a modulation amplitude of 4G.



## 2.2 Laccase Lcc5 from *Coprinopsis cinerea*

Laccase Lcc5 of *Coprinopsis cinerea* was provided by Dr. Martin Rühl, Georg-August-University of Göttingen, Germany.

### 2.2.1 Crystallization

Initial three-dimensional crystals were obtained from the Footprint Screen I-III in a condition that contained 2 % (v/v) MPD and 1.8 M Na,K phosphate pH 8.5 at 20 °C. After refinement of the condition, the reservoir contained 2 % MPD (v/v) and 1.6 M Na,K phosphate pH 8.5, while the drop contained 1 µl protein solution (7 mg ml<sup>-1</sup>) and 1 µl reservoir solution.

Blue crystals appeared after around 12 h to 2 days. Three crystals forms could be observed: cubic-like, cuboid-like, and crystals with an irregular shape. The crystals were sensitive towards the cryoprotective buffer that contained the reservoir solution and 20 % (v/v) MPD as cryoprotectant. The concentration of MPD was therefore increased in 4 steps of 5 %.

### 2.2.2 Data collection and processing

Diffraction data were collected on beam lines X06SA at the Swiss Light Source, Paul Scherrer Institute, Villigen, Switzerland and on an inhouse rotating copper anode (Rigaku, Japan).

Collected data were indexed and processed with MOSFLM and SCALA (255) of the CCP4 suite (256).

All three crystal forms diffracted better than 2 Å and belonged to space group  $P2_12_12_1$  with unit cell parameters  $a = 79.4$  Å,  $b = 82.1$  Å,  $c = 91.0$  Å,  $\alpha = \beta = \gamma = 90.0^\circ$ . Calculation of the Matthews coefficient (257,258) with a molecular mass of 60 kDa per monomer suggested one monomer per asymmetric unit and a solvent content of 58 %.

### 2.2.3 Molecular replacement

Laccase Lcc5 of *Coprinopsis cinerea* shows a sequence identity of 53 % to Lcc1 (pdb: 1hfu, (216)) from the same organism. The protein was therefore used as search model for molecular replacement using the program MOLREP of the CCP4 suite (256). The rotation and translation functions were done within the resolution range of 91.0 Å to 2.5 Å.

### 2.2.4 Model building and refinement

The structural model was rebuilt according to the electron density map and the sequence of *C. cinerea* Lcc5 using the program COOT (260). The model was refined using REFMAC5 (261) with anisotropic B-factor refinement to a resolution of 1.2 Å to final  $R_{\text{cryst}}$  and  $R_{\text{free}}$  of 15.0 % and 17.2 %, respectively.

The current model consists of 4 copper atoms, 3 phosphate molecules, 4 N-acetylglucosamine (NAG) molecules, and 4,061 non-hydrogen atoms and 749 solvent molecules in the asymmetric unit. The final r.m.s.d. values are 0.012 Å for bond length and 1.61° for bond angles. A summary of the data collection statistics and refinement statistics can be found in Tab. 3 in the appendix.

## V Results and discussion

### 1 Nitrous oxide reductase of *Pseudomonas stutzeri*

#### 1.1 Crystallization

Purple crystals of *P. stutzeri* N<sub>2</sub>OR appeared after 2-4 days with different forms depending on the crystallization temperature (Fig. 17). At 293 K the crystals were in most cases cubic, which at higher temperature (298 K) tended to be more of a hexagonal shape. This ratio was not strict but rather a smooth transition.

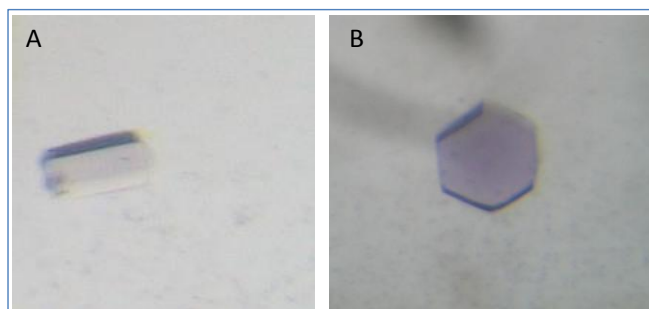


**Fig. 17** Crystals of purple *P. stutzeri* N<sub>2</sub>OR. Crystal shape depended on the crystallization temperature. At 293 K, crystals had a cuboid-like shape (A), whereas at higher temperatures (298 K) crystals tended to be of hexagonal shape (B).

The cuboid-shaped crystals belonged to space group *P1* with unit cell parameters  $a = 96.6 \text{ \AA}$ ,  $b = 106.5 \text{ \AA}$ ,  $c = 130.8 \text{ \AA}$ ,  $\alpha = 111.4^\circ$ ,  $\beta = 107.3^\circ$  and  $\gamma = 90.7^\circ$  and contained 4 dimers per asymmetric unit with a solvent content of 46 % according to Matthews (257,258). The hexagonal crystals, however,

belonged to space group *P6<sub>5</sub>* with  $a = b = 70.3 \text{ \AA}$ ,  $c = 399.7 \text{ \AA}$  and  $\alpha = \beta = 90^\circ$ ,  $\gamma = 120^\circ$  with one dimer per a.s.u. and a solvent content of 45 %.

Even though the hexagonal crystals diffracted to slightly higher resolutions (1.7 Å), the overall diffraction power from crystal to crystal was not consistent ranging from 1.7 to 5 Å whereas the cubic shaped crystals diffracted in most cases between 2 and 2.5 Å. Both crystal forms had almost the same solvent content (between 44 and 46 %) and crystal density was comparable. However, the hexagonal crystals diffracted anisotropically and due to the long cell axis reflections were close together especially if the rotation axis was orthogonal to *c*. Moreover, these crystals seemed to be more fragile as judged by easy

cracking during crystal harvesting from the drop and as well during pressurization with nitrous oxide.

Even though a high humidity in the pressure cell was assured, the drop in the loop containing the crystal became cloudy after around 5 minutes or cracked if the applied pressure exceeded 5 to 10 bars. Diffraction tests after pressurization revealed a complete loss of diffraction power or very high mosaicity leading to strong overlapping especially of the long cell axis reflections which made further processing of the data impossible.

On the other hand, the cubic shaped crystals did not exhibit any visible cracks and diffracted even when pressurized with 25 bars for 20 minutes. Therefore, all obtained data sets of N<sub>2</sub>O-gassed crystals belonged to space group *P*1.

## 1.2 Crystal structure

Nitrous oxide reductase from *P. stutzeri* shows the same quaternary structure as the previously described structures with an overall shape like a butterfly (Fig. 18).

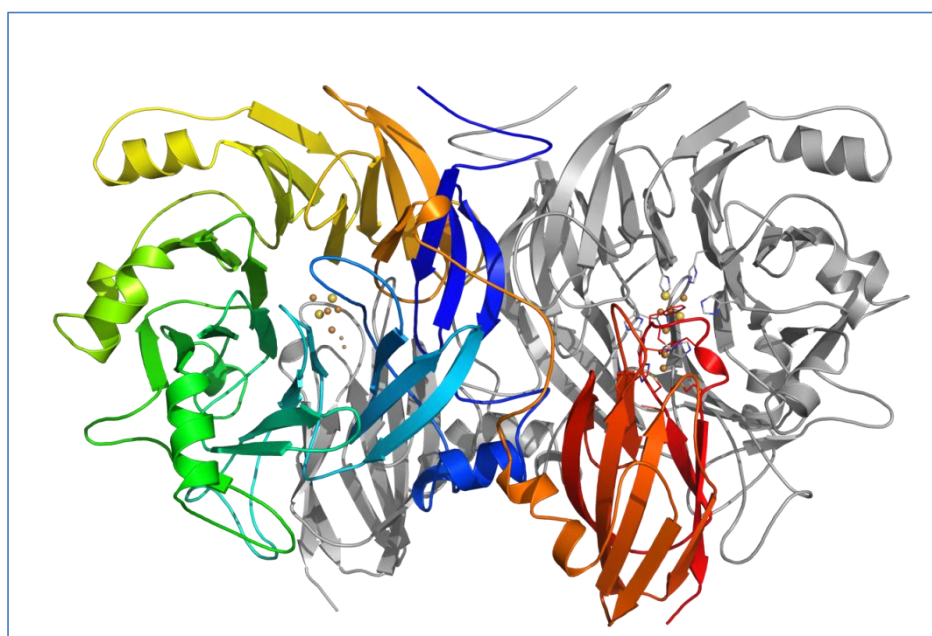


**Fig. 18** Dimer of *Pseudomonas stutzeri* nitrous oxide reductase. Monomer 1 in rainbow colors, monomer 2 in grey. Copper ions in orange, sulfur ions in yellow.

Each monomer consists of two distinct domains (Fig. 19), the N-terminal seven-bladed  $\beta$ -propeller with the tetranuclear  $\text{Cu}_Z$  site and the C-terminal cupredoxin-like domain with the  $\text{Cu}_A$  site.

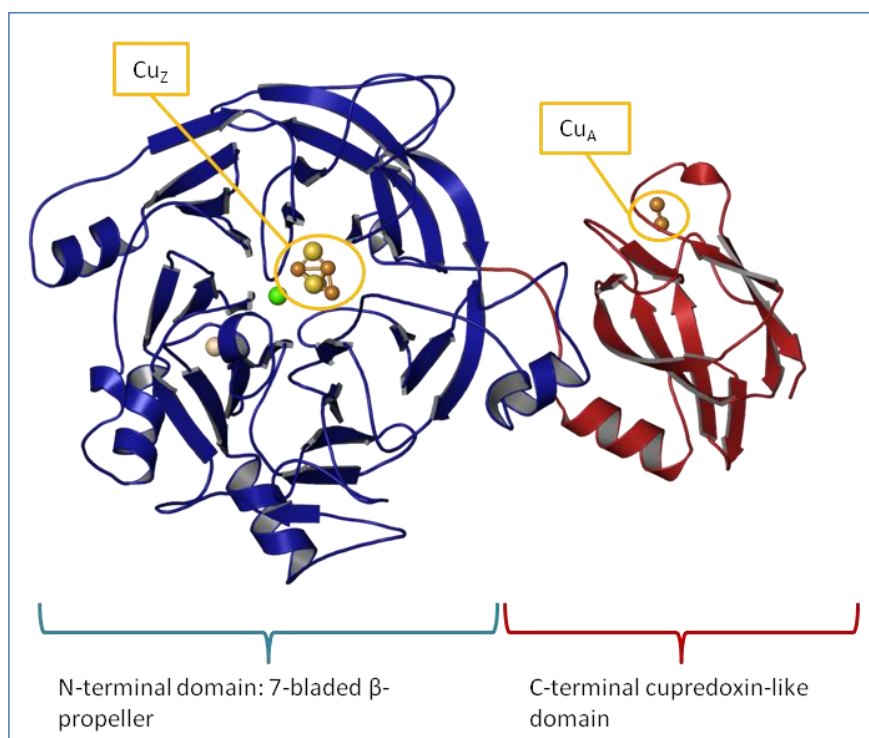


**Fig. 19** Monomer of *P. stutzeri* nitrous oxide reductase. Tetranuclear  $\text{Cu}_Z$  site is situated in the N-terminal  $\beta$ -propeller domain (blue), chloride (green), calcium (rose). The binuclear  $\text{Cu}_A$  site resides in the C-terminal cupredoxin-like domain.

The two monomers lie head-to-tail to each other with the C-terminal domain of one monomer facing the N-terminal 7-bladed  $\beta$ -propeller of the second monomer and vice versa. This results in a large interface ( $\sim 5430 \text{ \AA}^2$ ) between the two monomers, corresponding to  $\sim 30.4\%$  of the solvent accessible surface<sup>1</sup>. The dimer is stabilized by several polar and non-polar interactions as well as by hydrogen bonds and chelating interactions. Additionally, a monovalent ion such as a potassium or sodium ion can be found at the dimer interface.

<sup>1</sup> The solvent accessible surface was calculated with AREAIMOL of the CCP4 suite (256) that calculates the accessible surface area for protein atoms only and ignores water and other solvent molecules.

Sequence comparisons of the N<sub>2</sub>OR of *P. denitrificans* (17), *A. cycloclastes* (18) and *M. hydrocarbonoclasticus* (70) with the enzyme of *P. stutzeri* show only a moderate identity of 56 % and 55 % for the first two organisms and a significantly higher identity (75 %) for the last one (alignment of all four sequences can be found in the appendix). However, the structural models of all four proteins are strikingly similar as seen in a superposition of the structures and by the small r.m.s.d. values of 0.467 Å, 0.563 Å and 0.582 Å for the C<sub>α</sub>-atoms, respectively (Fig. 20).

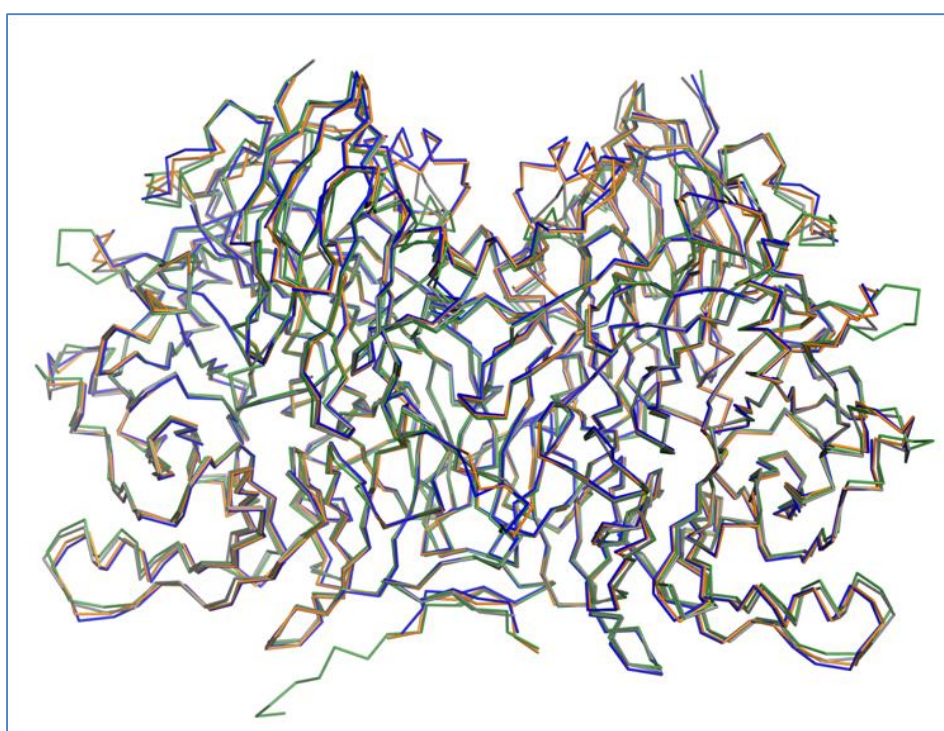


**Fig. 20** Superposition of the four available crystal structures of nitrous oxide reductase. *A. cycloclastes* (orange), *P. denitrificans* (blue), *M. hydrocarbonoclasticus* (grey) and *P. stutzeri* (green).

One major difference between the *P. stutzeri* and *M. hydrocarbonoclasticus* structures and the ones from *P. denitrificans* and *A. cycloclastes* is the absence of the small loop (Thr70 – Lys85 in *A. cycloclastes*, highlighted by a red circle (Fig. 21)) connecting the first and second blade of the N-terminal  $\beta$ -propeller in the latter ones.

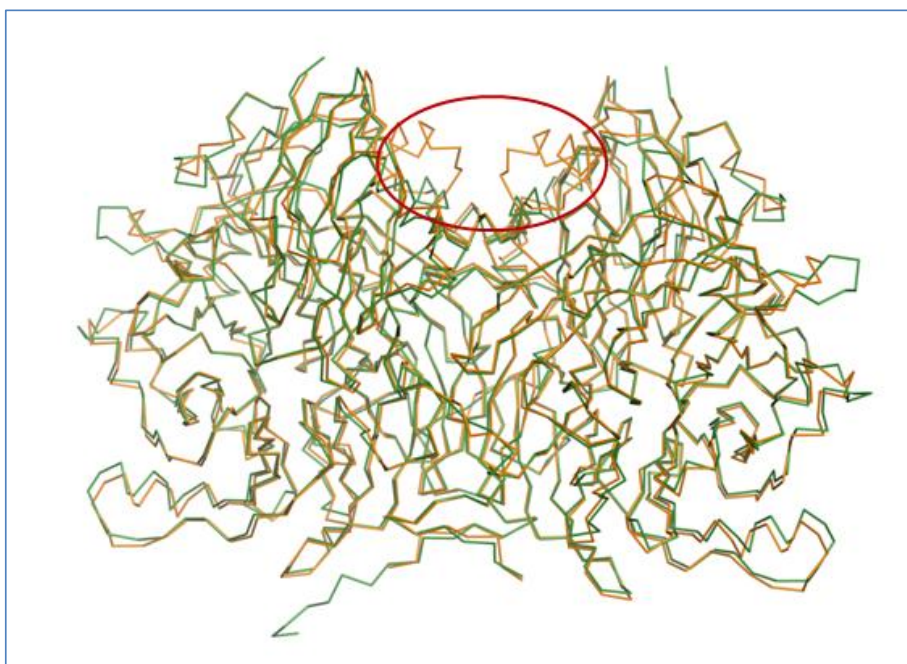


**Fig. 21** Superposition of N<sub>2</sub>OR of *A. cycloclastes* (orange) and *P. stutzeri* (green). The additional loop that connects the first and second blade of the N-terminal β-propeller is highlighted by a red circle. This loop can be found as well in the structure of *P. denitrificans*, but neither in *P. stutzeri* nor *M. hydrocarbonoclasticus* nitrous oxide reductase.

### 1.2.1 The Cu<sub>A</sub> site

The Cu<sub>A</sub> center is similar to the one found in cytochrome *c* oxidase subunit II (58,57) and it is situated in the C-terminal cupredoxin-like domain.

The two copper atoms are bridged by two cysteine residues (Cys622 and Cys618). Cu<sub>A1</sub> is additionally ligated by one methionine residue (Met629) and Cu<sub>A2</sub> by one histidine (His626) and the main chain O carbonyl of a tryptophan (Trp620) which confirms the already identified ligands for the Cu<sub>A</sub> site as described by Charnock *et al.* (71).

In the structures of COX and N<sub>2</sub>OR from *P. denitrificans* (70) and *M. hydrocarbonoclasticus* (both form III), (17)) and form II of *A. cycloclastes* (18), it can be seen that Cu<sub>A1</sub> is like Cu<sub>A2</sub> ligated by a histidine residue. The conformation of the Cu<sub>A</sub> site in its oxidized form in *A. cycloclastes* N<sub>2</sub>OR and its reduced form in *M. hydrocarbonoclasticus* and *P. denitrificans* are basically identical.

However, instead of coordinating the copper, the corresponding histidine (His583) in *P. stutzeri* N<sub>2</sub>OR forms in most observations a hydrogen bond from its N $\delta$ 1 atom to the O $\gamma$  atom of a close-by serine (Ser550) and from Ne2 with the  $\beta$ -carboxy group of an aspartate residue (Asp576) with distances of around 2.5 Å and 2.8 Å, respectively (Fig. 22). Interestingly, both residues, Ser550 and Asp576, are conserved among the N<sub>2</sub>OR reductases (Fig. 23) indicating a functional role as discussed in paragraph 1.3.1.

In a minor fraction of our structures, His583 is seen to be turned back and ligate the Cu<sub>A1</sub>, however the distance between the N $\delta$ 1 atom of His583 and the copper atom gets never shorter than 2.7 Å in the substrate-free enzyme which is larger than the bond lengths observed for COX and the other described N<sub>2</sub>O reductases (1.9 to 2.2 Å (57,58,17,18,70)). The absence of the histidine ligands results in a rearrangement of the Cu<sub>A</sub> cluster. The now three-coordinated Cu<sub>A1</sub> atom is drawn into the plane formed by the sulfur atoms of Cys618, Cys622 and Met629 thereby forming rather a kite than a regular tetrahedron. However, the distance between the two copper atoms in Cu<sub>A</sub> remains unchanged at 2.5 Å.

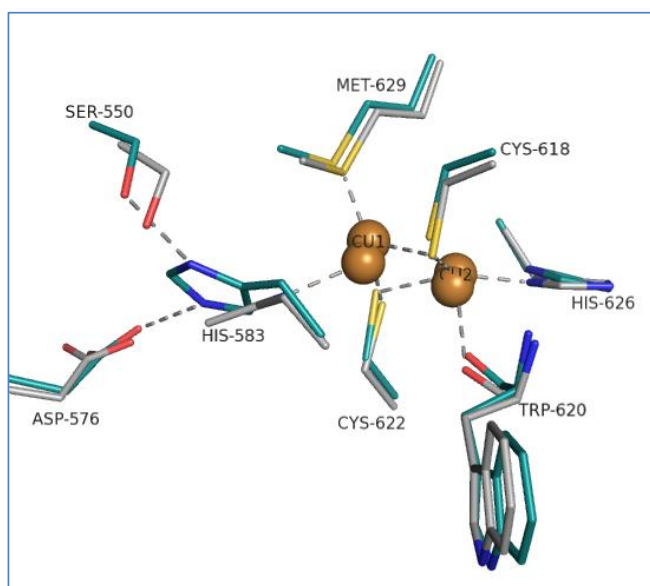


**Fig. 22** Cu<sub>A</sub> site of *P. stutzeri* (cyan) and *A. cycloclastes* (grey). The residues are labeled accordingly to *P. stutzeri*. His583 is rotated and no longer a ligand to Cu<sub>A1</sub> but instead forming hydrogen bonds with a close-by serine (Ser550) and aspartate residue (Asp576), whereas in *A. cycloclastes* the histidine residue is bound to Cu<sub>A1</sub> with its Ne2-atom.



**Fig. 23** Sequence alignment shows the conservation of the serine and aspartate residue (yellow boxes) that are involved in ligation of histidine H583 in *P. stutzeri*



### 1.2.2 The Cu<sub>z</sub> site

The Cu<sub>z</sub> center is situated in the hub of the β-propeller of the N-terminal domain, almost in one plane with the surface side that forms contact to the second monomer. The four copper ions are ligated by seven histidines (Fig. ) belonging to 6 of the 7 propeller blades: Cu<sub>z1</sub>, Cu<sub>z2</sub> and Cu<sub>z3</sub> have two amino acid ligands each (Nε2-His326 and Nε2-His382, Nδ1-His129 and Nε2-His178, Nε2-His130 and Nε2-His433, respectively) whereas Cu<sub>z4</sub> has just one ligand (Nδ1-His494).

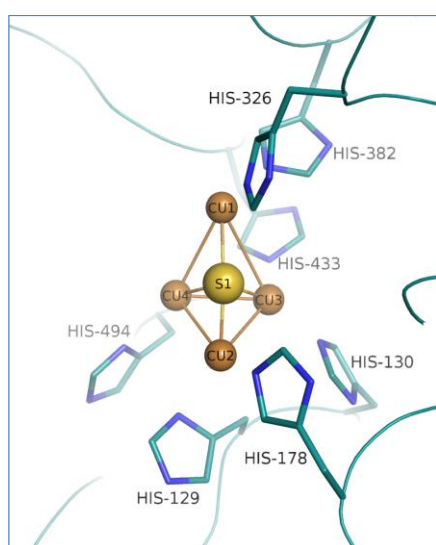


**Fig. 24** Cu<sub>z</sub> site of *P. stutzeri* N<sub>2</sub>OR. Cu<sub>z1</sub>, Cu<sub>z2</sub> and Cu<sub>z3</sub> have three histidine ligands each, whereas Cu<sub>z4</sub> has only one. The four copper are bridged by an inorganic sulfur.

The copper content for *P. stutzeri* N<sub>2</sub>OR was determined to be approximately 8 Cu per dimer (87,65). However, this was not consistent with the finding of a binuclear Cu<sub>A</sub> and a tetranuclear Cu<sub>z</sub> cluster which would result in 12 copper atoms per dimer. The explanation for this can be found in the structure itself. The electron density maps are best modeled with occupancies between 0.5 and 0.8 for the tetranuclear Cu<sub>z</sub> cluster and the best fit was for the intact center only. The calculation of 8 Cu/dimer is therefore due to the partial occupancy of the Cu<sub>z</sub> site. The loss of one of the metals goes along with loss of the complete cluster. This is in contrast to the observations made for *M.*

*hydrocarbonoclasticus* N<sub>2</sub>OR, where Cu<sub>z3</sub> and Cu<sub>z4</sub> seemed to be lost first (17).

Even though low occupancy of the cluster led to decreased electron density, all structural features were clear. The positions of the single copper atoms and the sulfide were modeled by the occurrence of positive or negative electron density according to the best resolved solutions in several monomers of different data sets.

### 1.2.2.1 Second sulfur

In the structures of *M. hydrocarbonoclasticus* and *A. cyclostastes* N<sub>2</sub>OR, one or two additional ligands can be seen at the edge of Cu<sub>Z1</sub> and Cu<sub>Z4</sub> that are assumed to be water or hydroxyl molecules. Surprisingly, if water was built in this position in *P. stutzeri* N<sub>2</sub>OR, positive difference electron density could be observed (Fig. 25-A), indicating an atom with more electrons. The positioning of an additional sulfur atom at this position explained very well the observed electron density (Fig. 25-B).

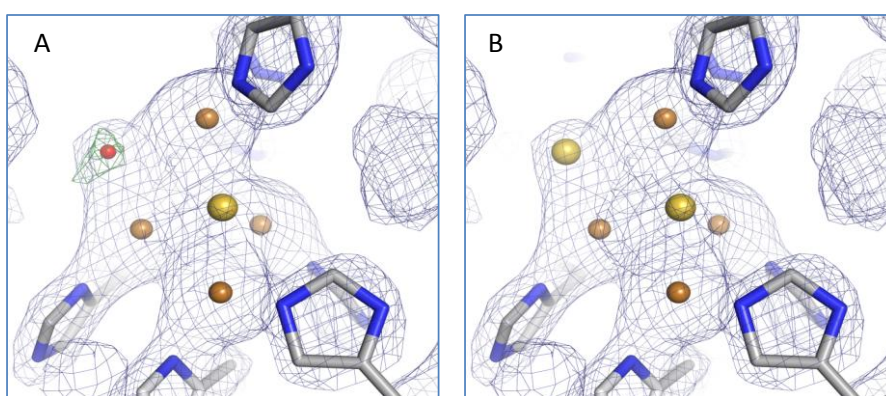


**Fig. 25** Cu<sub>2</sub> site of *P. stutzeri* N<sub>2</sub>OR. The four copper are shown in brown, sulfur in yellow. Upon building a water ligand at the edge of Cu<sub>Z1</sub> and Cu<sub>Z4</sub>, positive difference electron density could be observed. This indicated an atom with more electrons. The positioning of an additional sulfur instead of the water ligand explained this observation very well. 2F<sub>o</sub>-F<sub>c</sub> electron density is contoured at 1.0  $\sigma$ . The difference electron density (F<sub>o</sub>-F<sub>c</sub>) is contoured at 3.0  $\sigma$ .

Several facts back up this interpretation. The second sulfur is ligated to Cu<sub>Z1</sub> and Cu<sub>Z4</sub> with bond distances of 2.5 Å and 2.3 Å, respectively (Fig. 27), which speaks rather for a Cu-S coordinative bond than for a Cu-O bond.

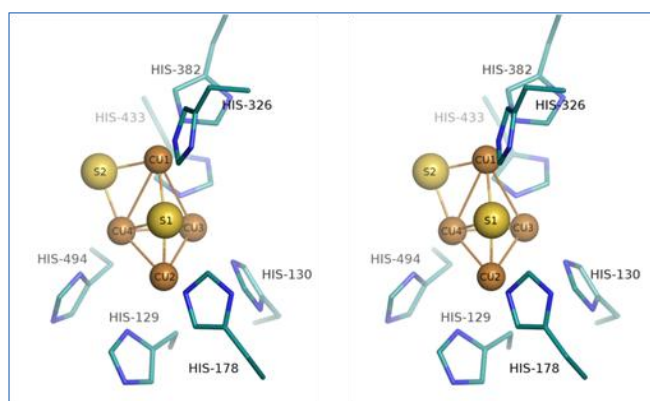


**Fig. 26** Stereo representation of the Cu<sub>2</sub> site with two sulfur.

coordinative bond than for a Cu-O bond.

Additionally, a N<sub>2</sub>OR crystal structure of *A. cyclostastes* with bound iodide is available (pdb: 2IWK (18)). The soaking experiments were done to study the effect of iodide on protein

inhibition which had been reported earlier (262) and will be discussed in paragraph V.1.3.5. However, one of the iodide ions was bound in exactly the same position where the second sulfur for the N<sub>2</sub>OR of *P. stutzeri* is proposed (18). According to the spectrochemical series, iodide is a strong field ligand that can replace S<sup>2-</sup> (263).

The Cu<sub>2</sub> site with two sulfur and 4 copper atoms offers explanations for several spectroscopic features that can be seen in the different forms of nitrous oxide reductase.

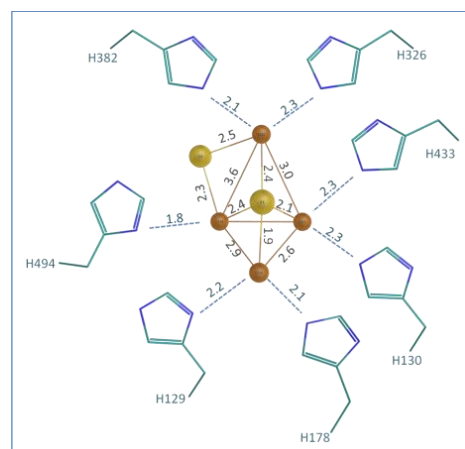


**Fig. 27** Scheme of the [4Cu:2S] Cu<sub>2</sub> site of *P. stutzeri* with bond distances in Å. Sulfur is shown in yellow, copper in brown.

### 1.2.2.2 Spectroscopic characterization of Cu<sub>2</sub>, Cu<sub>2</sub>\* and Cu<sub>2</sub><sup>0</sup>

The UV/vis spectrum of the catalytically active purple form of *P. stutzeri* (form I) exhibits three absorption bands that can be assigned to Cu<sub>A</sub>: 485 nm, 525 nm and 790 nm. The tetranuclear Cu<sub>2</sub> site is represented by two absorption bands at 538 nm and 660 nm (Fig. 28-C).

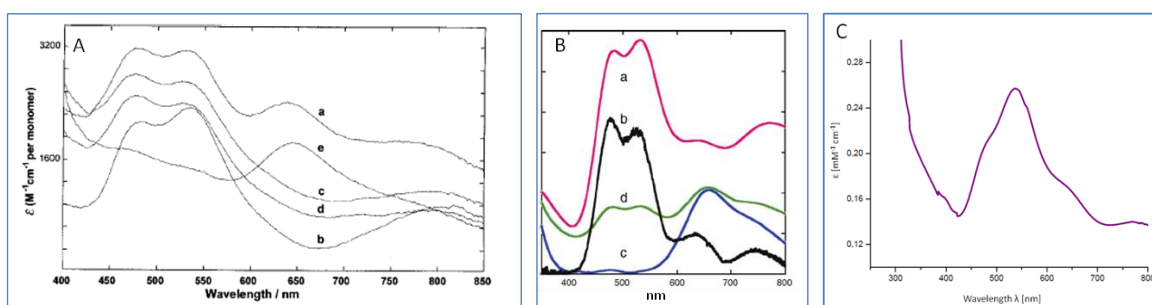


**Fig. 28** UV/vis spectra of nitrous oxide reductase. **A:** N<sub>2</sub>OR form III after reduction with dithionite (a) from *Paracoccus denitrificans* (Reprinted from (17) with kind permission from Portland Press). **B:** N<sub>2</sub>OR form II after aerobic purification (a) from *Achromobacter cycloclastes* (Reprinted from (18) with kind permission from Elsevier). **C:** *Pseudomonas stutzeri* N<sub>2</sub>OR form I after an anaerobic purification.

On the contrary, the spectra of pink N<sub>2</sub>OR (form II) of *A. cycloclastes* (Fig. 28-B) and the blue form (form III obtained after reduction of form II) of *P. denitrificans* N<sub>2</sub>OR show only

a single absorption maximum at around 650 nm. The one at 538 nm is absent (Fig. 28-A). This coincides with the observation of just one sulfur atom in the  $\text{Cu}_2$  site. Both absorption maxima seen for the purple form of *P. stutzeri*  $\text{N}_2\text{OR}$  can therefore be tentatively assigned to a sulfur-to-copper charge transfer transition mainly involving the  $3d$  and  $3p$  orbitals of copper and sulfur, respectively.

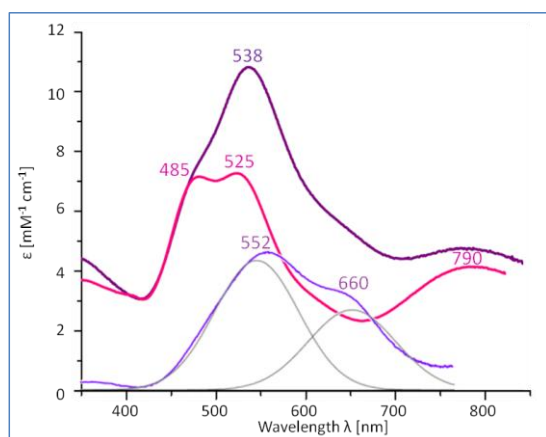


**Fig. 29** Deconvoluted UV/ vis spectra of form I (purple) and form V (MK402 variant, pink)  $\text{N}_2\text{OR}$  (kindly provided by O. Einsle). The difference between both spectra (violet) corresponds to the  $\text{Cu}_2$  site observed in purple *P. stutzeri*  $\text{N}_2\text{OR}$ . It can be deconvoluted into two separate bands. The band at 552 nm is a LMCT from  $\text{S}_{22}$  to copper, whereas the second band at 660 nm corresponds to  $\text{S}_{21} \rightarrow \text{Cu}$  LMCT transition.

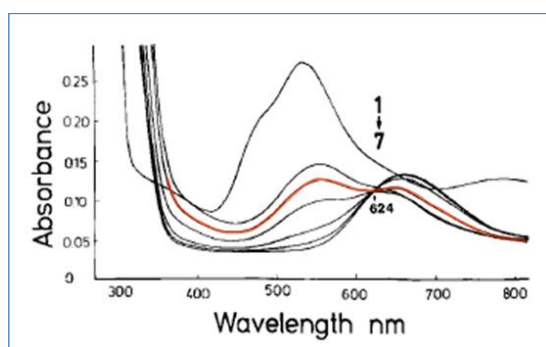


**Fig. 30** UV/ vis spectra of *P. stutzeri*  $\text{N}_2\text{OR}$  (Reprinted from (64) with kind permission from John Wiley & Sons). Anaerobic reduction with sodium dithionite. The two bands corresponding to two  $\text{S} \rightarrow \text{Cu}$  LMCT transitions of  $\text{Cu}_2$  can be seen before the cluster is further reduced (marked in orange).

A deconvolution of the UV/ vis spectra allows the allocation of a maximum at 552 nm to the second sulfur-copper LMCT transition whereas the maximum at 660 nm is the LMCT transition of the sulfur in the center of  $\text{Cu}_2$  (Fig.).

The second sulfur is close to a putative gas channel and thereby possibly exposed to dioxygen that might diffuse into the protein upon contact with air. The loss of the second sulfur leaves the remaining core cluster unaffected and corresponds therefore only to a loss of the second absorption maximum. It goes along with a decrease in enzymatic activity. The remaining catalytic activity can be assigned to residual  $[\text{4Cu}_2\text{S}]$ . Exposure of the  $\text{N}_2\text{OR}$  site to dioxygen leads therefore to a transition of  $\text{Cu}_2$  to  $\text{Cu}_2^*$ .

The maximum assigned to the second sulfur will be lost as well if form III of  $\text{N}_2\text{OR}$  is obtained by reduction of the purple form I as a result of reduced copper that will no longer participate in a charge

transfer transition with sulfur (Fig.). It is therefore possible to regain form I if the oxidation is done by titration with ferricyanide under strict anoxic conditions (64), which will oxidize the copper but prevents loss of the second sulfur. Interestingly, before complete reduction of the  $\text{Cu}_2$  site, both bands, which correspond to the two LMCT transitions between sulfur and copper and which have been determined by deconvolution of the form I and form V UV/vis spectrum can be seen (Fig., marked with orange color).

We therefore conclude that  $\text{Cu}_2$  is the active form in a  $[\text{4Cu}_2\text{S}]$  state whereas the  $[\text{4Cu}_1\text{S}]$  represents the inactive  $\text{Cu}_2^*$  form.

The correspondence between the  $\text{Cu}_2^*$  form and the loss of one sulfur provides a possible role for NosR and NosX. Even though NosX has been identified for a limited number of denitrifying bacteria, its role is suggested to be similar to NosR which is encoded in most *nos* gene clusters. Inactivation of both proteins results in an  $\text{N}_2\text{OR}$  phenotype similar to the pink form obtained under aerobic conditions (153,154,140). This indicates that those proteins may be involved in sulfur incorporation during the maturation of nitrous oxide reductase. It implies as well that the second sulfur is incorporated into  $\text{Cu}_2$  after the  $[\text{4Cu}_1\text{S}]$  core is synthesized but before insertion of the cluster into the protein.

An interesting observation that can be seen in context with the absence of a second sulfur is a study done by Alvarez *et al.* to prove that the bridging atom in the  $\text{Cu}_2$  cluster is rather sulfur than oxygen (139). Cells grown under the sulfur limiting conditions expressed  $\text{N}_2\text{OR}$  that - when purified under anoxic conditions - exhibited low activity and the typical features of  $\text{Cu}_2^*$  under UV/vis and resonance Raman spectroscopy equivalent to an enzyme one would obtain under oxic conditions. It can therefore be argued that the sulfur content in the growth media was high enough to allow for the initial  $[\text{4Cu}_1\text{S}]$  formation, but due to the low availability of sulfur only a small fraction of enzyme was equipped with the complete  $\text{Cu}_2$  site.

### 1.2.3 The putative gas channel

In all published structures of  $N_2OR$ , a channel can be found (Fig. 31) that is almost exclusively lined by apolar amino acids, whereas coordinated water molecules are absent creating a hydrophobic environment that indicates a gas channel. It ends close to the  $Cu_z$  site and the resulting cavity is large enough to accommodate a nitrous oxide molecule. Close to this cavity a pool of water molecules can be found. The positioning and the cavity above the  $Cu_{z1}-S_{z1}-Cu_{z2}-S_{z2}-Cu_{z4}$  plane are similar in all structures of  $N_2OR$  published so far.

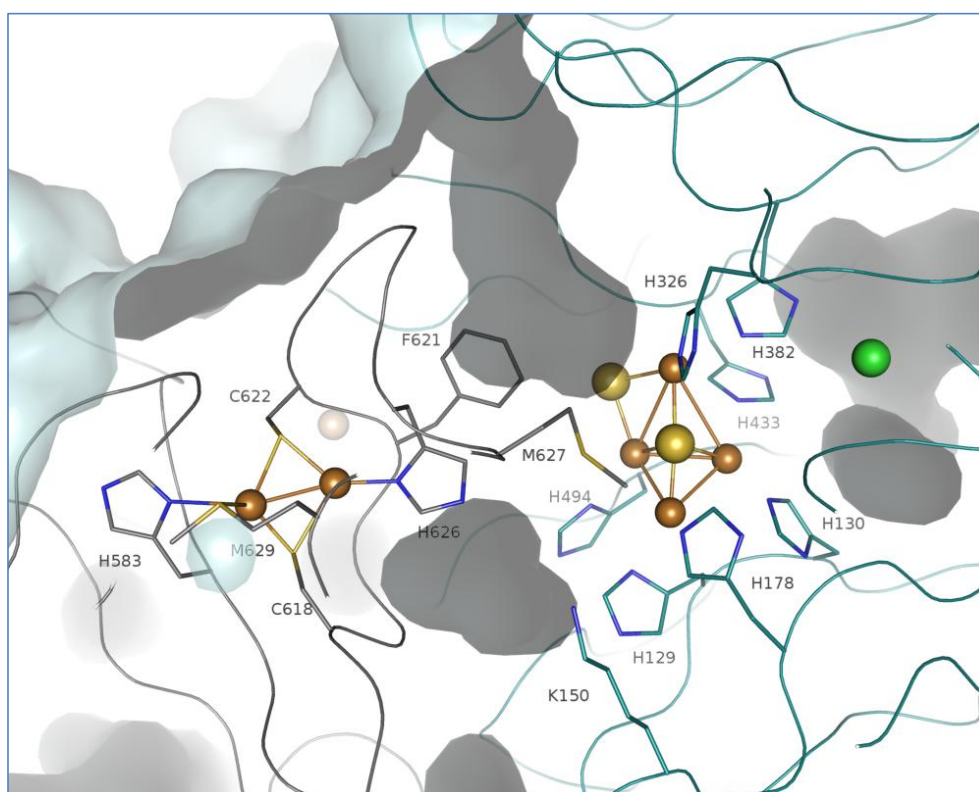


**Fig. 31**  $Cu_z$  and  $Cu_A$  center with putative gas channel. The channel is almost exclusively lined by apolar amino acids. Water molecules are absent, thereby creating a hydrophobic environment. Surface of the protein is shown in light blue.  $Cu_A$  belongs to monomer 1 (grey) and  $Cu_z$  to monomer 2 (cyan). Both centers are connected by a phenylalanine (F621). A monovalent ion (potassium or sodium, colored in light orange) is at the interface in between both monomers. A chloride ion (green) is close to the  $Cu_z$  site, sharing one of the histidine ligands with  $Cu_{z1}$ . Copper is colored in brown, sulfur in yellow.

The question that arises immediately from the observed presence of a second sulfur atom is how  $N_2O$  can bind to the enzyme. As described earlier, the edge of  $Cu_{z1}$  and  $Cu_{z4}$  was assumed to be the possible substrate binding site due to the modeled water molecules that indicated an open position for  $N_2O$ . But the crystal structure of the catalytically active purple  $N_2OR$  of *P. stutzeri* shows a second sulfur atom in this position. Therefore, some crystals of *P. stutzeri*  $N_2OR$  have been pressurized with  $N_2O$  to study the binding mechanism of the substrate to the catalytic site.

Three datasets could be collected with electron density maps that showed mainly the  $Cu_z$  cluster with the second sulfur present and the previously described decreased occupancy. Additionally, an elongated electron density at the  $Cu_z$  site of several monomers could be observed which could be perfectly modeled with a nitrous oxide molecule. In previously solved structures of *P. stutzeri*  $N_2OR$  that were not pressurized with nitrous oxide, no additional electron density indicating a water or other molecule bound to the active site could be observed. And indeed, the modeling of one or two water molecules resulted in occurrence of positive difference electron density between the two waters indicating a single molecule rather than one or two water. After refinement, the  $N_2O$  and  $Cu_z$  exhibited B-factors close to the surrounding amino acids.

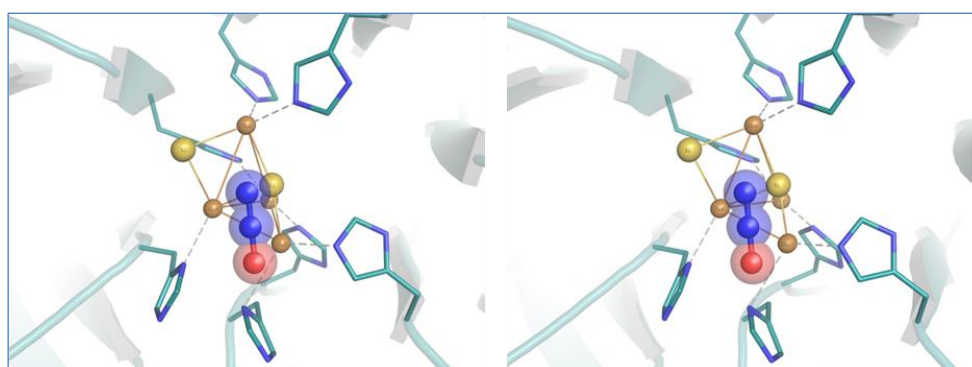


**Fig. 32** Stereo representation of the  $Cu_z$  site with bound substrate. View from above along the axis of the  $\beta$ -propeller domain.  $N_2O$  in blue (nitrogen) and red (oxygen). Copper is shown in brown, sulfur in yellow.

The structure of the *P. stutzeri* enzyme with bound  $N_2O$  shows clearly, that the substrate binds in a side on manner above the plane created by  $Cu_{z4}$ ,  $Cu_{z2}$  and  $S_{z1}$  and not, as previously suggested, parallel at the edge of  $Cu_{z1}$  and  $Cu_{z4}$  (Fig. 32 and Fig. 33). Here, the

second sulfur is sitting, blocking substrate access. The binding position of  $N_2O$  showed slight variations as can be seen by superposition of the  $Cu_z$  with bound substrate, but the overall orientation and positioning were consistent.

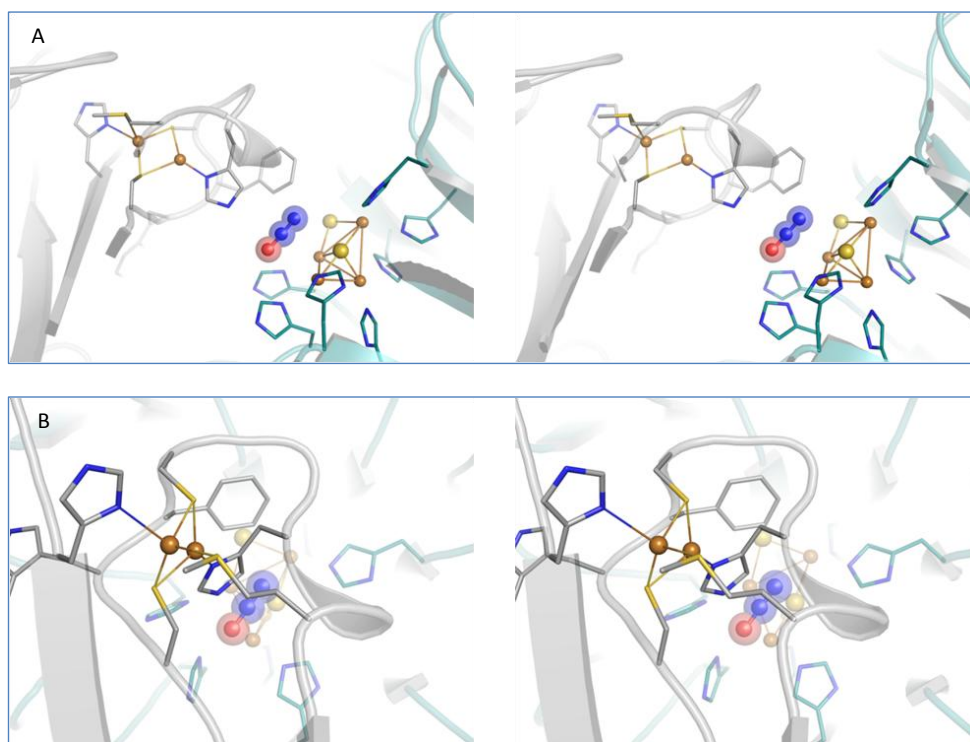


**Fig. 33** Stereo representation of  $N_2O$  binding between  $Cu_A$  and  $Cu_z$ . Monomer 1 is shown in grey, monomer 2 in cyan.  $N_2O$  is in red (oxygen) and blue (nitrogen), located above the plane created by  $Cu_{z4}$ ,  $S_{z1}$  and  $Cu_{z2}$  between the  $Cu_A$  and the  $Cu_z$  site. A phenylalanine and a methionine residue assist in correct positioning and orientation of the substrate. A:  $N_2O$  is binding between the  $Cu_A$  and the  $Cu_z$  site. B: view from the  $Cu_A$  site (monomer 1) into the hub of the  $\beta$ -propeller (monomer 2).

The putative substrate channel that had been described earlier ends directly at the  $Cu_z$  site with the nitrous oxide molecule sitting in a narrow pocket between the  $Cu_A$  and the  $Cu_z$  site lined by three amino acid residues, Phe621, His626 and Met627 (Fig. 34). They belong to the cupredoxin domain of the opposite monomer. The histidine residue is a ligand of  $Cu_{A2}$  which brings the substrate in direct contact to the  $Cu_A$  site. The methionine residue is close to a cavity that contains several water molecules, while the phenylalanine residue is located between the  $N_2O$  binding side and the gas channel. Both residues are conserved among the  $N_2OR_A$  sequences (16) and form a barrier around the substrate. They



might therefore be involved in orienting the  $N_2O$  molecule so that its O-atom is positioned towards the water pool while the nitrogen faces the putative substrate channel. In this way, the dinitrogen obtained after reduction of  $N_2O$  might emerge the same way as nitrous oxide entered the catalytic site while the product  $H_2O$  is kept in the water-filled cavity.

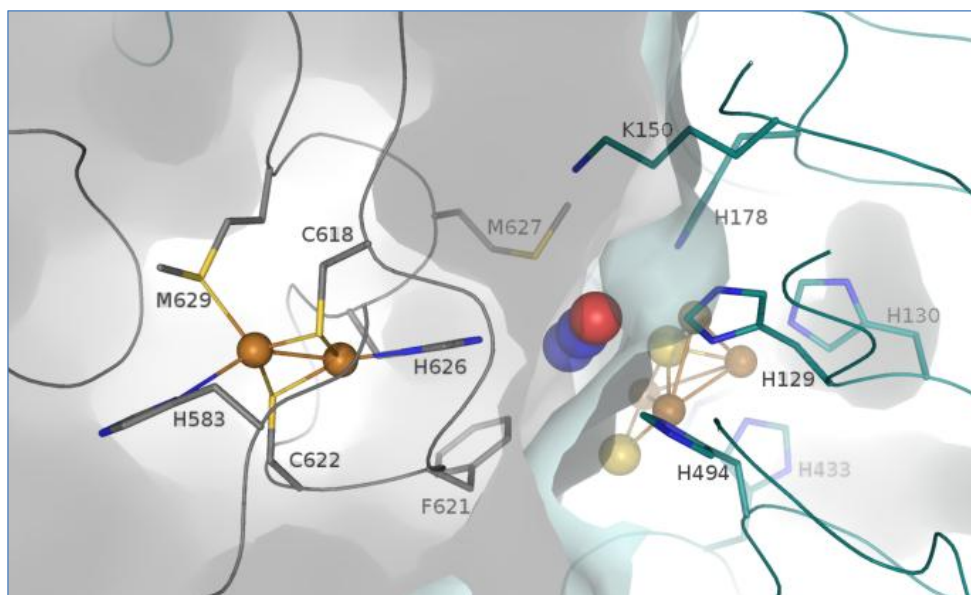


**Fig. 34** Representation of the catalytic site of *P. stutzeri*  $N_2OR$ . View from the water pool close to the  $Cu_2$  site towards the substrate channel. Monomer 1 with  $Cu_A$  center is shown in cyan, monomer 2 with  $Cu_B$  site in grey with light brown for copper and yellow for sulfur. The surface for each monomer has been calculated separately to show the binding pocket for the substrate  $N_2O$ , which is situated between both copper centers. The phenylalanine (F621) might function as a barrier of the gas channel while the methionine (M627) is closely to the O-atom of the substrate to assure the right orientation and positioning of  $N_2O$ .

Another interesting observation connected with the substrate binding is the behavior of His583 that was no longer a ligand to  $Cu_{A1}$  as described in paragraph V1.2.1: The copper-histidine distance (1.9-2.2 Å, (16,17,18,58,57)) observed in other enzymes could never been verified for the *P. stutzeri* structure. Instead, the histidine is rotated about 125° and forms a hydrogen bridge with a nearby serine residue (Ser550).

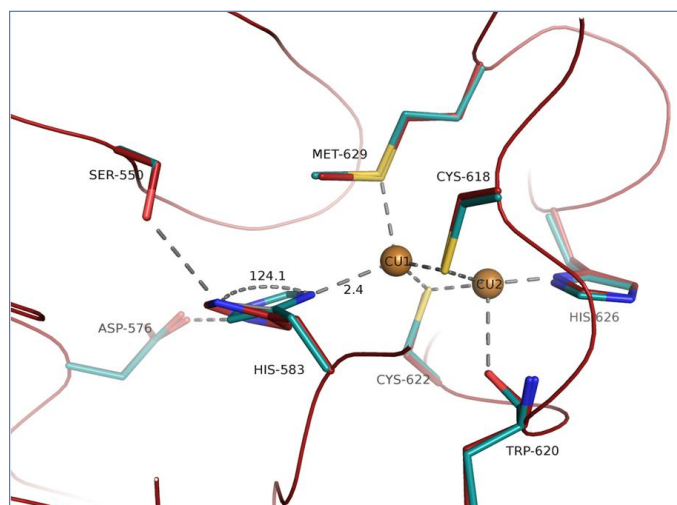


**Fig. 35**  $\text{Cu}_A$  site. Upon binding of the substrate  $\text{N}_2\text{O}$ , His583 rotates back by around  $125^\circ$  towards the  $\text{Cu}_{A1}$ , even though the distance is with  $2.4 \text{ \AA}$  higher than observed for other  $\text{N}_2\text{O}$  reductases.

Nevertheless, this flexibility seemed to decrease upon binding of  $\text{N}_2\text{O}$ . The histidine moves back towards the  $\text{Cu}_{A1}$  atom upon binding of the substrate nitrous oxide, even though it never approaches closer than  $2.4 \text{ \AA}$  (Fig. 35).

### 1.3 Implications for the reaction mechanism

#### 1.3.1 Electron transfer from a putative electron donor

As described in chapter V1.2.1, histidine (His583) is no longer a ligand for  $\text{Cu}_{A1}$  in *P. stutzeri*  $\text{N}_2\text{OR}$  but it rotates back towards the copper upon binding of substrate to the catalytic site (Fig. 35). Histidine has usually a  $\text{pK}_a$  of around 6.0–6.5 for its side chain. But an influence of the pH used for crystallization on the protonation state of His583 can be excluded because the  $\text{N}_2\text{OR}$  structures of *M. hydrocarbonoclasticus*, *P. denitrificans* and *A. cycloclastes* were crystallized at pH 9.5, pH 6.5 and pH 6.5 (16,70,17,18) and show all the same conformation for the corresponding histidine ligand. On the other hand, *P. stutzeri*  $\text{N}_2\text{OR}$  has been crystallized at pH 7.0. The major difference is that only the structure of this protein represents the physiologically active purple form. Some kind of participation of His583 in the catalytic cycle is therefore likely.

The delocalized electron of the Cu<sub>A</sub> site is distributed over the Cu<sub>2</sub>S<sub>2</sub> core. The observed variations in geometry of this cluster are rather limited. Even upon loss of His583 as a ligand of Cu<sub>A1</sub>, the planarity of this core is maintained, and the features are less affected than they would be in the case of a mononuclear copper center.

The pK<sub>a</sub> of a histidine is normally around 6.0 and 6.5 for the second protonation. But the hydrogen bond between histidine and aspartate will increase this pK<sub>a</sub>, turning it thereby into a stronger base that is able to deprotonate the serine residue. This leaves the histidine with a positive charge facilitating electron transfer. Under these conditions, histidine will be even protonated, if the surrounding pH is high thereby increasing the redox potential and facilitate electron transfer. Comparisons with other N<sub>2</sub>OR reveal conservation of both residues as well as location close to the surface.

Docking studies of the putative physiological electron donor for *P. denitrificans* revealed Asp519 to be close to the surface and involved in binding. The homologous cluster in COX of the same organism is Asp178, which has been shown to be important for cytochrome *c* binding (264). The corresponding residue in *P. stutzeri* N<sub>2</sub>OR is Asp576 that forms a hydrogen bond to His583. So docking of an electron donor on the surface above these residues would thus offer an effective route for electron transfer to the Cu<sub>A</sub> site.

Under denitrifying conditions, nitrous oxide reductase is expressed together with pseudoazurin and/ or *c*-type cytochromes, some of them are essential for N<sub>2</sub>O reduction (131,150,152,77,265). For the nitrous oxide reductase of *M. hydrocarbonoclasticus* cytochrome *c*<sub>552</sub> has been identified as putative physiological electron donor (143). Furthermore, gene deletion studies on *P. denitrificans* showed that a double mutant lacking cytochrome *c*<sub>550</sub> and a pseudoazurin is unable to denitrify, whereas a single deletion of just one gene results in wildtype phenotype (265,266).

### 1.3.2 Explanation for the pH dependence of N<sub>2</sub>OR by an engineered Cu<sub>A</sub> azurin

Fujita *et al.* proposed that the active-site conformation around Cu<sub>A</sub> can be influenced by pH changes that are catalytically relevant and might fine-tune the reactivity of the Cu<sub>A</sub> center in inter- and intramolecular electron transfer (267). They could show that both, Cu<sub>Z</sub>\* and especially Cu<sub>A</sub>, are affected in the oxidized state of *A. cycloclastes* N<sub>2</sub>OR. Similar effects have been observed for COX of *P. denitrificans* (268,269).

These observations can partially be explained by studies on engineered Cu<sub>A</sub> azurin: The first azurin that was engineered with a Cu<sub>A</sub> center was published in 1996 (62). Since then a lot of studies have been done to help in characterization of the Cu<sub>A</sub> site and to provide insight into its functions.

The T1-copper protein azurin and the C-terminal domain of N<sub>2</sub>OR both contain a cupredoxin fold. It was possible to replace the loop in azurin carrying the type-1 copper with the loop of cytochrome *c* oxidase which contained the ligands to bind Cu<sub>A</sub> (62). The thereby obtained new protein, Cu<sub>A</sub> azurin (Cu<sub>A</sub>-Az), binds a Cu<sub>A</sub> site and shows similar spectroscopic features to native COX and N<sub>2</sub>OR (270,76,271,272). A high-resolution crystal structure proved that the engineered Cu<sub>A</sub> and the native one of cytochrome *c* oxidase are almost identical (273).

A recent study on Cu<sub>A</sub>-Az showed the pH-dependence of the electron transfer: At pH 7.0 the Cu<sub>A</sub> exhibits the typical delocalized mixed-valence [Cu<sup>1.5+</sup>:Cu<sup>1.5+</sup>] state with the characteristically seven-line hyperfine EPR spectrum. But a shift to pH 4.0 resulted in a four-line EPR spectrum that is typical for a trapped valence like in a type-1 copper center even though this transformation is reversible if the pH is altered back to higher values. This suggests that it is possible to transform the mixed-valent state into a trapped valence by lowering the pH. Further experiments to determine the residues that might be protonated under these conditions showed the His120 to be a candidate. And indeed, measurements of the reduction potential of Cu<sub>A</sub> azurin as a function of pH showed an increase of 180 mV vs. NHE at pH 4 when the Cu<sub>A</sub> obtained the trapped valence state. However, UV/vis spectra did not show any difference to the mixed-valent state (274).

This histidine corresponds to the histidine ligand of Cu<sub>A2</sub> in *P. stutzeri* N<sub>2</sub>OR (His626) that is at the dimer interface close to the Cu<sub>Z</sub> site. Additionally, its Nε2-atom is pointing towards the cavity close-by the Cu<sub>Z</sub> site that contains several coordinated water molecules suggesting involvement in this hydrogen bonding network. The described observations for Cu<sub>A</sub> azurin might therefore offer an explanation for the slow electron transfer from Cu<sub>A</sub> to Cu<sub>Z</sub> in nitrous oxide reductase (64,141).

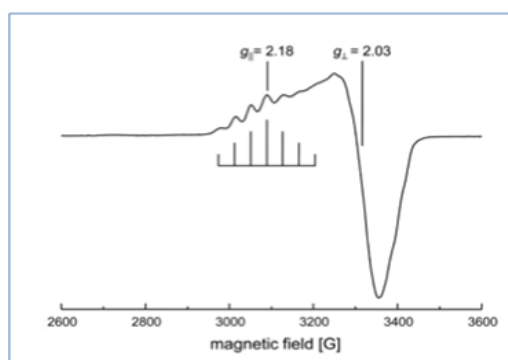


**Fig. 36** X-band EPR spectrum of purple N<sub>2</sub>O reductase of *P. stutzeri* showing the characteristically 7-line hyperfine pattern with a 1:2:3:4:3:2:1 intensity ratio.

However, a trapped valence state for the Cu<sub>A</sub> site in *P. stutzeri* N<sub>2</sub>OR can be excluded because the EPR spectrum showed the seven-line hyperfine signatures (Fig. 36). The electron is delocalized with around 95 % on the Cu<sub>2</sub>S<sub>2</sub>-rhomb of the Cu<sub>A</sub> center, whereas only ~5 % is distributed over the histidine residues. But protonation of His626 might increase the redox potential of the Cu<sub>A</sub> site which could result in prevention of electron

transfer to Cu<sub>Z</sub>. It might therefore play an important role in regulation of the proton-coupled electron transfer.

The crystal structure of *P. stutzeri* N<sub>2</sub>OR with bound substrate shows that N<sub>2</sub>O binds in close distance to the Nε2-atom (~3.5 Å) of His626 (Fig. 37). It might therefore form a hydrogen bond with the O-atom of N<sub>2</sub>O and/ or transfer protons and electrons to the substrate. This would suggest as well that Cu<sub>A</sub> and Cu<sub>Z</sub> are involved in reduction of nitrous oxide.

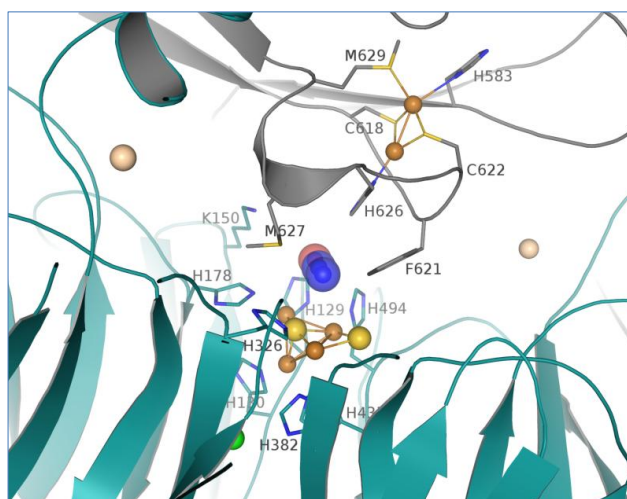


**Fig. 37** Catalytic site of N<sub>2</sub>OR with bound substrate. N<sub>2</sub>O (oxygen: red, nitrogen: blue) binds between Cu<sub>A</sub> and Cu<sub>Z</sub>. It is lined by F621 and a M627) that might be involved in positioning of the substrate.

### 1.3.3 A structural role for $S_{Z2}$

The discovery of a second sulfur atom in the  $Cu_z$  site of the purple *P. stutzeri*  $N_2OR$  eliminates the possibility of substrate binding to the edge of  $Cu_{Z1}$  and  $Cu_{Z4}$  as previously suggested. The bound  $N_2O$  is located above the plane created by  $Cu_{Z4}$ ,  $S_{Z1}$  and  $Cu_{Z2}$  (Fig. 33 and 37). The second sulfur takes on an important structural role.

A complex network of hydrogen bonds has been suggested to maintain the geometry of the  $[4Cu1S]$  site (17). Calculation showed that the histidine side chains will reorient if not supported by hydrogen bonds (172). The  $Cu_{Z4}$ , which is only ligated by one histidine residue would obtain a linear geometry with the  $S_{Z1}$  and its imidazole ligand in its reduced state ( $S-Cu-N(\text{his})$  angle is  $180^\circ$ ). The cluster would therefore move towards a trigonal bipyramide geometry (172) with  $Cu_{Z1}$ ,  $Cu_{Z2}$ ,  $Cu_{Z3}$  and  $S_{Z1}$  at the base to reach an energy minimum. The binding site for the substrate created by  $Cu_{Z4}-S_{Z1}-Cu_{Z2}$  will therefore be lost. To avoid this, the strain energies have to be minimized by hydrogen bonds and support of the protein backbone.

On the contrary, the second sulfur supports the tetrahedral conformation and lowers the strain energy. The geometry of the  $Cu_z$  site is therefore less affected by pH changes.

### 1.3.4 Two distinct ways of $N_2O$ reduction in $Cu_z$ and $Cu_z^*$

Enzymatic activity of the form II and form III  $N_2OR$  of various sources has been reported to depend on long-term exposure of up to several hours to dithionite and redox mediators such as methyl viologen or benzyl viologen (143,70,171,173). The mechanism suggested for  $N_2OR$  on the base of crystal structures of *A. cycloclastes*, *P. denitrificans* and *M. hydrocarbonoclasticus* requires the fully reduced  $[4Cu^+]$  state (171,172,143).

In contrast to these enzymes the nitrous oxide reductase of *P. stutzeri* is the only example of the purple form. It is, upon anaerobic purification, catalytically active (64,63) even in its oxidized state, while a further reduction of  $Cu_z^*$  or  $Cu_z$  to a  $[4Cu^+]$  state under physiological conditions is impossible. It is therefore unlikely that the reductively activated enzyme represents a physiologically relevant form.

Several facts support this conclusion. Cells of a  $\Delta nosR$  mutant show complete loss of activity even though *in vitro* activity could be shown upon extended exposure to dithionite and methyl viologen resulting again in a fully reduced  $[4Cu^+]$  state (154).

Moreover, as described for *P. stutzeri*  $N_2OR$ , binding and reduction of substrate did not change UV/vis spectroscopic features (64), like in contrast to many inhibitors while binding of  $N_2O$  to  $Cu_2^*$  in aerobically isolated protein of *M. hydrocarbonoclasticus* resulted in substantial changes (143). Despite the fact that this protein has been described to be of purple color, a comparison of the UV/vis spectra of both enzymes shows that the peak at 640 nm is unusually high compared to the band at 540 nm. It is therefore necessary to analyze whether the purple form of *M. hydrocarbonoclasticus*  $N_2OR$  is identical to the one of *P. stutzeri*.

Physiologic activity depends highly on the presence of the second sulfur in the  $Cu_2$  site. The observed reductive activation necessary for form II and III might therefore be required to deliver a second electron to the substrate which is under physiological conditions no longer possible due to loss of the second sulfur.

A possibility to study the physiological relevance of  $Cu_2^*$ , would be to grow a cell culture under sulfur limiting conditions. This leads, as described by Alvarez *et al.*, to expression of  $N_2OR$  with the spectroscopic and kinetic features of  $Cu_2^*$  (139). These cells should therefore be unable to grow any longer or with very slow growth rates because catalytic activity of the  $N_2OR$  is limited to those proteins that contain the complete  $Cu_2$  cluster.

### 1.3.5 Iodide as an inhibitor for $N_2OR$

The observation of one or two water ligands to the edge of  $Cu_{Z1}$  and  $Cu_{Z4}$  in the  $N_2OR$  models of *P. denitrificans* (17) and *A. cycloclastes* (18) resulted the assumption of this location being the putative substrate binding site.

This idea has been supported by Paraskevopoulos and co-workers: the structural model of *A. cycloclastes*  $N_2OR$  with bound iodide shows that this anion is binding at the edge of  $Cu_{Z1}$  and  $Cu_{Z4}$  (18). Iodide had been reported earlier as an inhibitor of this enzyme (262),

the observation of the iodide binding position was therefore interpreted as its occupation of the substrate binding site.

The finding of the second sulfur in *P. stutzeri* N<sub>2</sub>OR leads to another interpretation for the effect of iodide: First of all, the ion radius of iodide is larger than that of sulfur (2.2 Å instead of 1.8 Å), which might interfere with the binding of nitrous oxide to the Cu<sub>z</sub> site simply by deforming the Cu<sub>z</sub> cluster. This effect can be seen already by comparison of the as-isolated structure and the iodide-bound one. The sulfur bridging the four copper is drawn closer to Cu<sub>z2</sub>, resulting in complete disturbance of the cluster geometry which prevents binding of N<sub>2</sub>O (Fig. 38).

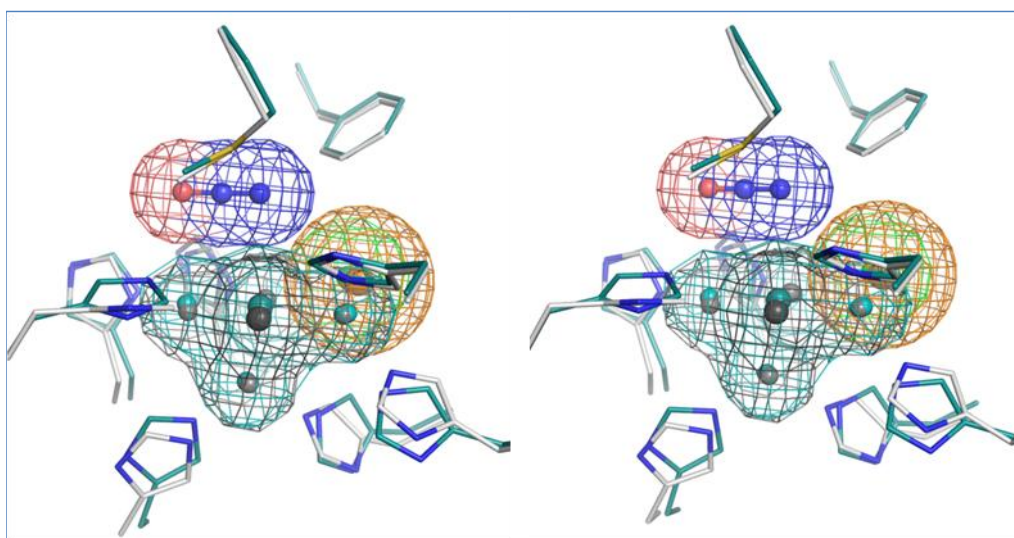


**Fig. 38** Stereo representation of the Cu<sub>z</sub> site with bound N<sub>2</sub>O of *P. stutzeri* (cyan) and the Cu<sub>z</sub> site substituted with iodide of *A. cycloclastes* (grey, **18**). Iodide is bound in exactly the same position as the additional sulfur in *P. stutzeri*. It has been suggested to inhibit the protein by binding to the so far assumed substrate binding site at the edge of Cu<sub>z1</sub> and Cu<sub>z4</sub>. It might as well prevent N<sub>2</sub>O binding by disturbing the Cu<sub>z</sub> geometry because the ion radius of iodide is larger than the one of sulfur (mesh).

### 1.3.6 Biosynthetic models of Cu-S cluster

The unique Cu<sub>z</sub> cluster has inspired several studies on biosynthetic multicopper-sulfide models.

A first mixed-valent Cu-S cluster with N-ligands has been synthesized by the group of W. B. Tolman (275). Interestingly, this cluster contains two sulfur atoms and three copper



and is able to reduce  $\text{N}_2\text{O}$  to  $\text{N}_2$  at low temperatures (Fig. , (276)). Although this cluster differs from  $\text{Cu}_2$  in its coordination regarding a bridging disulfide instead of the single sulfur bridging  $\text{Cu}_{21}$  to  $\text{Cu}_{24}$ , the overall UV/ vis spectroscopic features are similar to the one of  $\text{Cu}_2$ .

The calculation of transition state (TS) structures with bound substrate resulted in a low-energy structure with  $\text{N}_2\text{O}$  bound via its oxygen (Fig. (276)). This is different from the binding mode observed for purple  $\text{N}_2\text{OR}$  of *P. stutzeri* and the one proposed by Solomon *et al.* where  $\text{N}_2\text{O}$  is thought to bind via a  $\mu$ -1,3-bridged mode at the edge of  $\text{Cu}_{21}$  and  $\text{Cu}_{24}$  (172). However, it has to be studied whether the binding of  $\text{N}_2\text{O}$  to synthetic models differ compared to binding to  $\text{Cu}_2$  in the protein. The conformational strains by the protein backbone might result in a completely different binding mode.

#### 1.4 Conclusions and Outlook

In this study, the first structure of a catalytically active nitrous oxide reductase has been solved. It could be shown, that the  $\text{Cu}_2$  center is a  $[\text{4Cu:2S}]$  cluster, whereas  $\text{Cu}_2^*$  describes a  $[\text{4Cu:1S}]$  site. Additionally, a second structure could be solved with  $\text{N}_2\text{O}$  bound to the active site. This represents the first structure of a metal  $\text{N}_2\text{O}$  complex.

The results of this study open new question on the reaction mechanism of nitrous oxide reductase. The so far suggested model was calculated by DFT based on the structures of

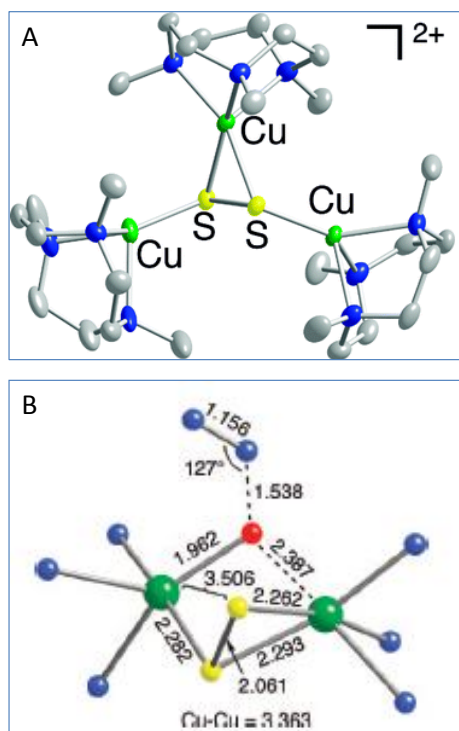


**Fig. 39** **A:** X-ray structure of cationic portion of mixed valent  $[\text{3Cu:2S}]$  cluster with all nonhydrogen atoms shown as 50% thermal ellipsoids. **B:** Transition state structure for the N-O bond cleavage computed at the M06L DFT level with selected interatomic distances (Å). Key: green = Cu, blue = N, yellow = S, and red = O (Reprint from (276) with kind permission from the American Chemical Society).

*Marinobacter hydrocarbonoclasticus*, *Paracoccus denitrificans* and *Achromobacter cycloclastes* (172,171,138). These were either of form II or form III obtained under oxic conditions and therefore with a sulfur-depleted  $\text{Cu}_Z^*$  site. This open coordination site had been suggested for substrate binding (171). However, the observed binding mode of  $\text{N}_2\text{O}$  in form I  $\text{N}_2\text{OR}$  differs to the one proposed. In purple nitrous oxide reductase,  $\text{N}_2\text{O}$  binds between the  $\text{Cu}_A$  and  $\text{Cu}_Z$  site indicating that both copper centers act in concert. This offers an explanation for observed slow electron transfer rates from  $\text{Cu}_A$  to  $\text{Cu}_Z$ : The binding position of  $\text{N}_2\text{O}$  in between the two copper sites allows direct electron transfer from  $\text{Cu}_A$  to the substrate. It is therefore not necessary to reduce  $\text{Cu}_Z$  to an  $[\text{4Cu}^+]$  state because a one-electron reduction is provided directly by  $\text{Cu}_A$ . It would therefore be interesting to see the  $\text{N}_2\text{O}$  binding mode to  $\text{Cu}_Z^*$ . This might help to answer the question how the reaction mechanism between the reductively-activated form and the physiologically active  $\text{N}_2\text{OR}$  differ.

However, the second sulfur and the observed  $\text{N}_2\text{O}$  binding mode might be an inspiration for new strategies to synthesize similar multicopper-sulfur complexes in order to study the enzyme reaction.

In this context it is highly interesting to see how the multicopper oxidase McoP of *Pyrobaculum aerophilum* is able to reduce  $\text{N}_2\text{O}$  as has been shown recently (125).

## 2 Laccase Lcc5 of *Coprinopsis cinerea*

### 2.1 Crystallization

Crystals with an intense blue color appeared in most cases after 12 hours. Three different crystal shapes could be observed: a cubic form, a cuboid-like shape and irregularly shaped crystals. Even though, all crystals diffracted better than 1.7 Å, the best resolution could be obtained with crystals of irregular shape (Fig. 40).

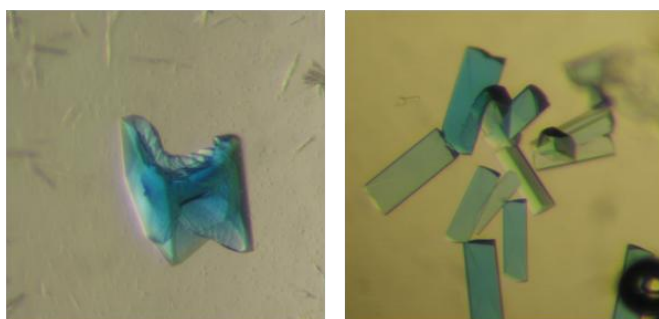


**Fig. 40** Crystals of Lcc5 of *Coprinopsis cinerea*. Three forms could be observed: cubic-shaped (not shown), cuboid-shaped (right) and crystals with irregular shape (left).

The crystals were insensitive upon harvesting but dissolved easily in various cryoprotectants such as MPD, glycerol, polyethylene glycols or 2*R*,3*R* butane diol. Because MPD was part of the crystallization condition, a step-wise increase from the initial XX to a final concentration of 20 %

(v/ v) offered the best solution. However, in almost all collected datasets, ice rings could be observed. Independent of the shape, all crystals belonged to space group  $P2_12_12_1$  with similar cell parameters ( $a=79.4$  Å,  $b=82.1$  Å,  $c=91.0$  Å,  $\alpha=\beta=\gamma=90^\circ$ ). The asymmetric unit contained one monomer with a solvent content of 58 % according to Matthews (257,258).

### 2.2 Sequence analysis

Sequence analysis of Lcc5 from *Coprinopsis cinerea* show the four highly conserved regions (L1-L4) that had been described for other laccases (Fig. 41). They accommodate the ligands of the mononuclear and trinuclear copper site. Between L2 and L3, four less conserved loops can be found, which are involved in substrate binding (277,208).

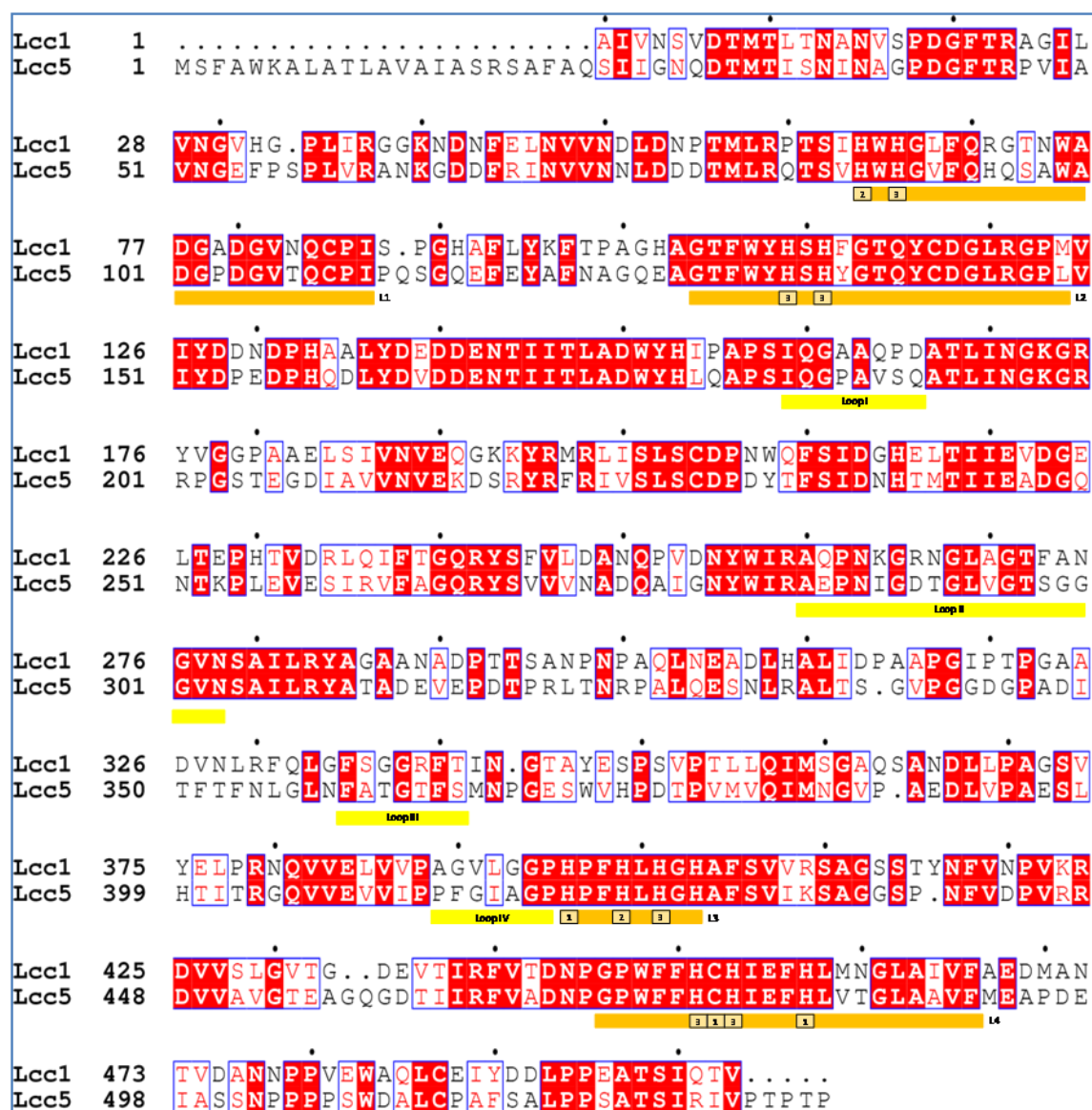


**Fig. 41** Alignment of the *Coprinopsis cinerea* laccases Lcc1 and Lcc5. The cysteine and histidine residues involved in copper ligation are indicated by boxes and numbered according to the ligated copper (1 type-1, 2 type-2 and 3 type-3). Orange bars mark the highly conserved regions L1-L4 and yellow bars the conserved loops involved in substrate binding.

### 2.3 Crystal structure

Laccase Lcc5 of *Coprinopsis cinerea* is a monomer and consists of three  $\beta$ -barrel cupredoxin-like domains forming a tight globule (Fig. 42). Two disulfide bonds stabilize the structure (Fig. 42-C and D): one of them connects domain 1 (Cys142) and 2 (Cys229)

and a second one can be found between domain 1 (Cys109) and 3 (Cys512). Domain 2 and 3 are connected by a large loop.

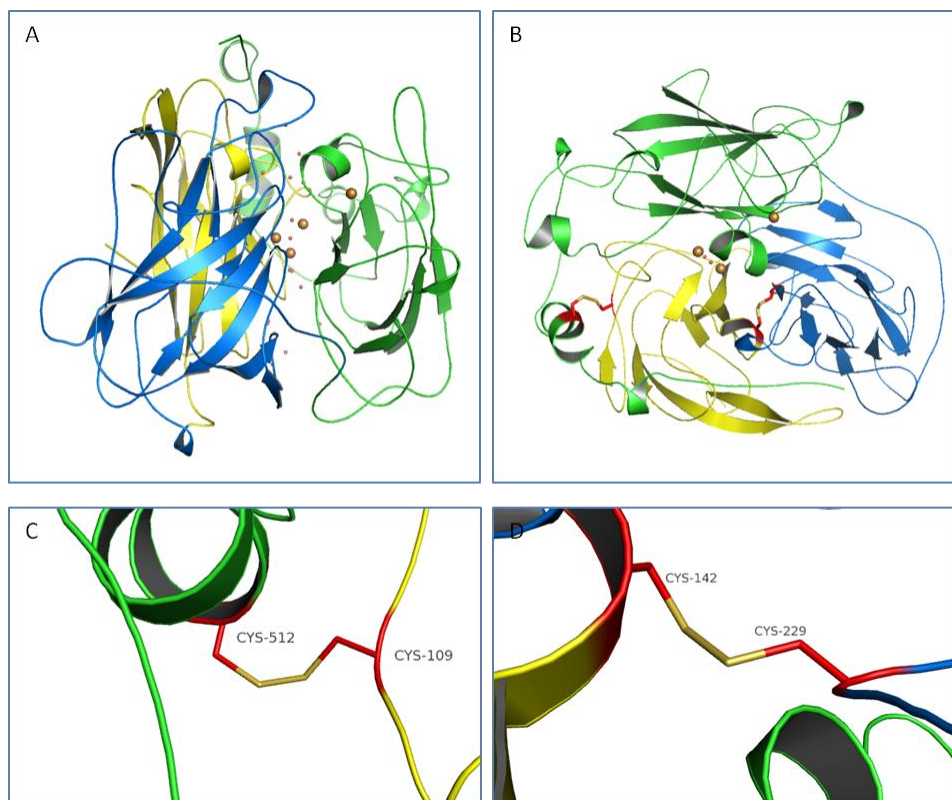


**Fig. 42** Lcc5 of *Coprinopsis cinerea*. A: Cartoon representation of the overall structures. The three cupredoxin-like domains are colored in yellow (domain 1), blue (domain 2) and green (domain 3) from N- to C-terminus. The mononuclear copper site is located in domain 1. The trinuclear copper site is at the interface of domain 1 and 3. Copper is colored in brown, water molecules in red. B: Cartoon representation. View from the mononuclear copper site to the trinuclear center. Disulfide bonds connecting domain 1 (yellow) and domain 2 (blue), and domain 1 and domain 3 (green) are colored in red. C and D: Disulfide bonds connecting the domains. Same color code as A and B.

Superposition of Lcc1 and Lcc5 displays the high structural similarity (53 % sequence identity) between both proteins, which is reflected in small r.m.s.d. of  $0.479 \text{ \AA}^2$  for the  $C_{\alpha}$ -atoms (Fig. 43-A).

A cleft, which can accommodate a variety of substrates, is formed by four loops of domain 2 and 3. It is similar in both proteins regarding depth and wideness. Loop 1 is not defined for the Lcc1 structure and seems to be more flexible than loop 2 to 4 in the structure of Lcc5 (residue 184 to 191) judged by B-factor depended coloring. Loop 2

(residue 285 to 303), loop 3 (residue 356 to 366) and loop 4 (residue 414 to 420) show similar shapes as the loops in Lcc1 (Fig. 43).

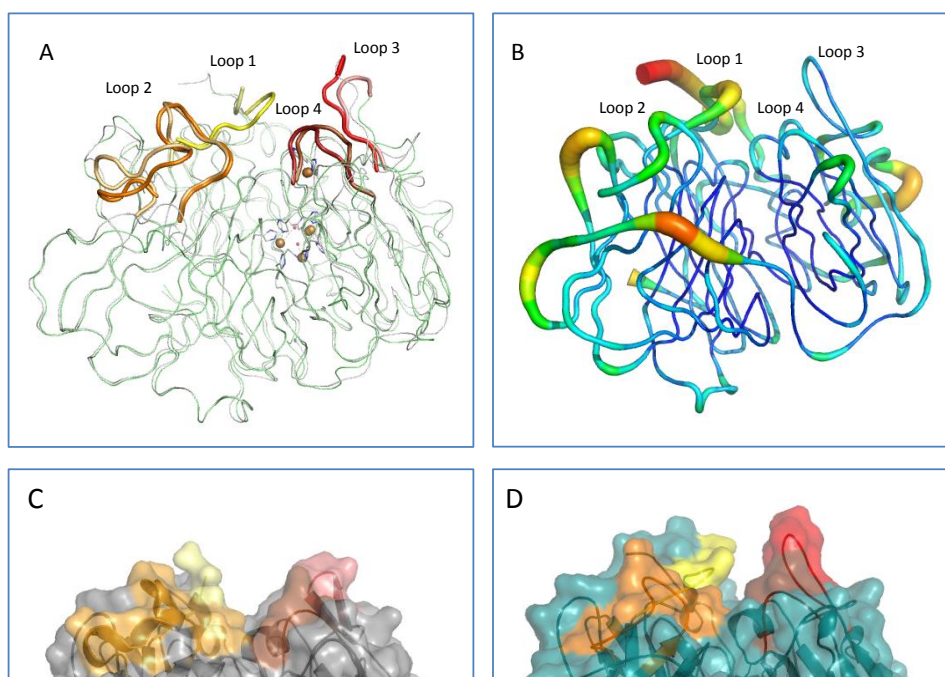


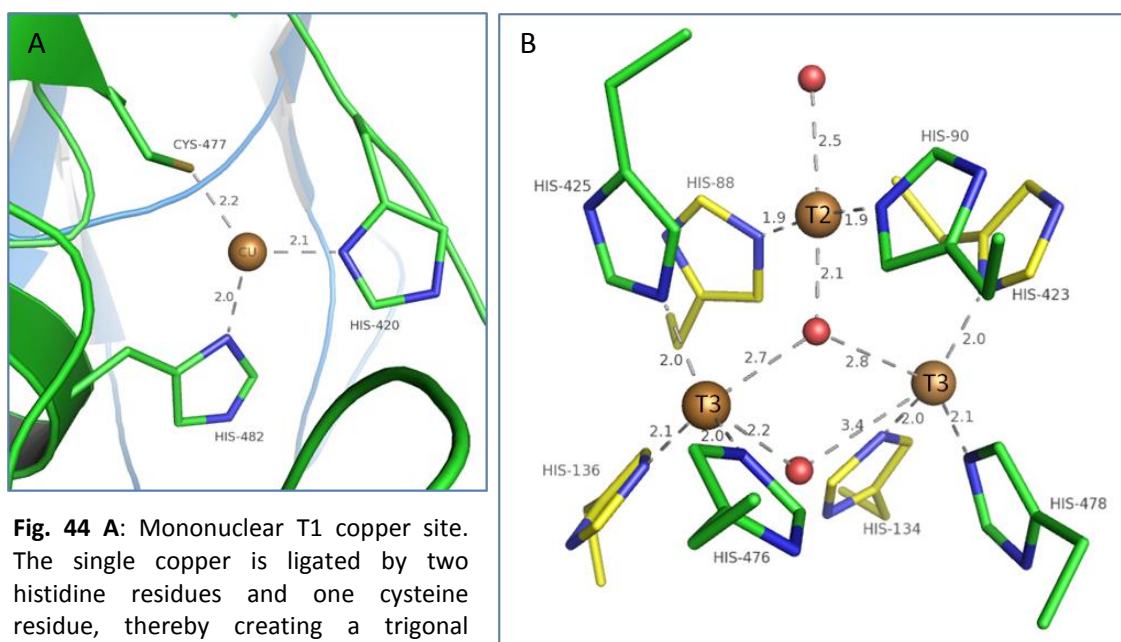
**Fig. 43** **A:** Superposition of Lcc1 (grey) and Lcc5 (cyan). The four loops that create the substrate binding cavity are highlighted in yellow/ light yellow (1), orange/ light orange (2), red/ pink (3) and brown/ sand (4) for Lcc5 and Lcc1, respectively. **B:** B-factor putty representation of Lcc5 to demonstrate the flexibilities of the different loops. Loop 1 is most flexible, whereas loop 3 and 4 show B-factor similar to the surrounding loops that connect the  $\beta$ -strands. **C:** Close-up of the substrate binding cavity of Lcc1. Loop 1 (yellow) is not completely modeled. The cavity seems therefore larger than for Lcc5 (**D**)

### 2.3.1 The two copper sites

The type-1 copper site is the primary electron acceptor and responsible for substrate oxidation. It is located in the C-terminal cupredoxin-like domain close to the surface near loop 3 and 4. The single copper is ligated by two histidine residues (His482-N $\delta$ 1 and His420-N $\delta$ 1) and one cysteine residue (Cys477) arranging the cluster in a trigonal planar geometry (Fig. 44). A fourth axial ligand is absent.

The trinuclear center is located between the N-terminal and the C-terminal cupredoxin-like domain. It is involved in dioxygen binding and reduction to two water molecules.

The eight histidine residues ligating the three copper atoms are derived from both domains (Fig. 44-B): the type-2 copper is ligated by His90-N $\epsilon$ 2 from domain 3 and His88-N $\epsilon$ 2 from domain 1. The type-3 copper atoms are ligated by His134-N $\epsilon$ 2, His423-N $\delta$ 1 (both domain 1) and His478-N $\epsilon$ 2 (domain 3) for the first copper atom, and His425-N $\epsilon$ 2, His476-N $\epsilon$ 2 (both domain 3) and His136-N $\epsilon$ 2 (domain 1) for the second copper. Three water or hydroxyl molecules can be found at the trinuclear site. The first one is



coordinated to the T2 copper in a distance of 2.5 Å. The second one is ligating all three copper atoms with 2.1 Å, 2.7 Å and 2.8 Å distant to T2 and T3, respectively. A third water or hydroxyl molecule is bound between the two T3 copper atoms.

The structure of Lcc1 is depleted in T2 copper (216), which leads to rearrangement of its histidine ligands. His399 (His423 in Lcc5) acquires a second conformation by turning towards one of the T3 copper, which is therefore ligated by four histidine residues. This increases the distance between both type-3 copper from 4.9 Å observed in Lcc5 to 5.3 Å

(Fig. 45). The water ligand, that is bridging the three copper as observed for Lcc5 is lost, if the T2 copper is absent.

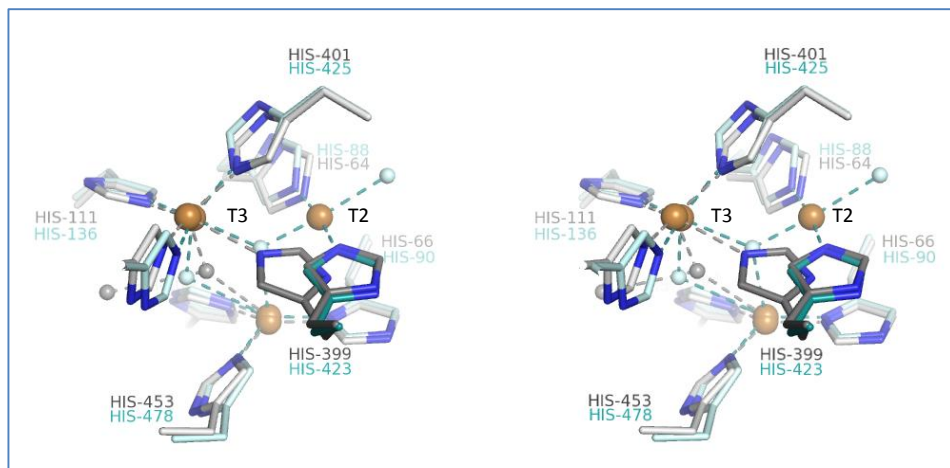


**Fig. 45** Stereo representation of the trinuclear site of Lcc1 (grey) and Lcc5 (cyan). Water or hydroxyl molecules are represented by small spheres. Lcc1 is depleted in type-2 copper (T2). This leads to an alternative conformation of His399 by turning towards one of the type-3 copper (T3), which is now ligated by 4 histidine residues. This results eventually in increase of the distance between both type-3 copper from 4.9 Å to 5.3 Å.

The mononuclear and trinuclear copper site are separated by around 12 Å. They are connected by a tripeptide consisting of the cysteine ligand (Cys477) of the T1 site and two histidine ligands (His476 and His478) of the trinuclear site (Fig. 46). This CHC-motif is highly conserved among laccases and involved in electron transfer.

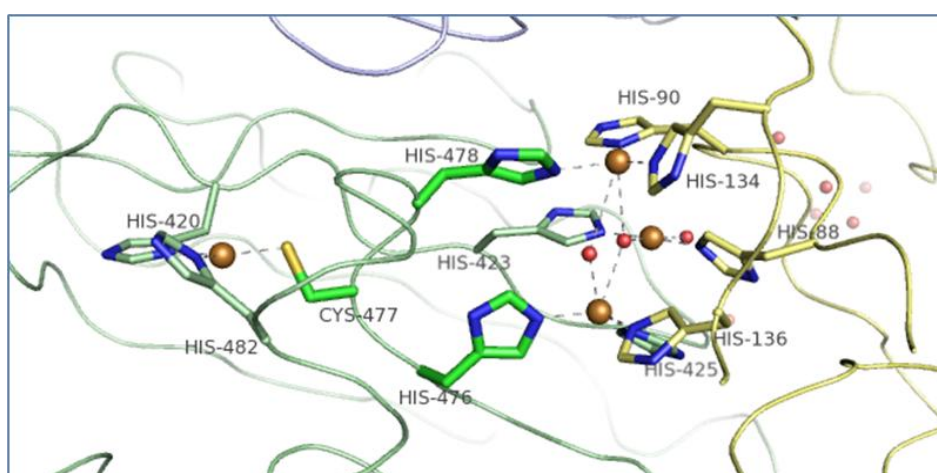


**Fig. 46** Two histidine (His478 and His476) together with a cysteine residue (Cys477) form a highly conserved tripeptide (bright green), which is involved in electron transfer. Copper is colored in brown, water/ hydroxyl molecules in red.



### 2.3.2 Glycosylation of Lcc5

The structure of Lcc5 reveals four glycosylation sites, which were already predicted (225). One O-linked N-acetyl glucosamine is present close to the C-terminus at residue Thr523 (O $\gamma$ 1) and Thr530 (O $\gamma$ 1), respectively, while a third O-linked N-acetyl glucosamine can be found at an aspartate residue (Asp79-O $\delta$ 2) belonging to a loop of domain 1 that is close-by to the first two glycosylation sites (Fig. 47). The fourth glycosylation site is located in domain 2, where an N-acetyl-D-glucosamine is N-linked to asparagine residue 239.

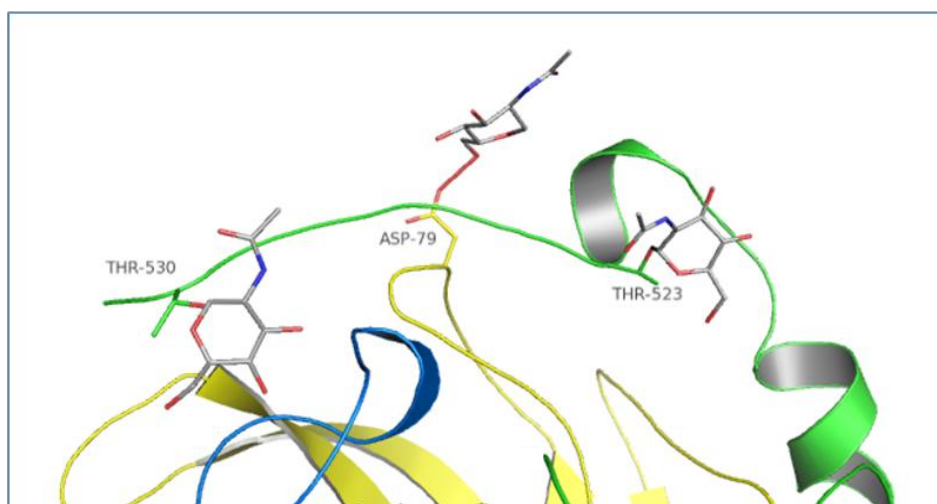


**Fig. 47** Glycosylation sites of Lcc5. An O-linked N-acetyl glucosamine (grey) can be found at residue Thr523 and Thr530 close to C-terminal domain 3. A third N-acetyl glucosamine is O-linked to Asp79 of domain 1. Domain 1, 2 and 3 are colored yellow, blue and green, respectively.

## 3 Conclusions and Outlook

The overall structure of Lcc5 is highly similar to the one of Lcc1. In contrast to the latter enzyme, Lcc5 contains all four copper ions. The intact trinuclear site of Lcc5 confirms the observation described for the type-2 depleted Lcc1 (216). Superposition of both structures showed the rearrangement of the trinuclear site due to the loss of the T2 copper.

The easy generation of high-diffracting crystals of this laccase offers a practical tool for further crystallographic studies such as protein-substrate complexes.

## VI Appendix

### Abbreviations

Å	Ångström; 1 Å = 10 <sup>-10</sup> m	N <sub>2</sub> O	nitrous oxide
a.s.u.	asymmetric unit	N <sub>2</sub> OR	nitrous oxide reductase
COX	cytochrome c oxidase	ODP	ozone-depleting potential
Da	Dalton; 1 Da = 1 g · mol <sup>-1</sup>	ODS	ozone-depleting substance
DFT	density function theory	ppm	parts per million
EPR	electron paramagnetic resonance	UHP	ultra-high purity
LMCT	ligand-to-metal charge transfer	r.m.s.d.	root-mean-square deviation
MPD	2-methyl-2,4-pentane diol	v/ v	volume per volume
NHE	Normal hydrogen electrode	w/ v	weight per volume

### Amino acids

A	Ala	alanine	N	Asn	asparagine
C	Cys	cysteine	P	Pro	proline
D	Asp	aspartate	Q	Gln	glutamine
E	Glu	glutamate	R	Arg	arginine
F	Phe	phenylalanine	S	Ser	serine
G	Gly	glycine	T	Thr	threonine
H	His	histidine	V	Val	valine
I	Ile	isoleucine	W	Trp	tryptophan
K	Lys	lysine	Y	Tyr	tyrosine
L	Leu	leucine			
M	Met	methionine			

**Tab. 2** X-ray data processing and refinement statistics for *Pseudomonas stutzeri* N<sub>2</sub>OR. Wavelength for all datasets is 1.0 Å. Data sets recorded at X06SA at the Swiss Light Source, Paul Scherrer Institute, Villigen, Switzerland.

<i>P. stutzeri</i> Nitrous oxide reductase	Native 1	Native 2	N <sub>2</sub> O adduct
<b>Space group</b>	<i>P</i> 1	<i>P</i> 6 <sub>5</sub>	<i>P</i> 1
<b>Cell constants <i>a, b, c</i> (Å); <math>\alpha, \beta, \gamma</math> (°)</b>	96.9 106.7 131.1 111.3 107.3 90.7	70.3 70.3 399.7 90 90 120	96.6 106.5 130.9 111.5 107.2 90.7
<b>Resolution range (Å)</b>	46.11-2.1	50.0-1.69	115.283-2.24
<b>Completeness overall (%)</b>	94.7 (91.8)	98.3 (89.5)	94.6 (90.5)
<b>Reflections, unique</b>	255620 (36175)	121422 (16139)	208149 (29124)
<b>Multiplicity (%)</b>	2.1 (2.0)	5.4 (3.9)	3.8 (3.7)
<b><i>R</i><sub>merge</sub> overall<sup>1</sup></b>	0.107 (0.492)	0.096 (0.485)	0.09 (0.417)
<b><i>R</i><sub>value</sub> overall (%)<sup>2</sup></b>	0.1779	0.1691	0.1697
<b><i>R</i><sub>value</sub> free (%)</b>	0.2422	0.2039	0.2448
<b>Non hydrogen protein atoms</b>	36801	9191	36916
<b>Non hydrogen ligand atoms</b>	0	0	12
<b>Solvent molecules</b>	2474	706	2556
<b>Mean <i>I</i> / Sig(<i>I</i>)</b>	56.7 (1.6)	10.6 (2.0)	12.8 (3.9)
<b>Cruickshanks DPI</b>	0.2684	0.0228	0.4213
<b>FOM</b>	0.8586	0.8411	0.8219
<b>R.m.s. deviations from ideal values</b>			
<b>Bond lengths (Å)</b>	0.0209	0.0299	0.0191
<b>Bond angles (°)</b>	1.9203	2.406	1.7921
<b>Average <i>B</i> values (Å<sup>2</sup>)</b>			
<b>Protein main chain atoms</b>	22.827	27.284	18.151
<b>Protein all atoms</b>	23.542	28.456	18.755
<b>Ligand</b>	0	0	55.342
<b>Solvent</b>	28.865	35.970	24.106
<b><math>\Phi, \Psi</math> angle distribution for residues<sup>3</sup></b>			
<b>In most favoured regions (%)</b>	94.7	87.5	93.6
<b>In additional allowed regions (%)</b>	4.6	11.1	5.2
<b>In generously regions (%)</b>	0.6	0.7	2.0
<b>In disallowed regions (%)</b>	0.1	0.7	0.2
<sup>1</sup> $R_{\text{merge}} = \frac{\sum_{hkl} [(\sum_i  I_i - \langle I \rangle ) / \sum_i I_i]}{\sum_{hkl} I_i}$ <sup>2</sup> $R_{\text{value}} = \frac{\sum_{hkl} ( F_{\text{obs}}  -  F_{\text{calc}} ) / \sum_{hkl}  F_{\text{obs}} }{\sum_{hkl}  F_{\text{obs}} }$ $R_{\text{free}}$ is the cross-validation <i>R</i> factor computed for the test set of 5 % of unique reflections <sup>3</sup> Ramachandran statistics as defined by PROCHECK			

**Tab. 3** X-ray data processing and refinement statistics for *Coprinopsis cinerea* laccase Lcc5. Wavelength for is 1.0 Å. Data sets recorded at X06SA at the Swiss Light Source, Paul Scherrer Institute, Villigen, Switzerland.

	Native
<b>Space group</b>	<i>P2<sub>1</sub>2<sub>1</sub>2<sub>1</sub></i>
<b>Cell constants <i>a, b, c</i> (Å); <math>\alpha, \beta, \gamma</math> (°)</b>	79.375, 82.116, 91.009 90.0, 90.0, 90.0
<b>Resolution limit (Å)</b>	91.0-1.2
<b>Completeness overall (%)</b>	94.1
<b>Reflections, unique</b>	3,002,266
<b><i>R</i><sub>merge</sub> overall<sup>1</sup></b>	0.119
<b><i>R</i><sub>value</sub> overall (%)<sup>2</sup></b>	0.15
<b><i>R</i><sub>value</sub> free (%)</b>	0.172
<b>Non hydrogen protein atoms</b>	4061
<b>Non hydrogen ligand atoms</b>	0
<b>Solvent molecules</b>	749
<b>Mean <i>I</i> / Sig(<i>I</i>)</b>	5.6
<b>Cruickshanks DPI</b>	0.036
<b>FOM</b>	0.914
<b>R.m.s. deviations from ideal values</b>	
<b>Bond lengths (Å)</b>	0.012
<b>Bond angles (°)</b>	1.61
<b>Average <i>B</i> values (Å<sup>2</sup>)</b>	
<b>Protein main chain atoms</b>	12.873
<b>Protein all atoms</b>	13.583
<b>Ligand</b>	0
<b>Solvent</b>	28.449
<b><math>\Phi, \Psi</math> angle distribution for residues<sup>3</sup></b>	
<b>In most favoured regions (%)</b>	88.9
<b>In additional allowed regions (%)</b>	10.6
<b>In generously regions (%)</b>	0.5
<b>In disallowed regions (%)</b>	0
<sup>1</sup> $R_{\text{merge}} = \frac{\sum_{hkl} [(\sum_i  I_i - \langle I \rangle )]}{\sum_i I_i}$ <sup>2</sup> $R_{\text{value}} = \frac{\sum_{hkl}   F_{\text{obs}}  -  F_{\text{calc}}  }{\sum_{hkl}  F_{\text{obs}} }$ $R_{\text{free}}$ is the cross-validation <i>R</i> factor computed for the test set of 5 % of unique reflections <sup>3</sup> Ramachandran statistics as defined by PROCHECK	

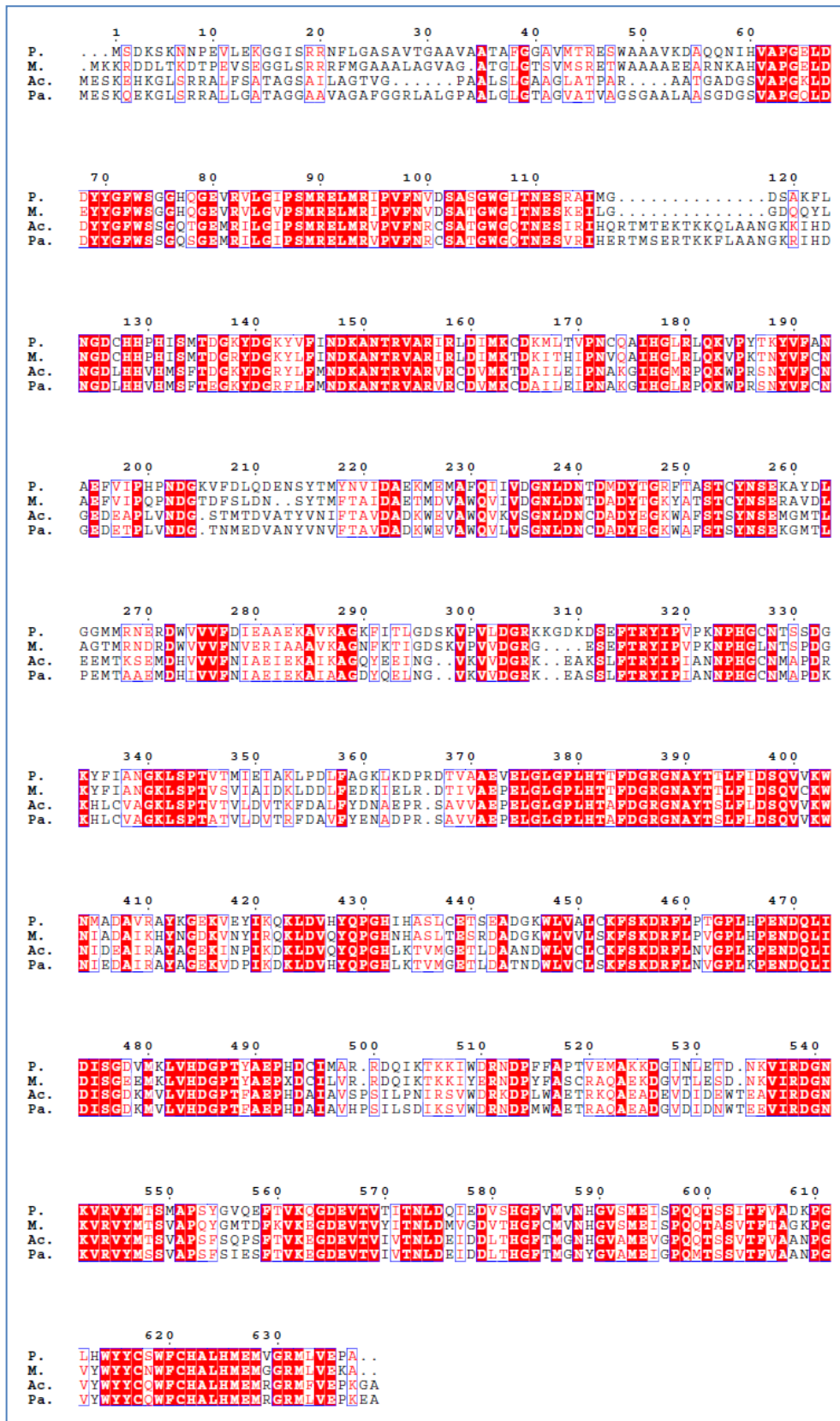


**Fig. 48** Sequence alignment of the four structural described nitrous oxide reductases. P = *Pseudomonas stutzeri*, M = *Marinobacter hydrocarbonoclasticus*, Ac = *Achromobacter hydrocarbonoclasticus*, Pa = *Paracoccus denitrificans*

## VII References

1. Holm, R. (1996) *Chem. Rev.* **96**, 2239.
2. Crichton, R. R., Pierre, J.L. (2001) *Biometals* **14**, 99.
3. Abolmaali, B. (1998) *Structure and Bonding* 91 - Evolutionary Aspects of Copper Binding Centers in Copper Proteins. Springer Verlag, Heidelberg.
4. Kasting, J. F. (2006) *Phil. Trans. R. Soc. B.* **361**, 1733.
5. Farquhar, J., Wing, B. A. (2003) *Earth Planet Sci. Lett.* **1**, 213.
6. Tian, F. (2005) *Science* **308**, 5724.
7. Abolmaali, B. (1998) *Struct. Bond* **91**, 91.
8. Sykes, A. G. (1991) *Adv. Inorg. Chem.* **36**, 377.
9. Lancaster, K. M. (2009) *Nat. Chem.* **1**, 711.
10. Malkin, R., Malmström, B. G. (1970) *Adv. Enzymol. Relat. Areas Mol. Biol.* **33**, 177.
11. Koval, I. A. (2006) *J. Chem. Soc. Rev.* **35**, 814.
12. Belle, C. (2005) *J. Inorg. Biochem.* **99**, 1929.
13. Murphy, M. EP. (1997) *Prot. Sci.* **6**, 761.
14. Murphy, L. M. (2002) *J. Mol. Biol.* **315**, 859.
15. Godden, J. W. (1991) *Science* **253**, 438.
16. Brown, K. (2000) *NatureLett.* **7**, 191.
17. Haltia, T. (2003) *Biochem. J.* **369**, 77.
18. Paraskevopoulos, K. (2006) *J. Mol. Biol.* **362**, 55.
19. Romero, A. (1993) *J. Mol. Biol.* **229**, 1997.
20. Guckert, J. A. (1995) *JACS* **117**, 2817.
21. Pascher, T. (1993) *Eur. J. Biochem.* **212**, 289.
22. Machonkin, T. E. (1998) *Biochem.* **37**, 9570.

23. Xu, F. (1996) *Biochim. Biophys. Acta* **1292**, 303.
24. Hough, M. A. (2001) *Acta Cryst. D* **57**, 355.
25. Crichton, R. R. *Biological Inorganic Chemistry: An Introduction..*
26. Morozova, O. V. (2007) *Biochem. (Moscow)* **72**, 1136.
27. Randall, D. W. (2000) *J. Biol. Inorg. Chem.* **5**, 16.
28. Einsle, O. (2000) *J. Biol. Inorg. Chem.* **5**, 666.
29. Chapman, G. V. (1977) *J. Mol. Biol.* **110**, 187.
30. Solomon, E. I. (1996) *Chem. Rev.* **96**, 2563.
31. Arciero, D. M. (2002) *Biochem.* **41**, 1703.
32. Lieberman, R. L. (2001) *Biochem.* **40**, 5674.
33. Basumallick, L. (2005) *JACS* **127**, 3531.
34. Fusetti, F. (1998) *J. Biol. Chem.* **273**, 16962.
35. Gacheru, S. N. (1990) *J. Biol. Chem.* **265**, 19022.
36. Malmström, B. G. (1968) *Biochim. Biophys. Acta* **156**, 67.
37. Eisensmith, R. C. (1991) *Molec. Biol. Med.* **8**, 3.
38. Ito, N. (1991) *Nature* **350**, 87.
39. LaCroix, L. B. (1996) *JACS* **118**, 7755.
40. Yoon, J. (2009) *PNAS* **106**, 6585.
41. Longa, S. D. (1996) *J. Biol. Chem.* **271**, 21025.
42. Klabunde, T. (1998) *Nat. Struct. Biol.* **1084**, 5.
43. Magnus, K. A. (1994) *Prot. Struct. Funct. Genet.* **19**, 302.
44. Messerschmidt, A. (1992) *J. Mol. Biol.* **224**, 179.
45. Zaitseva, I. (1996) *J. Biol. Inorg. Chem.* **1**, 15.
46. Osaki, S. (1966) *J. Biol. Chem.* **241**, 5053.
47. Osaki, S. (1966) *J. Biol. Chem.* **241**, 2746.



48. Osaki, S., Walaas, O. (1968) *Arch. Biochem. Biophys.* **125**, 918.
49. Osaki, S., Walaas, O. (1967) *J. Biol. Chem.* **242**, 2653.
50. Huber, C. T., Frieden, E. (1970) *J. Biol. Chem.* **245**, 3973.
51. Carver, F. J. (1982) *Biol. trace Elem. Res.* **4**, 1.
52. Chidambaram, M. V. (1983) *FEBS Lett.* **159**, 137.
53. Samuel, T. K., Gitlin, J. D. (2006) *Nat. Chem. Biol.* **2**, 486.
54. Shiva, S. (2006) *Nat. Chem. Biol.* **2**, 486.
55. Beinert, H. (1962) *J. Biol. Chem.* **237**, 2337.
56. Suharti, S. (2001) *Biochem.* **40**, 2632.
57. Iwata, S. (1995) *Nature* **376**, 660.
58. Tsukihara, T. (1995) *Science* **269**, 1069.
59. Wilmans, W. (1995) *PNAS* **92**, 11955.
60. Kroneck, P. MH. (1988) *FEBS Lett.* **242**, 70.
61. Savelieff, M. G. (2010) *J. Biol. Inorg. Chem.* **15**, 461.
62. Hay, M. (1996) *PNAS* **93**, 461.
63. Coyle, C. L. (1985) *Eur. J. Biochem.* **153**, 459.
64. Riester, J. (1989) *Eur. J. Biochem.* **178**, 751.
65. Zumft, W. G., Kroneck, P. MH. (2006) *Adv. Microbial. Physiol.* **52**, 109.
66. Antholine, W. E. (1992) *Eur. J. Biochem.* **209**, 875.
67. Kroneck, P. MH. (1989) *FEBS Lett.* **248**, 212.
68. Neese, F. (1997) *Electronic structure and spectroscopy of novel copper chromophores in biology*. Ph. D. Dissertation, University of Konstanz, Germany.
69. Farrar, J. A. (1991) *FEBS Lett.* **294**, 11.
70. Prudencio, M. (2000) *Biochem.* **39**, 3899.
71. Charnock, J. M. (2000) *Eur. J. Biochem.* **267**, 1368.
72. Zickermann, V. (1997) *Biochem.* **36**, 3232.

73. Zickermann, V. (1995) *Eur. J. Biochem.* **234**, 686.
74. Wang, K. (2002) *Biochem.* **41**, 2298.
75. Zhen, Y. (2002) *Biochem.* **41**, 2288.
76. DeBeer, G. D. (2001) *JACS* **123**, 5757.
77. Rasmussen, T. (2005) *Dalton Trans.*, 3501.
78. Chen, P. (2002) *JACS* **123**, 576.
79. Rasmussen, T. (2000) *Biochem.* **39**, 12753.
80. Atkins, P. W., Beran, J. A. (1998) In : *Chemie: einfach alles* 2nd edn. Wiley-VCH, Weinheim.
81. Einsle, O., Kroneck, P. MH. (2004) *Biol. Chem.* **385**, 875.
82. Payne, W. J. (1973) *Bact. Reviews* **37**, 409.
83. McCarty, G., Bremner, J. M. (1992) *PNAS* **89**, 453.
84. Buresh, R. J. (1978) *Soil Sci. Soc. Am. J.* **42**, 913.
85. Cole, J. A. (1980) *FEMS Microbiol. Lett.* **7**, 65.
86. Bonin, P. (1996) *FEMS Microbiol. Ecol.* **19**, 27.
87. Zumft, W. G. (1997) *Microbiol. Molec. Biol. Rev.* **61**, 533.
88. Hendriks, J. (2000) *Biochim. Biophys. Acta* **1459**, 266.
89. Strous, M. (1999) *Nature* **400**, 446.
90. Strous, M. (1999) *Appl. Environ. Microbiol.*, 3248.
91. Jolly, W. L. (1964) *The inorganic chemistry of nitrogen*. Benjamin, New York.
92. Staehelin, J. (2001) *Rev. Geophys.* **39**, 231.
93. Ravishankara, A. R. (2009) *Science* **326**, 123.
94. IPCC *Climate Change 2007*. 4th Assessment Report.
95. Crutzen, P. J. (2008) *Atmos. Chem. Phys.* **8**, 389.
96. Priscu, J. C. (1996) *Limnol. Oceanogr.* **41**, 1544.
97. Conrad, R. (1996) *Microbiol. Rev.* **60**, 609.

98. Dickinson, R. E., Cicerone, R. J. (1986) *Nature* **319**, 109.
99. Reilly, J. (1999) *Nature* **401**, 549.
100. IPCC (2006) Chapter 11: N<sub>2</sub>O emissions from managed soils, and CO<sub>2</sub> emissions from lime and urea application. In : *IPCC Guidelines for National Greenhouse Gas Inventories 4*. National Greenhouse Gas Inventories Programme, Hayama, Japan.
101. Skiba, U., Smith, K. A. (2000) *Glob. Change Sci.* **2**, 379.
102. Crutzen, P. J. (1970) *Meteorol. Soc.* **96**, 320.
103. Johnston, H. (1971) *Science* **173**, 517.
104. (1987) *Layer, The Montreal Protocol on Substances that Deplete the Ozone.*, Montreal, Canada.
105. Otte, S. (1999) *Appl. Microbiol. Biotechnol.* **51**, 255.
106. Anders, HJ. (1995) *Proteobacteria Int. J. Syst. Bacteriol.* **45**, 327.
107. Greenberg, E. P., Becker, G. E. (1977) *Can. J. Microbiol.* **23**, 903.
108. Doi, M., Shoi, Y. (1991) *Plant Cell Physiol.* **32**, 365.
109. Shiba, T. (1991) *Syst. Appl. Microbiol.* **14**, 140.
110. Casella, A. (2006) *Biochem. Soc. Trans.* **34**, 130.
111. Renner, E. D., Becker, G. E. (1970) *J. Bacteriol.* **101**, 821.
112. Kaspar, H. F. (1982) *Arch. Microbiol.* **133**, 126.
113. Yoshinari, T. (1980) *App. Environ. Microbiol.* **39**, 81.
114. Simon, J. (2004) *FEBS Lett.* **569**, 7.
115. Huston, A. L. (2000) *Environ. Microbiol.* **2**, 383.
116. Methe, B. A. (2005) *PNAS* **102**, 10913.
117. Völkl, P. (1993) *Appl. Environ. Microbiol.* **59**, 2918.
118. Anton, J. (2002) *Int. J. Syst. Evol. Microbiol.* **52**, 485.
119. ZoBell, C. E., Oppenheimer, C. H. (1950) *J. Bacteriol.* **60**, 771.
120. Beyer, \*. (2009) *J. Mol. Microbiol. Biotechnol.* **16**, 187.

121. Baliga, N. S. (2004) *Genome Res.* **14**, 2221.
122. Mullakhabbhai, M. F., Larsen, H. (1975) *Arch. Microbiol.* **104**, 207.
123. Grant, W. D. (2001) Class III Halobacteria. In : *Bergey's Manual of Systematic Bacteriology The Archaea and the Deeply Branching and Phototrophic Bacteria.* Springer, New York.
124. Fitz-Gibbon, S. T. (2002) *PNAS* **99**, 984.
125. Fernandez, A. T. (2010) *FEBS* **277**, 3176.
126. Zumft, W. G., Matsubara, T. (1982) *FEBS Lett.* **148**, 107.
127. Rhodes, M. (1963) *Can. J. Microbiol.* **9**, 799.
128. Matsubara, T., Iwasaki, H. (1972) *J. Biochem.* **71**, 747.
129. Iwasaki, H. (1980) *Plant Cell Physiol.* **21**, 1573.
130. Iwasaki, H., Terai, H. (1982) *J. Gen. Appl. Microbiol. Tokyo* **28**, 189.
131. Berks, B. C. (1993) *Eur. J. Biochem.* **212**, 467.
132. Yamaguchi, K. (2003) *J. Biochem.* **134**, 853.
133. McEwan, A. G. (1985) *J. Bacteriol.* **164**, 823.
134. Teraguchi, S., Hollocher, T. C. (1989) *J. Biol. Chem.* **264**, 1972.
135. SooHoo, C. K., Hollocher, T. C. (1991) *J. Biol. Chem.* **266**, 2203.
136. Zhang, CS. (1991) *J. Biol. Chem.* **266**, 2199.
137. Suharti, S., de Vries, S. (2005) *Biochem. Soc. Trans.* **33**, 130.
138. Ghosh, S. (2007) *JACS* **129**, 3955.
139. Alvarez, M. L. (2001) *JACS* **123**, 576.
140. Rasmussen, T. (2002) *Biochem. J.* **364**, 807.
141. Riester, J. (1989) *Dissertation: Distickstoffoxid-Reduktase, ein Multikupferenzym in denitrifizierenden Bakterien* 248. Hartung-Gorre Verlag, University of Konstanz, Germany.
142. Chan, J. M. (2004) *JACS* **126**, 3030.

143. Dell'Acqua, S. (2008) *Biochem.* **47**, 10852.
144. Ferretti, S. (1999) *Eur. J. Biochem.* **259**, 651.
145. Zumft, W. G. (1992) *Eur. J. Biochem.* **208**, 31.
146. Scott, R. A. (1989) *PNAS* **86**, 4082.
147. Greenwood, C. (1983) *Biochem. J.* **215**, 303.
148. Winkler, J. R. (2000) *Curr. Opin. Chem. Biol.* **4**, 192.
149. Itoh, M. (1989) *FEBS Lett.* **251**, 104.
150. Richardson, D. J. (1991) *Eur. J. Biochem.* **199**, 677.
151. Mattila, K., Haltia, T. (2005) *Proteins* **59**, 708.
152. Zhang, CS., Hollocher, T. C. (1993) *Biochim. Biophys. Acta* **1142**, 253.
153. Wunsch, P. (2003) *J. Bacteriol.* **185**, 885.
154. Wunsch, P., Zumft, W. G. (2005) *J. Bacteriol.* **187**, 1992.
155. Honisch, U., Zumft, W. G. (2003) *J. Bacteriol.* **185**, 1895.
156. Velasco, L. (2004) *Antonie Leeuwenhoek* **85**, 229.
157. Arai, H. (2003) *Microbiol. (UK)* **149**, 29.
158. Heikkilä, M. P. (2001) *J. Bacteriol.* **183**, 1663.
159. Dreusch, A. (1995) *Liganden der Kupferzentren der N<sub>2</sub>O-Reduktase von Pseudomonas stutzeri sowie Untersuchungen zur Biosynthese und Prozessierung des Enzyms*. Ph. D. Dissertation, University of Karlsruhe, Germany.
160. Dreusch, A. (1997) *Biochim. Biophys. Acta* **1319**, 311.
161. Dreusch, A. (1996) *Eur. J. Biochem.* **237**, 447.
162. McGuirl, M. A. (2001) *J. Biol. Inorg. Chem.* **6**, 189.
163. Saunders, N. FW. (2000) *J. Bacteriol.* **182**, 5211.
164. Chan, YK. (1997) *Microbiol. (UK)* **143**, 2817.
165. Otte, S. (1996) *Appl. Environ. Microbiol.* **62**, 2421.
166. Körner, H., Zumft, W. G. (1989) *Appl. Environ. Microbiol.* **55**, 1670.

167. Baumann, B. (1996) *J. Bacteriol.* **178**, 4367.
168. Chen, P. (2002) *JACS* **124**, 10497.
169. Chen, P. (2002) *JACS* **124**, 744.
170. Organesyan, V. S. (2004) *Dalton Trans.*, 996.
171. Ghosh, S. (2003) *JACS* **126**, 3030.
172. Gorelsky, S. I. (2006) *JACS* **128**, 278.
173. Chen, P. (2004) *Angew. Chem. Int. Ed.* **43**, 4132.
174. Claus, H. (2004) *Micron*. **35**, 93.
175. van der Ham, J. L. (2007) *Crustaceana* **80**, 755.
176. O'Malley, D. M. (1993) *Plant J.* **4**, 751.
177. Yoshida, H. (1883) *J. Chem. Soc.* **43**, 472.
178. Omura, T. (1961) *J. Biochem. (Tokyo)* **50**, 264.
179. Sterjiades, R. (1992) *Plant. Physiol.* **99**, 1162.
180. Bao, W. (1993) *Science* **260**, 672.
181. Gavnholt, B. (2002) *Plant Sci.* **162**, 873.
182. Caparros-Ruiz, D. (2006) *Plant Sci.* **171**, 217.
183. Andreasson, L. E. (1976) *Biochem. Biophys. Acta* **438**, 370.
184. Richardson, A. (2000) *Tree Physiol.* **20**, 1039.
185. Gavnholt, B., Larsen, K. (2002) *Physiol. Plant.* **116**, 273.
186. Mayer, A. M., Staples, R. C. (2002) *Phytochem.* **60**, 551.
187. Koschorreck, K. (2008) *Appl. Microbiol. Biotechnol.* **79**, 217.
188. Kataoka, K. (2007) *J. Mol. Biol.* **373**, 141.
189. Sharma, P. (2007) *J. Microbiol. Biotechnol.* **23**, 823.
190. Cha, S. J., Cooksey, D. A. (1991) *PNAS* **88**, 8915.
191. Claus, H. (2003) *Arch. Microbiol.* **179**, 145.

192. Sugumaran, M. (1992) *Arch. Ins. Biochem. Physiol.* **19**, 271.
193. Kramer, K. J. (2001) *Tetrahedron* **57**, 385.
194. Arakane, Y. (2005) *PNAS* **102**, 11337.
195. Decker, H. (2001) *J. Biol. Chem.* **276**, 17796.
196. Lee, S. Y., Soderhall, K. (2002) *Fish Shellfish Immun.* **12**, 421.
197. Sugumaran, M. (2002) *Pigm. Cell Res.* **15**, 2.
198. Liu, G. X. (2006) *Fish Shellfish Immun.* **20**, 47.
199. Hoegger, P. J. (2006) *FEBS J.* **273**, 2308.
200. Thurston, C. F. (1994) *Microbiol., UK* **140**, 19.
201. Baldrian, P. (2006) *FEMS Microbiol. Rev.* **30**, 215.
202. Das, N. (1997) *Appl. Environ. Microbiol.* **63**, 4120.
203. Leonowicz, A. (2001) *J. Basic Microbiol.* **41**, 185.
204. Blaich, R., Esser, K. (1975) *Arch. Microbiol.* **103**, 271.
205. Duran, N. (2002) *Enzyme Microbiol. Tech.* **31**, 907.
206. Palmieri, G. (1997) *J. Biol. Chem.* **272**, 31301.
207. Faraco, V. (2009) *Biodegrad.* **20**, 209.
208. Larrondo, L. F. (2003) *Appl. Environ. Microbiol.* **69**, 6263.
209. Klonowska, A. (2002) *Eur. J. Biochem.* **269**, 6119.
210. Yaver, D. S. (1996) *Appl. Environ. Microbiol.* **62**, 834.
211. Molitoris, H. P., Esser, K. (1970) *Arch. Microbiol.* **72**, 267.
212. Palmer, A. E. (2001) *JACS* **123**, 6591.
213. Enguita, F. J. (2003) *J. Biol. Chem.* **278**, 19416.
214. Garavaglia, S. (2003) *J. Mol. Biol.* **342**, 1519.
215. Bento, I. (2005) *Dalton Trans.* **21**, 3507.
216. Ducros, V. (1998) *Nat. Struct. Biol.* **5**, 310.

217. Messerschmidt, A. (1998) Metal sites in small blue copper proteins, blue copper oxidases and vanadium-containing enzymes, 37-68. In : *Metal sites in proteins and model redox centers*. Verlag Berlin/ Heidelberg, Berlin.
218. Hakulinen, N. (2002) *Nat. Struct. Biol.* **9**, 601.
219. Larrondo, L. F. (2004) *Appl. Environ. Microbiol.* **150**, 2775.
220. Kilaru, S. (2006) *Curr. Genet.* **50**, 45.
221. Giardina, P. (1999) *Biochem. J.* **341**, 655.
222. Giardina, P. (2010) *Cell Mol. Life Sci.* **67**, 369.
223. Ferraroni, M. (2007) *BMC Struct. Biol.* **7**, 60.
224. Tadesse, M. A. (2008) *Org. Biomol. Chem.* **6**, 868.
225. Rühl, M. (2009) *Dissertation: Laccases and other ligninolytic enzymes of the basidiomycetes Coprinopsis cinerea and Pleurotus ostreatus.*, University of Göttingen, Germany.
226. Solomon, E. I. (2008) *Dalton Trans.* **30**, 3921.
227. Quintanar, L. (2005) *JACS* **127**, 13832.
228. Zoppellaro, G. (2001) *J. Biochem.* **129**, 949.
229. Lee, S. K. (2002) *JACS* **124**, 6180.
230. Solomon, E. I. (2007) *Acc. Chem. Res.* **40**, 581.
231. Yoon, J. (2007) *PNAS* **104**, 13609.
232. Yoon, J., Solomon, E. I. (2007) *JACS* **129**, 13127.
233. Sakurai, T. (1992) *Biochem. J.* **284**, 681.
234. Gianfreda, L. (1999) *Bioremediation J.* **3**, 1.
235. Yaropolov, A. I. (1994) *Appl. Biochem. Biotech.* **49**, 257.
236. Pointing, S. B. (2001) *Appl. Microbiol. Biotech.* **57**, 20.
237. Novotny, C. (2004) *Soil Biol. Biochem.* **36**, 1545.
238. Ikehata, K. (2004) *J. Environ. Engin. Sci.* **3**, 1.



239. Minussi, R. C. (2002) *Tr. Food Sci. Tech.* **13**, 205.
240. Couto, S. R. (2006) *Biotech. Adv.* **24**, 500.
241. Riva, S. (2006) *Tr. Biotech.* **24**, 219.
242. Moreira, M. T. (1998) *J. Biotechnol.* **66**, 27.
243. Pandey, A. (2000) *Proc. Biochem.* **35**, 1153.
244. Hakala, T. K. (2005) *Enz. Microbial Tech.* **36**, 461.
245. Ibarra, D. (2006) *J. Chem. Tech. Biotech.* **81**, 1159.
246. Kharazipour, A. (1997) *J. Adh. Scie. Tech.* **11**, 419.
247. Felby, C. (2002) *Enz. Microbial. Tech.* **31**, 736.
248. Mai, C. (2004) *Appl. Microbiol. Biotech.* **63**, 447.
249. Fackler, K. (2008) *Holzforsch.* **62**, 223.
250. Hoppe, W. (1957) *Acta Cryst.* **10**, 750.
251. Huber, R. (1965) *Acta Cryst.* **19**, 353.
252. Rossmann, M. G., Blow, D. M. (1962) *Acta Cryst.* **15**, 24.
253. Patterson, A. L. (1934) *Phys. Rev.* **46**, 372.
254. Smith, P. K. (1985) *Anal. Biochem.* **150**, 76.
255. Evans, P. R. (2006) *Acta Cryst. D* **62**, 72.
256. Collaborative computational project, 4. (1994) *Acta Cryst. D* **50**, 760.
257. Matthews, B. W. (1968) *J. Mol. Biol.* **33**, 491.
258. Matthews, B. W. (1976) *Annu. Rev. Phys. Chem.* **27**, 493.
259. McCoy, A. J. (2007) *J. Appl. Cryst.* **40**, 658.
260. Emsley, P., Cowtan, K. (2004) *Acta Cryst. D* **60**, 2126.
261. Murshudov, G. N. (1997) *Acta Cryst. D* **53**, 240.
262. Hulse, C. L., Averill, B. A. (1990) *Biochem. Biophys. Res. Commun.* **166**, 729.
263. Shriver, D. F., Atkins, P. W. (2001) *Inorganic chemistry* 3rd edn. Oxford University Press, Oxford.

264. Witt, H. (1998) *J. Biol. Chem.* **273**, 5132.
265. Pearson, I. V. (2003) *J. Bacteriol.* **185**, 6308.
266. van Spanning, R. JM. (1990) *J. Bacteriol.* **172**, 986.
267. Fujita, K., Dooley, D. M. (2007) *Inorg. Chem.* **46**, 613.
268. Gupta, S. (2001) *Biochem.* **40**, 6180.
269. Lappalainen, P. (1993) *J. Biol. Chem.* **268**, 26416.
270. Epel, B. (2002) *JACS* **124**, 8152.
271. Xie, X. (2008) *JACS* **130**, 5194.
272. Lukoyanov, D. (2002) *Biophys. J.* **82**, 2758.
273. Robinson, H. (1999) *Biochem.* **38**, 5677.
274. Hwang, H. J., Lu, Y. (2004) *PNAS* **101**, 12842.
275. Brown, E. C. (2005) *JACS* **127**, 13752.
276. Bar-Nahum, I. (2009) *JACS* **131**, 2812.
277. Kumar, S. VS. (2003) *Biotechn. Bioeng.* **83**, 386.
278. Decker, H., Terwilliger, N. (2000) *J. Exp. Biol.* **203**, 1777.
279. Kitajima, N. (1992) *JACS* **114**, 1277.
280. Antholine, W. E. (1998) *Mol. Phys.* **95**, 1247.
281. Arai, H. (1997) *Mol. Microbiol.* **25**, 1141.
282. Kroneck, P. MH. (2001) Binculear Copper A. In : *Handbook of Metalloproteins 2*. Wiley, Chichester.
283. Randall, D. W. (2000) *J. Biol. Inorg. Chem.* **5**, 16.
284. Simon, J. (2002) *FEMS Microbiol. rev.* **26**, 285.
285. Adman, E. T. (1995) *Nat. Struct. Biol.* **2**, 929.
286. Boulanger, M. J. (2002) *J. Mol. Biol.* **315**, 1111.
287. Dell'Acqua, S. (2010) *J. Biol. Inorg. Chem.* **15**, 967.
288. Rasmussen, T. (2005) *Dalton Trans.*, 3501.

289. Williams, P. A. (1999) *Nat. Struct. Biol.* **6**, 509.
290. Chang, A. HH. (1993) *Chem. Phys.* **99**, 6824.
291. Tachikawa, H. (1995) *Phys. Chem.* **99**, 16630.
292. Nakamura, H. (1999) *Chem. Phys.* **110**, 9937.
293. Hwang, DY. (2000) *Chem. Phys.* **259**, 89.
294. Vagin, A. (1997) *J. Appl. Crystl.* **30**, 1022.
295. Krissinel, E., Henrick, K. (2007) *J. Mol. Biol.* **372**, 774.
296. Larkin, M. A. (2007) *Bioinform.* **23**, 2974.
297. Higgins, D. (1994) *Nucl. Acids Res.* **22**, 4673.
298. Hay, M. T. (1998) *Inorg. Chem.* **37**, 191.
299. Hoegger, P. J. (2004) *Curr. Gen.* **45**, 9.
300. Bollag, J. M., Leonowicz, A. (1984) *Appl. Environ. Microbiol.* **48**, 849.

## VIII Acknowledgements

Diese Arbeit entstand im Zeitraum von September 2006 bis September 2010 in der Abteilung für Molekulare Strukturbiologie der Universität Göttingen und dem Lehrstuhl für Biochemie an der Universität Freiburg.

Mein ganz besonderer Dank gilt Herrn Prof. Dr. Oliver Einsle, Universität Freiburg, nicht nur für dieses spannende Thema und die exzellente Betreuung sondern auch für die Geduld und das Vertrauen, sowie die Unterstützung und die vielen guten Ratschläge.

Dr. Susana Andrade möchte ich als erstes herzlich für die Übernahme des Korreferats danken sowie für die vielen freundlichen Gespräche, aufmunternden Worte und Ratschläge.

Ein herzliches Danke geht an Prof. Dr. Peter Kroneck und Prof. Dr. Walter Zumft, nicht nur für die Bereitstellung von Proteinproben und das in mich gesetzte Vertrauen, sondern vor allem auch für die vielen interessanten Diskussionen und Hilfestellungen vor allem im Rahmen der gemeinsamen Publikationen.

Ein großes Dankeschön geht an das Team der Swiss Light Source in Villigen für die exzellente Unterstützung.

Ebenso danke ich den Göttingern, vor allem Dr. Martin Rühl, und der AG Ficner für die schöne gemeinsame Zeit, besonderer Dank gilt hierbei Chrissoula, Kristina und Sohail.

Weiterer Dank gebührt dem Graduiertenkolleg IRTG1422 für die finanzielle Unterstützung und die Möglichkeit an vielen internationalen Treffen und Konferenzen teilzunehmen. Besonderer Dank geht an die Mitglieder für die vielen Diskussionen, Ideen und Anregungen, vor allem Frieda, Alexandra, Hanna und Florian für die lustige gemeinsame Zeit.

Herzlicher Dank geht an meine Kollegen in der AG Einsle, AG Andrade und AG Friedrich für die freundliche Atmosphäre, die Zusammenarbeit und Unterstützung und die

gemeinschaftlichen Dienstagabende. Vor allem Frau Williams, Frau Zähringer-Steffens und Herrn Hamacher möchte ich ganz speziell danken, da sie es irgendwie immer geschafft haben auch unmögliche Sachen zu vollbringen und ohne die diese Abteilung nicht das wäre, was sie heute ist.

Ein ganz besonders lieber Dank geht an meine Freunde Camila, Peer, Wei, Juan, Ramona, Thomas, Daniel, Emmanuel, Carlos, Maren und Daniel. Ihr habt die Zeit in Göttingen und Freiburg zu einer unvergesslich schönen und lustigen Zeit gemacht. Danke für die vielen Tips, die Diskussionen und vor allem die vielen gemeinschaftlichen Unternehmungen und Filmabende. Mit euch und kann auch noch ein mehrtägiger Synchrotron-Trip Spaß machen.

Nicht genug danken kann ich meinen "großen Bruder" Stefan für seine Geduld und Fachkenntnis bei Problemen aller Art. Ohne Dein Verständnis, Deine Herzlichkeit und unermüdliche Hilfe wäre diese Arbeit so nicht entstanden. Danke für alles!

Unendlicher Dank geht an Katrin, Katja, Anja, Sandra und Julia für euren Rückhalt und eure Freundschaft, auch trotz der teilweisen großen Distanz. Ihr seid die besten Freunde, die man sich wünschen kann. Besonders Julia gehört noch ein extragroßes Dankeschön für die gemeinsam durchlittene Schreibphase.

Mein größter Dank geht an meine Familie, besonders meine Eltern und meine Schwester Juliane für die grenzenlose Unterstützung, ihr Vertrauen, die aufbauenden Worte zu jeder Tag- und Nachtzeit, die ständige Aufmunterung und die tollen Kehrpakete.

## IX *Curriculum vitae*

### Personal data

Name: Anja Pomowski  
born: June 4<sup>th</sup>, 1981 in Jena, Germany

### Education

2000 Abitur, Gotthold-Ephraim-Lessing-Gymnasium, Neubrandenburg, Germany  
2000-2005 Studies of Biology, Georg-August-Universität Göttingen, Germany  
2005-2006 Diploma thesis "Charakterisierung der Distickstoffoxid-Reduktase aus *Wolinella succinogenes*", Georg-August-Universität Göttingen, Germany, supervisor Prof. Dr. Oliver Einsle  
2006-2010 Ph. D. studies, Georg-August-Universität Göttingen and Albert-Ludwigs-Universität Freiburg, Germany, supervisor Prof. Dr. Oliver Einsle

### Courses and working experience

2007 QIAGEN protein crystallography workshop, Göttingen  
2009 16. Arbeitstagung "Mikromethoden in der Biochemie", Martinsried

### Conference and workshop presentations

2010 Anja Pomowski, Walter G. Zumft, Peter M.H. Kroneck, Oliver Einsle: "Purple Nitrous Oxide Reductase from *Pseudomonas stutzeri* – New Insights into Cu<sub>2</sub>" 10<sup>th</sup> EUROBIC, Thessaloniki, Greece

